



Review

Lignans as Pharmacological Agents in Disorders Related to Oxidative Stress and Inflammation: Chemical Synthesis Approaches and Biological Activities

Dmitry I. Osmakov ^{1,2}, Aleksandr P. Kalinovskii ¹, Olga A. Belozorova ¹, Yaroslav A. Andreev ^{1,2}
and Sergey A. Kozlov ^{1,*}

¹ Shemyakin-Ovchinnikov Institute of Bioorganic Chemistry, Russian Academy of Sciences, ul. Miklukho-Maklaya 16/10, 117997 Moscow, Russia; osmadim@gmail.com (D.I.O.); kalinovskii.ap@gmail.com (A.P.K.); o.belozorova@gmail.com (O.A.B.); aya@ibch.ru (Y.A.A.)

² Institute of Molecular Medicine, Sechenov First Moscow State Medical University, 119991 Moscow, Russia

* Correspondence: serg@ibch.ru

Abstract: Plant lignans exhibit a wide range of biological activities, which makes them the research objects of potential use as therapeutic agents. They provide diverse naturally-occurring pharmacophores and are available for production by chemical synthesis. A large amount of accumulated data indicates that lignans of different structural groups are apt to demonstrate both anti-inflammatory and antioxidant effects, in many cases, simultaneously. In this review, we summarize the comprehensive knowledge about lignan use as a bioactive agent in disorders associated with oxidative stress and inflammation, pharmacological effects *in vitro* and *in vivo*, molecular mechanisms underlying these effects, and chemical synthesis approaches. This article provides an up-to-date overview of the current data in this area, available in PubMed, Scopus, and Web of Science databases, screened from 2000 to 2022.

Keywords: lignan; antioxidant; oxidative stress; anti-inflammatory; inflammation; chemical synthesis



Citation: Osmakov, D.I.; Kalinovskii, A.P.; Belozorova, O.A.; Andreev, Y.A.; Kozlov, S.A. Lignans as Pharmacological Agents in Disorders Related to Oxidative Stress and Inflammation: Chemical Synthesis Approaches and Biological Activities.

Int. J. Mol. Sci. **2022**, *23*, 6031.

<https://doi.org/10.3390/ijms23116031>

Academic Editors: Natália Cruz-Martins and Roberta Fusco

Received: 29 April 2022

Accepted: 24 May 2022

Published: 27 May 2022

Publisher's Note: MDPI stays neutral with regard to jurisdictional claims in published maps and institutional affiliations.



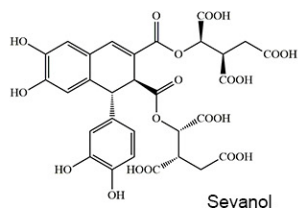
Copyright: © 2022 by the authors. Licensee MDPI, Basel, Switzerland. This article is an open access article distributed under the terms and conditions of the Creative Commons Attribution (CC BY) license (<https://creativecommons.org/licenses/by/4.0/>).

1. Introduction

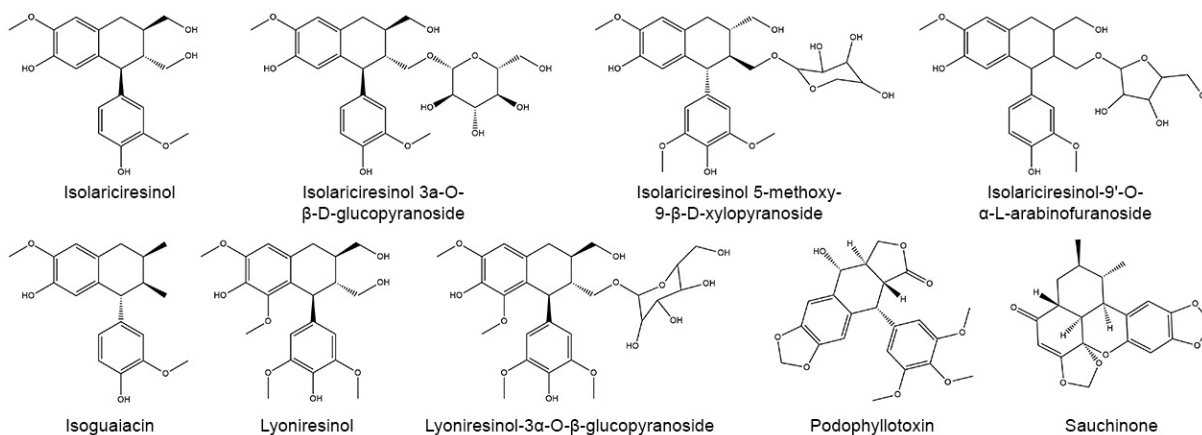
Through their vital activity, plants produce a wide range of pharmacologically active natural compounds. Phenylpropane (C₆C₃) units, provided by precursor phenylalanine and tyrosine, are found in many natural compounds, including lignans. Lignans are dimer compounds originating from cinnamic acid and its derivatives that also give rise to lignin, pre-eminent polymer component of the plant cell wall. The term “lignans” is often restricted to molecules in which two phenylpropane units are coupled at the central carbon of the side-chain (β - β' -coupling) while compounds with alternative coupling are referred to as neolignans [1]. The focus of this review is the group of lignans. Based on the patterns of cyclization and oxygen incorporation, lignans can be classified into eight subgroups: arylnaphthalenes, aryltetralins, dibenzocyclooctadienes, dibenzylbutanes, dibenzylbutyrolactones, dibenzylbutyrolactols, furans, and furofurans (Figure 1). Along with the diversity of structure, lignans exert a broad spectrum of biological activities, e.g., antitumor, antiviral, hepatoprotective, immunosuppressive, anti-platelet, and cardiovascular effects [2]. Additionally, some lignans can produce strong antioxidant and anti-inflammatory effects.

Oxidative stress is an imbalance of the oxidants/antioxidants tilting toward an oxidative status, which is characterized by a higher level of reactive oxygen species (ROS) and reactive nitrogen species (RNS) than in the normal physiological state. It could be triggered by heavy metals, xenobiotics, free radicals, drugs, and ionizing radiation. Exposure to these toxicants and oxidants impairs cellular components (e.g., lipids, proteins, and nucleic acids) and initiates the pathogenesis of diabetes mellitus, cancer, neurodegenerative, cardiovascular, lung diseases, etc. [3].

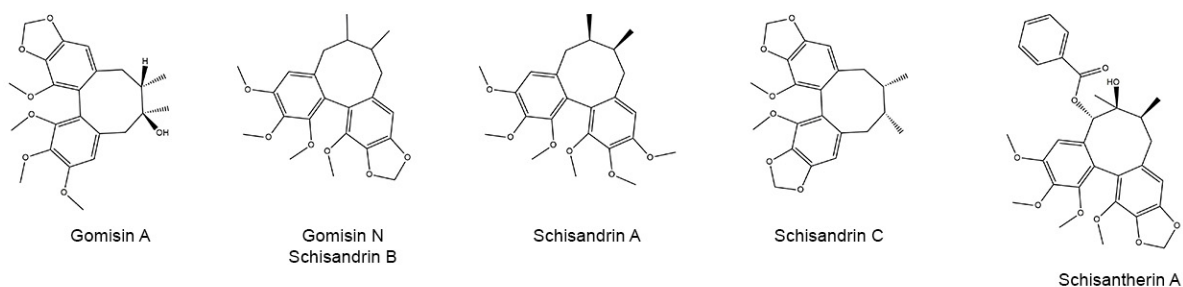
Arylnaphthalene structure group



Aryltetralin structure group



Dibenzocyclooctadiene structure group



Dibenzylbutane structure group

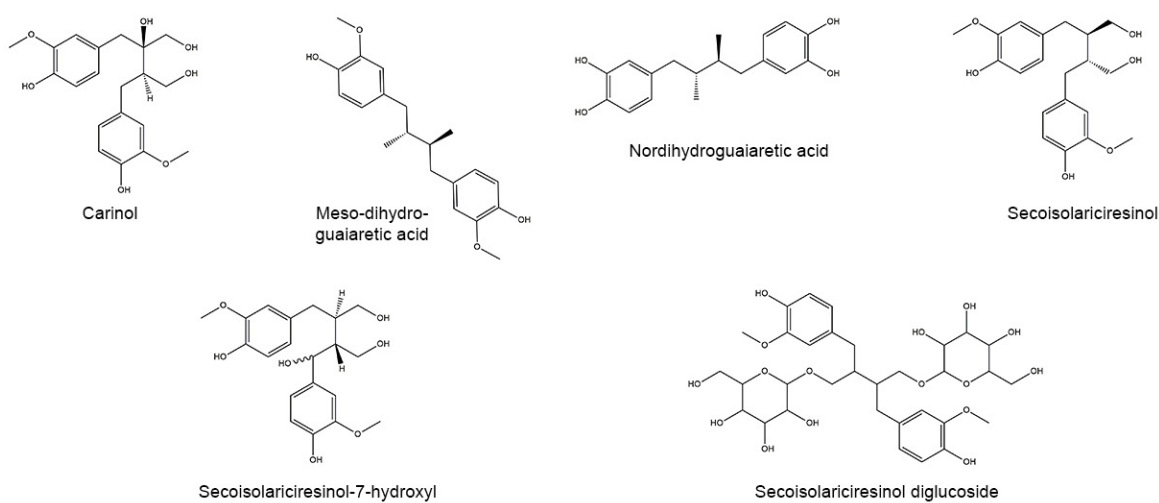


Figure 1. Cont.

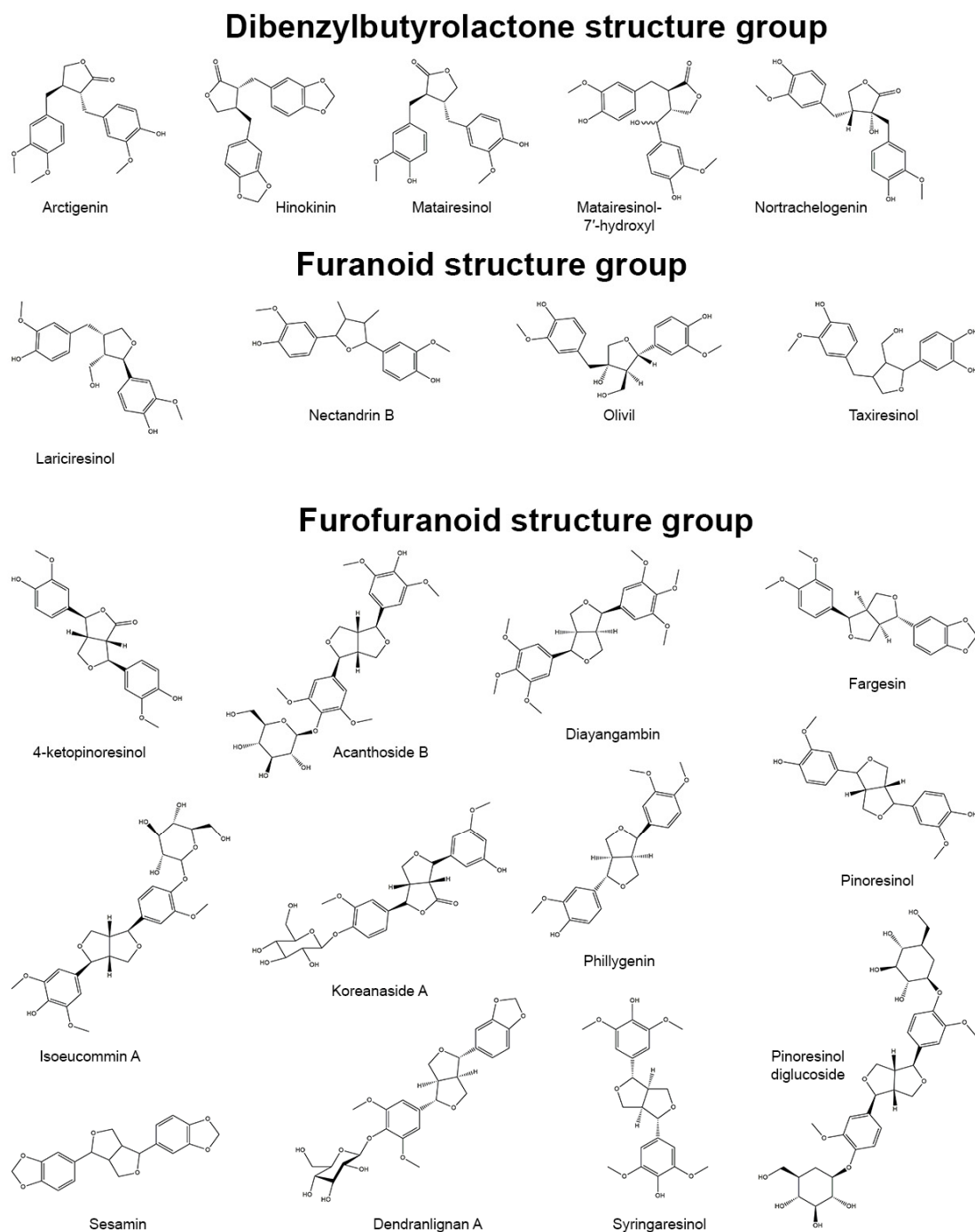


Figure 1. Representatives of plant lignans of various structural subgroups with antioxidant and anti-inflammatory properties.

Inflammation is an adaptive response induced by pathogens, tissue damage or ingestion of allergens or pollutants that includes activation of innate and adaptive immunity. This process is coordinated by a complex regulatory network of factors that fall into four functional categories: inducers, sensors, mediators, and effectors. Endogenous and exogenous inducers activate specialized sensors, e.g., toll-like receptors, inflammasome, IgE, TRP and ASIC channels, etc. They, in turn, elicit the production of specific sets of mediators (vasoactive amines, vasoactive peptides, fragments of complement components, eicosanoids, cytokines, chemokines, and proteolytic enzymes) that alter the functionality of tissues and organs (downstream effectors). Irrespective of injury or infection, long-term stress and

malfunction of tissues can also induce chronic low-level inflammation that is common to such disorders as obesity, type 2 diabetes, atherosclerosis, asthma, cancer, autoimmune and neurodegenerative diseases [4]. The pathological effect of simultaneously developing oxidative stress and inflammation is enormous and requires pharmacological measures for control.

2. Molecular Mechanisms of Inflammation and Oxidative Stress

Signals of inflammation can be divided into damage-associated molecular patterns (DAMP), which are cell-derived and initiate immunity in response to trauma and tissue damage, and pathogen-associated molecular patterns (PAMP), which are derived from microorganisms [5,6]. They stimulate protective reactions via the interaction with pattern recognition receptors with the subsequent formation of inflammasomes. Activation of the inflammasome requires two events: priming and activation. For example, the priming can include recognition of a bacterial lipopolysaccharide (LPS) by toll-like receptor 4 (TLR4) which leads to the activation of a cascade of reactions resulting in the translocation of nuclear factor kappa-light-chain-enhancer of activated B (NF- κ B) into the cell nucleus (Figure 2). Activation of NF- κ B is the general event in the inflammatory reaction of a cell and includes two main signaling pathways: canonical and non-canonical (or alternative). The main mechanism of the canonical activation of NF- κ B is the induced degradation of the NF- κ B-I κ B complex triggered by site-specific phosphorylation by I κ B kinase (IKK) [7]. The inhibitory subunit I κ B α then leaves the complex and, via ubiquitinylation, is degraded in the proteasome [8]. Non-canonical activation of NF- κ B does not involve I κ B α degradation, but depends on the processing of NF- κ B2 precursor protein, called p100, by NF- κ B-inducing kinase (NIK), which activates and functionally interacts with IKK. The processing of p100 with the degradation of its C-terminal I κ B-like structure leads to the formation of a mature NF- κ B2 p52 and the nuclear translocation of this non-canonical NF- κ B complex into the nucleus [9]. Canonical or alternatively activated NF- κ B in the nucleus promotes the transcription of NF- κ B-dependent genes, such as the NLR family pyrin domain containing 3 (NLRP3), pro-IL-1 β and pro-IL-18, which are necessary for the activation of the inflammasome. Mitochondrial damage, as well as plasma membrane damage and K⁺ efflux, are also considered upstream mechanisms that regulate inflammasome activation [10]. Finally, activated inflammasome produces inflammatory mediators for excretion, which includes the maturation of pro-inflammatory cytokines such as interleukin-1-beta (IL-1 β), IL-6, and tumor necrosis factor-alpha (TNF- α) by caspase-1.

Nuclear factor erythroid-related factor 2 (Nrf2) is a redox-sensitive transcription factor that plays an essential role in the protection against oxidative stress and electrophilic injury by regulating a battery of cytoprotective genes. Under basal conditions, Nrf2 binds to its repressor Kelch-like ECH-associated protein 1 (Keap1) and is maintained at a low level in the cytosol through Keap1-mediated ubiquitinylation and 26S proteasome-mediated degradation. The activation of the Nrf2-mediated defensive response is an effective means of counteracting exogenous oxidative insults. Electrophilic and oxidative stressors, such as ROS, can activate Nrf2 promoting its dissociation from Keap1 or phosphorylation by several kinases, including advanced protein kinase B (Akt), extracellular signal-regulated kinase (ERK), p38 mitogen-activated protein kinase (p38 MAPK), and protein kinase C (PKC). The activated Nrf2 is guided into the nucleus, forms a heterodimer with a small musculo-aponeurotic fibrosarcoma (Maf) protein, binds to specific DNA sequences called the antioxidant responsive element (ARE) consensus and subsequently initiates the transcription of downstream cytoprotective genes. These ARE-containing genes include various redox-balancing proteins and phase II enzymes, such as heme oxygenase-1 (HO-1) and NAD(P)H:quinone oxidoreductase 1 (NQO1), γ -glutamyl cysteine synthetase (γ -GCS) and glutamate-cysteine ligase (GCL), thioredoxin (Trx), thioredoxin reductase (TrxR) and peroxiredoxin (Prx) as well as glutathione (GSH)-utilizing enzymes, such as superoxide dismutase (SOD), glutathione peroxidase (GPx) and catalase (CAT), glutathione S-transferase

(GST), glutathione reductase (GR). These proteins maintain the cellular redox capacity, eliminate ROS, promote excretion of toxicants, and ensure cytoprotection [11–13].

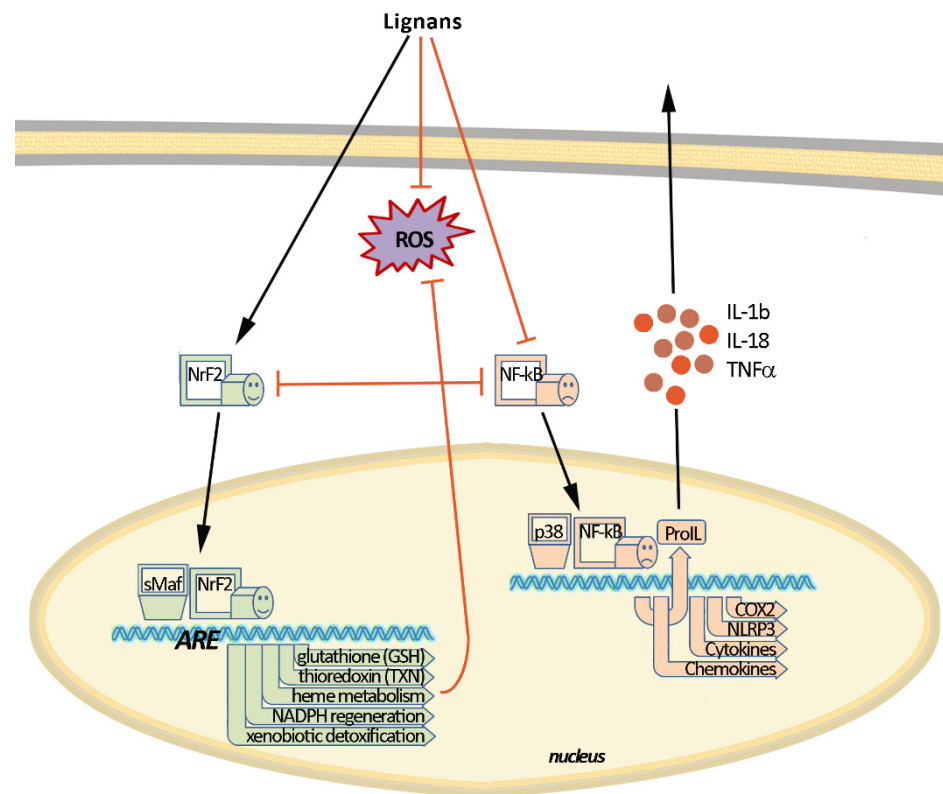


Figure 2. Molecular mechanisms of oxidative stress and inflammation and their interaction. Nuclear factor erythroid-related factor 2 (Nrf2) and nuclear factor kappa-light-chain-enhancer of activated B (NF-κB) are key factors mediating the antioxidant and anti-inflammatory effects of lignans.

The inflammation and ROS protection cascades regulate each other in several ways (Figure 2). For example, the Nrf2 transcription factor has been shown to negatively control the NF-κB signaling pathway through various mechanisms. First, Nrf2 inhibits the oxidative stress-mediated activation of NF-κB by reducing intracellular ROS levels [14]. The activation of Nrf2 has also been reported to inhibit the LPS-induced production of pro-inflammatory cytokines, including IL-6 and IL-1β, through an ROS-independent mechanism. This was due to the negative regulation of NF-κB-mediated transcription of pro-inflammatory cytokine genes and genes involved in the inflammasome assembly, such as NLRP3 and caspase 1 [15]. In addition, Nrf2 prevents IκB-α from degradation, thereby inhibiting the nuclear translocation of NF-κB [16]. NF-κB, in turn, prevents transcriptional co-activators from binding to Nrf2 and subsequent ARE transcription [17]. It was also found that GSH suppresses the activation of p38, as well as the expression of cyclooxygenase-2 (COX-2) in peritoneal macrophages of rats exposed to LPS stimulation [18], which shows that the content of GSH can strongly affect the activity and function of molecular and cellular mediators of inflammatory processes.

The mitochondrial status also plays an important role in the regulation of both inflammatory and oxidative stress processes. The degradation of mitochondria through the Bax/Bak pathway leads to an increase in intracellular ROS, oxidized lipids and mtDNA, which provokes the formation of the inflammasome and NF-κB-mediated inflammatory response. Mitochondrial biogenesis, as well as glucose transport and fatty acid oxidation, is improved by the transcription factor PGC-1α. The increase in both AMP/ATP and NAD⁺/NADH ratio triggers PGC-1α activation through its AMPK-mediated phosphorylation and SIRT1-mediated deacetylation [19,20]. PGC-1α can also activate Nrf2 by inhibiting the GSK3β regulator, which prevents the translocation of Nrf2 into the nucleus by phospho-

rylation. Under oxidative stress, GSK3 β is inactivated by p38, which is positively regulated by PGC-1 α , and, as a consequence, the antioxidant defense gets activated by Nrf2 [21].

p53 is another protein whose activity depends on the levels of ROS/RNS in oxidative stress conditions. p53 acts as a metabolic regulator or even an apoptosis inducer [22]. AMPK and p38 MAPK can phosphorylate p53 and induce its interaction with PGC-1 α to enhance Nrf2 response and reduce the effects of ROS/RNS [23].

3. Lignans with Antioxidant and Anti-Inflammatory Action

As shown in Figure 2, the response to ROS and RNS is unidirectional with the anti-inflammatory response. The antioxidant and anti-inflammatory effects of lignans measured in models have been summarized by us in separate tables for a better understanding. The antioxidant effects measured in vitro and ex vivo/in vivo are presented in Tables 1 and 2, respectively. Data on anti-inflammatory action obtained in experiments in vitro and ex vivo/in vivo are presented in Tables 3 and 4, respectively.

Table 1. Antioxidant activity of lignans in vitro.

Lignan	Source	Model/Assay	Target	Concentration	Ref.
Aryltetralinstructure group					
(–)-Isoguaiacin	<i>Machilusthunbergii</i> Sieb, et Zucc.	CCl ₄ -induced hepatotoxicity	↓GPT level	50–100 μ M	[24]
			↓MDA content, ↑GSH/GSSG level, ↑SOD1, ↑CAT	50 μ M	
(+)–Isolariciresinol	Riesling wine	TEAC assay	radical scavenging capacity	2.5 mmol Trolox/mmol	[25]
	<i>Ephedra viridis</i>	DCFH assay in HL-60 cells	↓iROS level	IC ₅₀ 21 μ g/mL	[26]
	<i>Euterpe oleracea</i> Mart.	HO assay	HO \bullet scavenging	IC ₅₀ 0.68 \pm 0.02 μ g/mL	[27]
DPPH assay		DPPH radical scavenging	IC ₅₀ 37.4 \pm 0.9 μ g/mL		
(\pm)–Isolariciresinol	Synthetic	DPPH assay	DPPH radical scavenging	IC ₅₀ 53.0 μ M	[28]
(–)-Isolariciresinol 5-methoxy-9- β -D- xylopyranoside	<i>Saracaasoca</i> (Roxb.) De Wilde	DPPH assay	DPPH radical scavenging	IC ₅₀ 44 μ M	[29]
(+)–Isolariciresinol 3a-O- β -D- glucopyranoside	<i>Carissa spinarum</i> Linn.	DPPH assay	DPPH radical scavenging	IC ₅₀ 45.7 \pm 1.5 μ M	[30]
		FRAP assay	ferric-reducing potentiality	33 mmol Fe ²⁺ /g	
		H ₂ O ₂ -induced L02 cells cytotoxicity	↓iROS level	5 μ M	
Isolariciresinol-9'- O- α -L- arabinofuranoside	<i>Pinus massoniana</i> Lamb.	H ₂ O ₂ -induced HUVECs cytotoxicity	↑PI3K, ↑p-Akt, ↑p-Bad, ↓Bax	31.3–125 μ g/mL	[31]
Lyoniresinol	<i>Berberis vulgaris</i> Linn.	HO assay	HO \bullet scavenging	IC ₅₀ 1.4 \pm 0.12 μ g/mL	[32]
	<i>Viscum album</i> Linn.	ABTS assay	ABTS radical scavenging	10–100 μ M	[33]
		DPPH assay	DPPH radical scavenging		

Table 1. Cont.

Lignan	Source	Model/Assay	Target	Concentration	Ref.
		Glu-treated HT22 cells	↓iROS level	25 μM	
(+)-Lyoniresinol-3α-O-β-glucopyranoside	<i>Strychnosvanprukii</i>	DPPH assay	DPPH radical scavenging	IC ₅₀ 31.2 μM	[34]
Sauchinone	Synthetic	AngII-induced mesangial cells	↓iROS level	1 μM	[35]
Dibenzocyclooctadiene structure group					
Gomisin A	Synthetic	ZnPP/high glucose-injured MC3T3 E1 cells	↓iROS level, ↑SOD, ↑HO-1	1–10 μM	[36]
		HeLa cells	↑iROS level	100 μM	[37]
Gomisin N	Synthetic	ethanol-treated HepG2 cells	↓iROS level, ↑GSH/GSSG level, ↑CAT, ↑SOD, ↑GPx, ↑SIRT1/AMPK, ↓CYP2E1	50–100 μM	[38]
	<i>Schisandra chinensis</i> Baill.	CCl ₄ -treated HepG2 cells	↓TBARS level, ↓iROS level	50 μM	[39]
		LPS-stimulated RAW 264.7 macrophages	↓iROS level, ↓Keap1, ↑Nrf2, ↑HO-1	200 μM	[40]
Schisandrin A		H ₂ O ₂ -induced C2C12 cell cytotoxicity	↓iROS level, ↑AMPK, ↑Bcl-2/Bax	200 μM	[41]
	Synthetic	DON-induced cytotoxicity in HT-29 cells	↓iROS level, ↓TBARS level, ↓CAT, ↓SOD, ↓GPx, ↑Nrf2, ↑HO-1, ↑GST, ↑GSH/GSSG level	2.5–10 μM	[42]
		RANKL-induced osteoclast differentiation model	↓iROS level, ↑Nrf2, ↑HO-1, ↑CAT, ↓TRAF6, ↓Nox1	50–200 μM	[43]
			↓TBARS level	50 μM	
	<i>Schisandra chinensis</i> (Turcz.) Baill.	CCl ₄ -treated HepG2 cells	↓iROS level, ↑CYP3A4 expression and activity	10–50 μM 50 μM	[39]
Schisandrin B		PQ-induced PC12 cells cytotoxicity	↓iROS level, ↑GSH/GSSG level	15 μM	[44]
	Synthetic	solar-irradiated BJ human fibroblast	↓iROS level, ↓MMP, ↑GSH/GSSG level	25–75 μM	[45]
		intact lymphocytes	↑iROS level, ↓GSH/GSSG level, ↑Nrf2, ↑HO-1, ↑TR, ↑GCLC	25–50 μM	[46]

Table 1. Cont.

Lignan	Source	Model/Assay	Target	Concentration	Ref.	
		H ₂ O ₂ -induced PC12 cells cytotoxicity	↓iROS level, ↓MDA content, ↑SOD	2.5–10 μM	[47]	
			↑Bcl-2/Bax, ↑p-Akt/Akt	10 μM		
		CsA-induced cytotoxicity in HK-2 cells	↓iROS level, ↑GSH/GSSG level, ↑Nrf2, ↑HO-1, ↑NQO1, ↑GCLM ↑Bcl-2/Bax	2.5–10 μM	[48]	
		tBHP-induced HaCaT cell injury	↓iROS level, ↑Nrf2, ↑HO-1, ↑SOD, ↑GPx, ↑CAT, ↑p-AMPK, ↑p-Akt, ↑p-Erk1/2, ↑p-JNK, ↑p-p38	2.5–10 μM	[49]	
		H/R-induced H9c2 cell injury	↓iROS level, ↑SOD, ↑GPx, ↑Nrf2, ↑NQO-1, ↑HO-1, ↓Keap1, ↑AMPK	20 μM	[50,51]	
Schisandrin C	Synthetic	solar-irradiated BJ human fibroblast	↓iROS level, ↓MMP, ↑GSH/GSSG level	25–75 μM	[45]	
		LPS-stimulated HDPCs	↓iROS level, ↑SOD ↑HO-1, ↑PGC-1α, ↑Nrf2, ↑p-Akt	10–20 μM	[52]	
Schisantherin A	<i>Schisandra chinensis</i> (Turcz.) Baill.	CCl ₄ -treated HepG2 cells	↓TBARS level	50 μM	[39]	
			↓iROS level	2–50 μM		
	<i>Schisandra sphenanthera</i>	H/R-induced HK-2 cells	↓iROS level, ↑SOD, ↑MDA content ↑Bcl2/Bax, ↑PI3K/AKT	5–20 μM	[53]	
			LPS-stimulated BV-2 microglial cells	↓iROS level, ↑HO-1, ↑NQO-1	2.5–50 μM	[54]
				↑Nrf2	50 μM	
Synthetic	LPS-stimulated NRK-52E cells	↑γGCS, ↑Nrf2	25–50 μM	[55]		
Dibenzylbutane structure group						
(–)-Carinol	Synthetic	DPPH assay	DPPH radical scavenging	IC ₅₀ 20.2 μM	[56]	
			DPPH radical scavenging	IC ₅₀ 4.4 μg/mL	[57]	
			↓xanthine oxidase enzyme	IC ₅₀ 219.4 μg/mL		
Meso-dihydroguaiaretic acid	<i>Machilusthunbergii</i> Sieb, et Zucc.	CCl ₄ -induced hepatotoxicity	↓GPT level	10–100 μM	[24]	
			↓MDA content, ↑GSH/GSSG level, ↑SOD1, ↑CAT	50 μM		

Table 1. Cont.

Lignan	Source	Model/Assay	Target	Concentration	Ref.
<i>Machilus philippinensis</i> Merr.		fMLF-activated human neutrophils	↓O ₂ ^{•-} level	IC ₅₀ 0.78 ± 0.17 μM	[58]
			↓iROS level	IC ₅₀ 0.79 ± 0.26 μM	
			↓p-ERK, ↓p-JNK, ↓p-Akt	10 μM	
		MMK-1-activated human neutrophils	↓O ₂ ^{•-} level	IC ₅₀ 1.17 ± 0.64 μM	
		PMA-activated human neutrophils	↓iROS level	IC ₅₀ 3.57 ± 3.93 μM	
		ABTS assay	ABTS radical scavenging	1–10 μM	
		DPPH assay	DPPH radical scavenging		
		ORAC assay	ROS scavenging		
XOD assay	superoxide anion scavenging				
<i>Larrea tridentate</i>		DCFH assay in HL-60 cells	↓iROS level	IC ₅₀ 0.7 μg/mL	[59]
		FL5.12 cells	↑p-ERK1/2, ↑p-JNK, ↑p-p38	20 μM	[60]
		HOCl assay	hypochlorous acid scavenging	IC ₅₀ 622 ± 42 μM	[61]
		O ₂ ^{•-} assay	superoxide anion scavenging	IC ₅₀ 15 ± 1 μM	
		OH assay	OH radical scavenging	IC ₅₀ 0.15 ± 0.02 μM	
		¹ O ₂ assay	singlet oxygen scavenging	IC ₅₀ 151 ± 20 μM	
		ONOO assay	ONOO anion scavenging	IC ₅₀ 4 ± 0.94 μM	
		H ₂ O ₂ /3-NP- induced CGNs neurotoxicity	↑Nrf2, ↑HO-1	20 μM	
Nordihydroguaiaretic acid	Synthetic	OH assay	OH radical scavenging	10 μM	[63]
		TPA-treated mouse model	↑GPx, ↑GR, ↑GST, ↑GSH/GSSG level, ↑SOD, ↑CAT	15–25 μM	[64]
		H ₂ O ₂ -induced LLC-PK1/MEFs cells cytotoxicity	↓iROS level, ↑Nrf2, ↑HO-1 ↑p-Akt, ↑p-ERK1/2, ↑p-p38, ↑p-JNK, ↑p-GSK-3	15 μM	[65]
		IAA/H ₂ O ₂ - induced cytotoxicity in MN and THP-1 cells	↓iROS level, ↑GSH/GSSG level ↑CD33	20 μM	[66]
		Daoy cells	↑GSH/GSSG level	75 μM	[67]

Table 1. Cont.

Lignan	Source	Model/Assay	Target	Concentration	Ref.
(–)- Secoisolariciresinol	<i>Taxus yunnanensis</i>	DPPH assay	DPPH radical scavenging	IC ₅₀ 28.9 μM	[68]
	<i>Araucaria angustifolia</i>	rat liver microsomes	↓lipid peroxidation activity	IC ₅₀ 0.1–0.15 μM	[69]
		O ₂ ^{•−} assay	superoxide anion scavenging	IC ₅₀ 4.8 nM	
	<i>Piceaabies</i>	ROO assay	peroxyl radicals scavenging	SF 3.1–4.0 mole/mole	[70]
		DPPH assay	DPPH radical scavenging	IC ₅₀ 9.0 ± 1.0 μM	
		<i>Linum usitatissimum</i> Linn.	L-α-phosphatidylcholine liposome/pBR322 plasmid DNA	AAPH radical scavenging DPPH radical scavenging	
	<i>Carissa spinarum</i> Linn.	DPPH assay	DPPH radical scavenging	IC ₅₀ 26.2 μM	[56]
Secoisolariciresinol-7-hydroxyl	<i>Piceaabies</i>	DPPH assay	DPPH radical scavenging	IC ₅₀ 12.7 ± 1.5 μM	[70]
	<i>Linum usitatissimum</i> Linn.	L-α-phosphatidylcholine liposome/pBR322 plasmid DNA	AAPH radical scavenging DPPH radical scavenging	10–100 μM 25–200 μM	[71]
		Synthetic	DPPH assay	DPPH radical scavenging	
Secoisolariciresinol diglucoside	<i>Linum usitatissimum</i> Linn.	iron treated H9c2 cells	↓iROS level, ↑SOD, ↑Bcl-2/Bax ↓MMP-2, ↓MMP-9, ↓FOXO3a, ↓p70S6K1, ↑AMPK	500 μM	[73]
		asbestos-exposed MFs	↓iROS level, ↓MDA content, ↓8-isoP, ↑Nrf2, ↑NQO-1, ↑HO-1, ↑GST, ↑TR, ↓nitrate/nitrite ratio	50–100 μM	
	Synthetic (LGM2605)	LPS-stimulated AC16 cells	↓iROS level	50 μM	[76]
	Dibenzylbutyrolactone structure group				
Arctigenin	Synthetic	glutamate-treated rat cortical cells	↓iROS level	IC ₅₀ 33.2 μM	[77]
		LPS-treated Raw264.7 cells	↓iROS level	5–50 μM	[78]
	<i>Arctium lappa</i> Linn.	glucose-starved A549 cells	↓iROS level	10 μM	[79]
		H ₂ O ₂ -treated L6 cells	↑Nrf2, ↑SOD, ↑GR, ↑GPx, ↑Trx1, ↑UCP2, ↑p-AMPK, ↑p-p53, ↑p21, ↑PGC-1α, ↑PPARα	1–20 μM	[80]

Table 1. Cont.

Lignan	Source	Model/Assay	Target	Concentration	Ref.	
	Synthetic	MDA-MB-231 cells	↑iROS level, ↓GSH/GSSG level, ↑Nox, ↑p-p38, ↑p-ATF-2, ↓Bcl-2	5 µM	[81]	
		H ₂ O ₂ -treated astrocytes	↓iROS level	10–20 µM	[82]	
		intact astrocytes	↑HO-1, ↑Nrf2, ↑c-Jun, ↑p-Akt			
			TGF-β1-induced HK-2 cells	↓iROS level, ↓Nox ↓p-Akt, ↓p-ERK1/2, ↓p-IκBα	0.5–1 µM	[83]
	<i>Arctium lappa</i> Linn.		DPPH assay	DPPH radical scavenging	IC ₅₀ 31.47 ± 2.33 µM	[84]
			H2DCF-DA assay	↓iROS level	10–100 µM	
	Synthetic	OA-treated WRL68 hepatocytes	↓MDA content ↑p-PI3K, ↑p-Akt, ↑p-AMPK	50 µM	[85]	
		Hep G2 cells	↑iROS level, ↓GSH/GSSG level	5–100 µM	[86]	
			↑p-p38, ↑p-JNK	20 µM		
			OGD-injured H9c2 cardiomyocytes	↓iROS level, ↓MDA content, ↑SOD ↑AMPK/SIRT1	50–200 µM	[87]
			silica-injured RAW 264.7 macrophages	↓iROS level	1 µM	[88]
Hinokinin	Synthetic	antioxidant assay	inhibition of H ₂ O ₂ produced by Trypanosoma cruzi mitochondria	IC ₅₀ 17.84 µM	[89]	
Matairesinol	<i>Cedrus deodara</i>	DPPH assay	DPPH radical scavenging	IC ₅₀ 33.24 ± 0.47 µM	[90]	
		rat liver microsomes	↓lipid peroxidation activity	IC ₅₀ 0.28 µM		
	<i>Piceaabies</i>	O ₂ ^{•-} assay	superoxide anion scavenging	IC ₅₀ 40 nM	[69]	
		ROO assay	peroxyl radicals scavenging	SF 1.0 mole/mole		
			DPPH assay	DPPH radical scavenging	IC ₅₀ 14.0 ± 0.0 µM	[70]
	<i>Arctium lappa</i>	DPPH assay	DPPH radical scavenging	IC ₅₀ 14.95 ± 0.38 µM	[84]	
		H2DCF-DA assay	↓iROS level	100 µM		
	Synthetic	DPPH assay	DPPH radical scavenging	20 µM	[91]	
O ₂ ^{•-} assay		superoxide anion scavenging				

Table 1. Cont.

Lignan	Source	Model/Assay	Target	Concentration	Ref.
		hypoxia-induced HeLa cells	↓miROS levels ↓HIF-1 α , ↓VEGF	10–50 μ M	[92]
		LPS-stimulated NSC-34 neurons and BV2 microglia	↓MDA content, ↑SOD, ↑CAT, ↑GPx, ↑Nrf2, ↑HO-1, ↑AMPK	5–20 μ M	[93]
Matairesinol-7'-hydroxyl	<i>Piceaabies</i>	rat liver microsomes	↓lipid peroxidation activity	IC ₅₀ 0.15–0.18 μ M	
		O ₂ ^{•-} assay	superoxide anion scavenging	IC ₅₀ 217 nM	[69]
		ROO assay	peroxyl radicals scavenging	SF 2.1–2.7 mole/mole	
		DPPH assay	DPPH radical scavenging	IC ₅₀ 15.7 \pm 0.6 μ M	[70]
		DPPH assay	DPPH radical scavenging	IC ₅₀ 20.0 \pm 0.1 μ M	[94]
(+)-Nortrachelogenin	<i>Wikstroemia indica</i>	DPPH assay	DPPH radical scavenging	IC ₅₀ 90.1 μ M	[95]
(–)-Nortrachelogenin	<i>Cedrus deodara</i>	DPPH assay	DPPH radical scavenging	IC ₅₀ 36.79 \pm 1.69 μ M	[90]
	<i>Pinus contorta</i>	rat liver microsomes	↓lipid peroxidation activity	IC ₅₀ 0.14–0.19 μ M	
		O ₂ ^{•-} assay	superoxide anion scavenging	IC ₅₀ 1.4 nM	[69]
	<i>Piceaabies</i>	ROO assay	peroxyl radicals scavenging	SF 2.0–2.2 mole/mole	
		DPPH assay	DPPH radical scavenging	IC ₅₀ 17.7 \pm 1.5 μ M	[70]
		<i>Carissa carandas</i> Linn.	DPPH assay	DPPH radical scavenging	IC ₅₀ 30.2 μ M
	<i>Carissa spinarum</i> Linn.	DPPH assay	DPPH radical scavenging	IC ₅₀ 35.8 μ M	[56]
<i>Galactites elegans</i>	DPPH assay	DPPH radical scavenging	IC ₅₀ 38.6 \pm 2.7 μ M		
	BHP-treated Jurkat cells	peroxyl radicals scavenging	50 μ M	[97]	
Furanoid structure group					
(+)–Lariciresinol	<i>Abies balsamea</i>	rat liver microsomes	↓lipid peroxidation activity	IC ₅₀ 0.17–0.35 μ M	
		O ₂ ^{•-} assay	superoxide anion scavenging	IC ₅₀ 35 nM	[69]
		ROO assay	peroxyl radicals scavenging	SF 1.0–2.6 mole/mole	
	<i>Hemerocallis fulva</i>	LUVs assay	↓lipid peroxidation activity	50 μ g/mL	[98]
	<i>Piceaabies</i>	DPPH assay	DPPH radical scavenging	IC ₅₀ 10.7 \pm 1.2 μ M	[70]

Table 1. Cont.

Lignan	Source	Model/Assay	Target	Concentration	Ref.	
	<i>Ephedra viridis</i>	DCFH assay in HL-60 cells	↓iROS level	IC ₅₀ 17.7 µg/mL	[26]	
	<i>Euterpe oleracea</i> Mart.	HO assay	HO• scavenging	IC ₅₀ 0.70 ± 0.13 µg/mL	[27]	
		DPPH assay	DPPH radical scavenging	IC ₅₀ 22.4 ± 3.0 µg/mL		
		ABTS assay	ABTS radical scavenging	12.5–50 µM	[99]	
		DPPH assay	DPPH radical scavenging			
		HO assay	HO• scavenging	1.5–6 µM		
		ORAC assay	↓ROO•-induced oxidation			
	<i>Rubia philippinensis</i>	CUPRAC assay	cupric-reducing potentiality	6.25–50 µM	[99]	
		FRAP assay	ferric-reducing potentiality			
		AAPH-treated RAW 264.7 cells	↓iROS level	12.5–50 µM		
		RAW 264.7 cells	↑Nrf2, ↑SOD1, ↑CAT, ↑GPx, ↑HO-1, ↑NQO1, ↑GCLc, ↑GCLm, ↑p-p38, ↑p-ERK1/2			
	Nectandrin B	DPPH assay	DPPH radical scavenging	5–50 µg/mL	[100]	
		old HDFs	↓p-AMPK, ↑p-PI3K, ↑p-Akt, ↓p-ERK1/2, ↓p-p38	10–20 µg/mL		
		H ₂ O ₂ /palmitic acid-treated old HDFs	↓iROS level, ↑SOD1,2			
(–)-Olivil	<i>Carissa spinarum</i> Linn.	DPPH assay	DPPH radical scavenging	IC ₅₀ 18.1 µM	[56]	
Taxiresinol	<i>Taxus yunnanensis</i>	DPPH assay	DPPH radical scavenging	IC ₅₀ 18.4 µM	[68]	
Furofuranoid structure group						
	4-ketopinoresinol	DPPH assay	DPPH radical scavenging	IC ₅₀ 52.7 ± 4.6 µg/mL	[101]	
		H ₂ O ₂ -induced HSC-3 cell cytotoxicity		↓iROS level	12.5–50 µM	[102]
				↑GSH/GSSG level	50 µM	
				↑Nrf2	6.25–50 µM	
				↑HO-1, ↑AKR1C1-3, ↑ABCC2, ↑GR, ↑GCLC, ↑GCLM, ↑TR, ↑ABCC5, ↑PI3K/Akt	25 µM	
	<i>Coixlachryma-jobi</i> Linn. var. <i>ma-yuen</i> Stapf					

Table 1. Cont.

Lignan	Source	Model/Assay	Target	Concentration	Ref.
	<i>Galactites elegans</i>	DPPH assay	DPPH radical scavenging	IC ₅₀ 143.3 ± 13.1 µM	[97]
		BHP-treated Jurkat cells	peroxyl radicals scavenging	50 µM	
Dendranlignan A	<i>Dendranthema morifolium</i> (Ramat.)	LPS-induced H9c2 cells	↓iROS level	10 µM	[103]
Isoeucommin A	<i>Eucommia ulmoides</i> Oliv.	high-glucose-stimulated HRMCs	↓MDA content, ↑SOD, ↑p-GSK-3β, ↑Nrf2, ↑HO-1	62.5–125 µM	[104]
Koreanaside A	<i>Forsythia koreana</i>	ORAC assay	↓ROO•-induced oxidation	25 µg/mL	[105]
		MOVAS cells	↓VCAM-1		
Pinoresinol	<i>Forsythia suspensa</i> (Thunb.)	Cu ²⁺ -induced LDL lipid peroxidation	↓lipid peroxidation activity	IC ₅₀ 1.39 µM	[106]
	<i>Eucalyptus globulus</i> Labill	rat liver microsomes	↓lipid peroxidation activity	IC ₅₀ 7.9 µg/mL	[107]
	<i>Piceaabies</i>	DPPH assay	DPPH radical scavenging	IC ₅₀ 17.7 ± 0.6 µM	[70]
	<i>Euterpe oleracea</i> Mart.	DPPH assay	DPPH radical scavenging	IC ₅₀ 34.7 ± 5.0 µg/mL	[27]
		HO assay	HO• scavenging	IC ₅₀ 1.8 ± 0.2 µg/mL	
	<i>Carissa spinarum</i> Linn.	DPPH assay	DPPH radical scavenging	IC ₅₀ 43.4 µM	[56]
	<i>Forsythia koreana</i>	ORAC assay	↓ROO•-induced oxidation	25 µg/mL	[105]
	<i>Galactites elegans</i>	DPPH assay	DPPH radical scavenging	IC ₅₀ 50.8 ± 3.1 µM	[97]
Cinnamon	intact Beas-2B cells		↑Nrf2, ↑NQO1, ↑γ-GCS	25 µM	[108]
		As(III)-induced Beas-2B cells injury	↓iROS level, ↑GSH/GSSG level		
Pinoresinol diglucoside	<i>Eucommia ulmoides</i>	oxLDL-induced HUVECs cytotoxicity	↓iROS level, ↓MDA content, ↑SOD	1 µM	[109]
Sesamin	<i>Sesamum indicum</i> Linn.	oxLDL-induced HUVECs cytotoxicity	↓iROS level, ↑SOD1, ↑Bcl-2/Bax level	12.5–100 µM	[110]
	Synthetic	KA-induced PC12 and BV-2 cells	↓iROS level, ↓MDA content	0.1–2 µM	[111]
	<i>Sesamum indicum</i> Linn.	dexamethasone-treated osteoblasts	↓iROS level, ↑Bcl-2/Bax, ↑p-Akt	5–20 µM	[112]

Table 1. Cont.

Lignan	Source	Model/Assay	Target	Concentration	Ref.
		H ₂ O ₂ -induced Caco-2 cell cytotoxicity	↓iROS, ↑GSH/GSSG level, ↓MDA content, ↑SOD, ↑Nrf2, ↓Keap1, ↑HO-1, ↑NQO1, ↑GCLC, ↑GCLM, ↑GR, ↑p-AKT, ↑p-ERK1/2	20–80 µM	[113]
		H ₂ O ₂ -induced SH-SY5Y cell cytotoxicity	↓iROS level, ↑SOD2, ↑CAT ↑FoxO3a, ↑SIRT1, ↑SIRT3	1 µM	[114]
	<i>Coixlachryma-jobi</i> Linn. var. <i>ma-yuen</i> Stapf	DPPH assay	DPPH radical scavenging	IC ₅₀ 24.6 ± 3.1 µg/mL	[101]
	<i>Euterpe oleracea</i> Mart.	DPPH assay	DPPH radical scavenging	IC ₅₀ 29.7 ± 2.0 µg/mL	[27]
		HO assay	HO• scavenging	IC ₅₀ 0.40 ± 0.13 µg/mL	
Syringaresinol	<i>Panax ginseng</i> C.A. Meyer	H/R-induced H9c2 cells	↓iROS level, ↑MnSOD, ↑CAT, ↑LC3, ↑Bcl-2/Bax, ↓HIF-1, ↑FoxO3a, ↓BNIP3, ↓cCYC, ↑mCYC	25 µM	[115]
	<i>Sargentodoxa cuneata</i>	high glucose-injured NRVMs	↑Nrf2, ↑NQO-1, ↑HO-1, ↓Keap1, ↑SOD, ↑Bcl-2/Bax	50–100 µM	[116]

3-NP, 3-nitropropionic acid; 8-isoP, 8-iso prostaglandin F2 α ; γ -GCS, γ -glutamyl cysteine synthetase; AAPH assay, 2,20-azo-bis(2-amidinopropane) dihydrochloride radical-scavenging method; ABCC, ATP-dependent drug efflux pumps (ATP-binding cassette), subfamily C (CFTR/MRP) members; ABTS assay, 2,2'-azino-bis(3-ethylbenzothiazoline)-6-sulfonic acid radical-scavenging method; AC16 cells, human ventricular cardiomyocyte-derived cell line; AKR1C1-3, aldo-keto reductase 1 subunits C-1-3; AKT, protein kinase B; AMPK, AMP-activated protein kinase; ATF-2, activator protein 1 (AP-1) transcription factor; BNIP3, Bcl-2 interacting protein 3; BV-2 cells, murine microglial cell line; CAT, catalase; CD33, myeloid cell-specific type 1 transmembrane glycoprotein; CsA, cyclosporine A; CUPRAC assay, cupric-reducing antioxidant capacity method; CYC c/m, cytochrom c in the cytosolic/mitochondrial fraction; CYP, cytochrome P450; DCFH-DA assay, 2',7'-dichlorofluorescein diacetate radical-scavenging method; DON, trichothecene toxin deoxynivalenol; DPPH assay, 1,1-diphenyl-2-picrylhydrazyl radical-scavenging method; ERK, extracellular signal-regulated kinase; fMLE, N-Formyl-Met-Leu-Phe; Fox, class O forkhead/winged helix transcription factor; FRAP assay, ferric reducing antioxidant power method; GCLC/M, γ -glutamylcysteine synthetase catalytic/modifier subunit; GPT level, serum glutamic pyruvic transaminase content; GPx, glutathione peroxidase; GR, glutathione reductase; GSH/GSSG level, ratio of reduced glutathione with oxidized glutathione; GSK-3, glycogen synthase kinase-3; GST, glutathione-S-transferase; H2DCF-DA assay, 2,7-dichlorodihydrofluorescein-diacetate; H9c2 cells, embryonic rat heart derived cell line; HDF, human diploid fibroblast; HDPCs, human dental pulp cells; HIF-1, hypoxia induction factor 1; HK-2, human renal tubular epithelial cells; HO-1, heme oxygenase-1; HO assay, hydroxyl radical scavenging method; H/R, hypoxia/reoxygenation; HRMCs, human renal mesangial cells; HUVECs, human umbilical vein endothelial cells; IAA, iodoacetate; I κ B α , inhibitor of κ B; JNK, c-Jun N-terminal kinase; KA, kainic acid; Keap1, kelch-like ECH-associated protein 1; LC3, microtubule-associated proteins 1A/1B light chain 3B; LPS, lipopolysaccharide; LUVs assay, inhibition of the oxidation of large unilamellar vesicles method; MDA, malondialdehyde; MDA-MB-231, ER-negative breast adenocarcinoma cells; MEFs, mouse embryo fibroblasts; MMK-1, Leu-Glu-Ser-Ile-Phe-Arg-Ser-Leu-Leu-Phe-Arg-Val-Met; MMP, matrix metalloproteinase; MnSOD, manganese superoxide dismutase; MOVAS, mouse vascular smooth muscle cell line; Nox, NADPH oxidase; NQO1, NADPH quinone acceptor oxidoreductase 1; Nrf2, nuclear transcription factor-erythroid 2 related factor; NRVMs, neonatal rat ventricular myocytes; OA, oleic acid; OGD, oxygen glucose deprivation; ORAC, oxygen radical absorbance capacity; ORAC antioxidant assay, inhibition of peroxy-radical-induced oxidation initiation by thermal decomposition of AAPH; oxLDL, oxidized low-density lipoprotein; p70S6K1, p70S6 Kinase 1; PC12 cells, rat pheochromocytoma cell line; PGC-1 α , peroxisome proliferator-activated receptor gamma coactivator 1-alpha; PI3K/AKT pathway, phosphatidylinositol 3-kinase/protein kinase B signaling; PMA, phorbol 12-myristate 13-acetate; POX, peroxidase; PPAR, peroxisome proliferator-activated receptor; PRDX3, peroxiredoxin 3; RANKL, receptor activator of NF- κ B ligand; ROO assay, peroxy radicals scavenging method; iROS, intracellular reactive oxygen species; SF, stoichiometric factor (moles

peroxyl radicals scavenged per mole of compound); SH-SY5Y, human neuroblastoma cell line; SIRT1, NAD-dependent deacetylase sirtuin-1; SOD, superoxide dismutase; SOD1, cytoplasmic copper/zinc superoxide dismutase; SOD assay, superoxide radical scavenging method; TBARS, thiobarbituric acid reactive substance; tBHP, tert-butylhydroperoxide; TEAC assay, Trolox equivalent antioxidant capacity test; TPA, 12-O-tetradecanoylphorbol-13-acetate; TR, thioredoxin reductase; TRAF6, TNF receptor associated factor 6; Trolox, 6-hydroxy-2,5,7,8-tetramethylchroman-2-carboxylic acid; Trx1, thioredoxin 1; UCP2, uncoupling protein 2; VEGF, vascular endothelial cell growth factor; XOD, xanthine oxidase; ZnPP, zinc protoporphyrin IX. Downward-pointing red arrows reflect the downregulatory action, upward-pointing green arrows reflect the upregulatory action.

3.1. Arylnaphthalene Skeletons

Sevanol

Sevanol, found in thyme of only one species *Thymus armeniacus* [117], was shown to possess acid-sensing ion channel (ASIC) inhibitory activity and a strong anti-inflammatory effect. Sevanol in vitro dose-dependently inhibited human and rat ASIC3 channels and, although with less efficiency, rat ASIC1a channels, heterologously expressed in oocytes of *Xenopus laevis*. In the model of neuronal-like cells, differentiated from the SH-SY5Y cell line by retinoic acid, sevanol showed an inhibitory effect on native human ASIC1a [118]. In Complete Freund's Adjuvant (CFA)-induced thermal hyperalgesia test in vivo, sevanol showed an anti-inflammatory effect by significantly increasing the withdrawal latency on a hot plate and reducing edema of the inflamed hind paw [119–121]. It is intriguing that oral administration provides a more pronounced anti-inflammatory and analgesic effect, which indicates the appearance of a more active metabolite during metabolism [121].

3.2. Aryltetralin Skeletons

3.2.1. Isoguaiacin

(-)-Isoguaiacin exerted diverse hepatoprotective activities by serving as a potent antioxidant. In primary cultures of rat hepatocytes injured with carbon tetrachloride (CCl₄), (-)-isoguaiacin significantly decreased the level of glutamic pyruvic transaminase (GPT), increased the level of reduced glutathione (GSH), decreased the production of malondialdehyde (MDA), a marker of lipid peroxidation, and preserved the activities of SOD, GPx and CAT [24].

3.2.2. Isolariciresinol and Isolariciresinol Glucoconjugates

Isolariciresinol exhibited potent antioxidant activities in hydroxyl radical scavenging, 2,2'-diphenyl-1-picrylhydrazyl (DPPH) radical scavenging and Trolox equivalent antioxidant capacity (TEAC) in vitro assays, and inhibited ROS generation in HL-60 cells [25–28]. Isolariciresinol-9'-O- α -L-arabinofuranoside isolated from *Pinus massoniana* Lamb. exerted protective effects against oxidative stress-induced apoptosis in human umbilical vein endothelial cells (HUVECs) via a mechanism involving the upregulation of phosphatidylinositol 3-kinase (PI3K) and phosphorylated Akt, which lead to upregulated levels of phosphorylated Bcl-2-associated agonist of cell death (p-Bad) [31]. (+)-Isolariciresinol-3 α -O- β -D-glucopyranoside extracted from *Carissa spinarum* exhibited moderate DPPH radical scavenging activity and high ferric reducing capacity (stronger than vitamin C), exerted significant hepatoprotective effects against H₂O₂-induced L02 cell injury by reducing ROS production, and also possessed a much better COX-2 inhibition activity compared with indomethacin [30]. (-)-Isolariciresinol-5-methoxy-9- β -D-xylopyranosyl showed the ability to scavenge DPPH radicals that were 1.5 times weaker than well-known antioxidant quercetin [29].

3.2.3. Lyoniresinol and Its Derivatives

Lyoniresinol together with its glycosylated analog (+)-lyoniresinol-3 α -O- β -glucopyranoside demonstrated significant capacity to scavenge DPPH radicals [33,34]. Lyoniresinol was also shown to effectively scavenge 2,2'-azino-bis(3-ethylbenzothiazoline)-6-sulfonic acid

(ABTS) and hydroxyl radicals as well as reduce the intracellular ROS (iROS) in glutamate treated HT22 cells [32,33].

3.2.4. Podophyllotoxin

Podophyllotoxin was found in plants of the genus Podophyllum, Linum, Callistris, and Juniperus. Due to its high toxicity and side effects, such as enteritis and depression of the central nervous system, the use of this compound is limited to a local antiviral agent. However, potent protective effects of podophyllotoxin formulation with rutin (G-003M) were demonstrated against radiation-induced lung injury. The formulation significantly attenuated oxidative and nitrosative stress and downregulated the expression of inflammatory and fibrogenic cytokines [122]. In another study, the efficacy of a more soluble and less toxic polyamidoamine dendrimer-conjugated podophyllotoxin was evaluated against chemically induced hepatocellular carcinoma (HCC) in mice. The administration of the drug significantly reduced histopathological changes in liver tissue and suppressed the progression of HCC by modulating the inflammatory and fibrogenic factors, which play important roles in HCC development [123].

3.2.5. Sauchinone

Sauchinone, isolated from the root of *Saururus chinensis*, exerted anti-inflammatory function in vitro by suppressing NF- κ B activity. Sauchinone was shown to dose-dependently inhibit the NF- κ B-mediated production of NO and expression of inducible nitric oxide (NO) synthase (iNOS), TNF α , and COX-2 in LPS-stimulated RAW264.7 cells [124,125] and attenuated renal inflammation by inhibiting NF- κ B/ROS pathway activation in angiotensin II (AngII)-induced human mesangial cells [35]. The lignan also showed anti-inflammatory functions in vivo in a murine model of allergen-induced airway inflammation. It suppressed neutrophil, lymphocyte, and eosinophil infiltration, and diminished pro-inflammatory cytokine production through the inhibition of GATA-3-driven T helper 2 (Th2) cell development, thereby attenuating tissue pathology [126].

Table 2. Antioxidant activity of lignans ex vivo and in vivo.

Lignan	Source	Model	Target	Dose, Road	Ref.
Dibenzocyclooctadiene structure group					
Gomisin A	<i>Schisandra chinensis</i> Baill.	CCl ₄ -induced hepatotoxicity	↓MDA content, ↑SOD	50–100 mg/kg of rat, i.p.	[127]
Gomisin N	Synthetic	ethanol-injured model	↓iROS, ↑GSH/GSSG, ↑CAT, ↑SOD, ↑GPx, ↑SIRT1/AMPK, ↓CYP2E1	5–20 mg/kg of mice, p.o.	[38]
Schisandrin A	Synthetic	ovariectomy-induced osteoporosis	↓iROS level, ↑Nrf2	100 mg/kg of mice, i.p.	[43]

Table 2. Cont.

Lignan	Source	Model	Target	Dose, Road	Ref.
Schisandrin B	<i>Schisandra chinensis</i> (Turcz.) Baill.	I/R injury model	↑GSH/GSSG level	1.2 mmol/kg of rat, e.v.p.	[128]
		CCl ₄ -induced hepatotoxicity	↑mtGSH/GSSG level, ↓mtMDA content, ↑GR, ↑GST, ↑GPx	2 mmol/kg of mice, p.o.	[129,130]
		ethanol-injured model	↓iROS, ↑GSH/GSSG level, ↑α-TOC, ↓MDA content, ↑GR, ↑GST, ↑MnSOD, ↑GPx	10 mg/kg of rat, i.g.	[131]
		Aβ-infused model	inhibition of ROO•-induced oxidation, ↑ORAC, ↑GSH/GSSG level, ↓MDA content, ↑SOD	25–50 mg/kg of rat, p.o.	[132]
	Synthetic	TSCI model	↑SOD	50 mg/kg of rat, p.o.	[133]
		I/R injury model	↓MDA content, ↑SOD	80 mg/kg of rat, p.o.	[134]
		STZ-induced diabetic model	↓iROS level, ↑Nrf2, ↑Bcl-2/Bax	20 mg/kg of mice, p.o.	[135]
		acute stress-induced anxiety	↓iROS level, ↓Keap1, ↑Nrf2, ↑SOD, ↑GSH/GSSG level	30–60 mg/kg of mice, p.o.	[136]
		pirarubicin-induced cardiotoxicity	↑SOD2, ↑CAT, ↑Bcl-2/Bax	50 mg/kg of rat, diet	[137]
	Schisandrin C	Synthetic	Ang II-induced endothelial deficit model	↓iROS level, ↑Nrf2, ↑NQO-1, ↑HO-1, ↓Keap1	10 mg/kg of mice, i.g.
Schisantherin A		Aβ-infused model	↓MDA content, ↑GSH/GSSG level, ↑SOD, ↑GPx	0.1 mg/kg of mice, i.c.v.	[139]
	<i>Schisandra chinensis</i> (Turcz.) Baill.	chronic fatigue/D-galactose-induced LMI model	↑GSH/GSSG level, ↓MDA content, ↓Keap1, ↑Nrf2, ↑HO-1, ↑SOD, ↑CAT, ↑Bcl-2/Bax	2.5–5 mg/kg of mice, i.g.	[140,141]
	Synthetic	MCAO/R-induced brain injury	↓MDA level, ↑SOD, ↑Trx, ↑PRDx, ↓NOX4	5–10 mg/kg of rat, i.g.	[142]
Dibenzylbutane structure group					

Table 2. Cont.

Lignan	Source	Model	Target	Dose, Road	Ref.
Nordihydroguaiaretic acid	Synthetic	ozone-induced lung injury	↓tyrosine nitration level	20 mg/kg of rat, Alzet osmotic pumps	[61]
		K ₂ Cr ₂ O ₇ -induced renal injury	↓NAG, ↑GPx	17 mg/kg of rat, mini-osmotic pumps	[143]
	<i>Larrea tridentata</i>	ALIOS-fed model	↑GPx4, ↑PRDx3, ↑PPARα	2.5 g/kg of mice, diet	[144]
Secoisolariciresinol diglucoside	<i>Linum usitatissimum</i> Linn.	metabolic syndrome model	↓TBARS, ↓iROS, ↑GSH/GSSG level, ↑SOD, ↑CAT, ↑GPx	20 mg/kg of rat, p.o.	[145]
	Synthetic	CCl ₄ -induced hepato- and nephrotoxicity	↓MDA content, ↑CAT, ↑SOD, ↑POX, ↓LPO	12.5–25 mg/kg of rat, p.o.	[72]
		MCT-induced heart failure	↓iROS level, ↑SOD, ↑CAT, ↑GPx	25 mg/kg of rat, p.o.	[146]
	Synthetic (LGM2605)	CLP-induced sepsis	↓iROS level	100 mg/kg of mice, i.p.	[76]
		NRC painful model	↓8-OHG	200 mg/kg of rat, s.c.	[147]
	<i>Linum usitatissimum</i> Linn.	CdCl ₂ -injured model	↑SOD, ↑CAT, ↑GPx, ↑GR	10 mg/kg of rat, s.c.	[148]
	Synthetic	BaP-injured model	↑GSH/GSSG, ↓MDA, ↑SOD, ↑CAT, ↓p-p38, ↓p-ERK, ↑MKP-1, ↓miR-101A	100 mg/kg of mice, i.g.	[149]
aging ovaries		↓iROS level	7–70 mg/kg of mice, i.g.	[150]	
Dibenzylbutyrolactone structure group					
Arctigenin	<i>Arctium lappa</i> Linn.	WFST model	↑Nrf2, ↑SOD, ↑GR, ↑GPx, ↑Trx1, ↑UCP2, ↑p-AMPK, ↑p-p53, ↑p21, ↑PGC-1α, ↑PPARα	15 mg/kg of rat, i.p.	[80]
		ethanol-induced gastric ulcer	↓MDA content, ↑SOD	0.05–0.45 mg/kg of rat, p.o.	[151]
Arctigenin	Synthetic	JEV-infected model	↓ROS level, ↑SOD1	10 mg/kg of mice, i.p.	[152]
		LPS-injured model	↑GSH/GSSG level, ↓MDA content, ↑SOD, ↑CAT, ↑HO-1	50 mg/kg of mice, i.p.	[153]
	Synthetic	I/R injury model	↓MDA content, ↑SOD, ↑GPx, ↑Nox1, ↑Trx1, ↑Nrf2	50–200 mg/kg of rat, i.g.	[154]
		AMI model	↓MDA content, ↑SOD, ↑GPx, ↑CAT, ↑HO-1	100–200 μmol/kg of rat	[155]

Table 2. Cont.

Lignan	Source	Model	Target	Dose, Road	Ref.
		Hep G2 xenograft model	↑p-p38, ↑p-JNK, ↑Bax, ↑TNF-α	20 mg/kg of mice, s.c.	[86]
		BLM-induced skin fibrosis	↑GSH/GSSG level, ↓MDA content, ↑SOD, ↑Nrf2, ↑HO-1	3 mg/kg of mice, i.p.	[156]
		I/R injury model	↓iROS level, ↓MDA content, ↑SOD, ↑AMPK/SIRT1	100 μmol/kg of rat, i.p.	[87]
		cadmium-intoxicated model	↑GSH/GSSG, ↓8-oxo-dG level, ↓MDA, ↑GSR, ↑GCL, ↑GPx, ↑CAT, ↑Nrf2, ↑HO-1, ↑NQO1	80 mg/kg of rat, i.g.	[157]
Hinokinin	Synthetic	HFD/STZ-induced type 2 diabetes	↓MDA, ↑SOD, ↑CAT, ↑GPx, ↑GST, ↑HO-1, ↑Nrf2, ↓Keap-1	20–40 mg/kg of mice, p.o.	[158]
Matairesinol	Synthetic	CLP-induced sepsis	↓MDA content, ↑SOD, ↑CAT, ↑GPx, ↑Nrf2, ↑HO-1, ↑AMPK	5–20 mg/kg of rat, p.o.	[93]
Furofuranoid structure group					
Fargesin	Synthetic	I/R injury model	↓MDA content, ↓ROS level, ↑SOD, ↑GPx, ↑CAT	15 μmol/kg of rat, i.v.	[159]
Isoeucommin A	<i>Eucommia ulmoides</i> Oliv.	H ₂ O ₂ -injured RTECs	↑SOD, ↑HO-1, ↑Nrf2	31.25–125 μM	[104]
			↑GSH/GSSG level	62.5–125 μM	
		STZ-induced diabetic nephropathy	↓MDA content	125 μM	
			↓MDA content, ↑GSH/GSSG level	2.5–10 mg/kg of rat, i.v.	
			↑SOD	5–10 mg/kg of rat, i.v.	
Pinoresinol diglucoside	Synthetic	Aβ-infused model	↓iROS level, ↓MDA content, ↑SOD, ↑CAT, ↑Nrf2, ↑HO-1, ↑Bcl-2/Bax	5–10 mg/kg of mice, i.g.	[160]
		MCAO model	↓iROS level, ↓MDA content, ↑GSH/GSSG level, ↑SOD, ↑GPx, ↑Nrf2, ↑NQO-1, ↑HO-1	5–10 mg/kg of mice, i.v.	[161]

Table 2. Cont.

Lignan	Source	Model	Target	Dose, Road	Ref.
Sesamin	Synthetic	STZ-induced diabetes	↓MDA content, ↑SOD	20 mg/kg of rat, p.o.	[162]
		nickel-induced hepatotoxicity	↓iROS, ↓TBARS, ↑GSH/GSSG level, ↓8-OHdG, ↑SOD, ↑CAT, ↑GPx ↑PI3K/AKT, ↑Bcl-2/Bax	60–120 mg/kg of mice, p.o.	[163]
		CCl ₄ -induced hepatotoxicity	↓iROS, ↓TBARS level ↓p-JNK, ↓p-c-Jun, ↓cCYC, ↓Bax, ↓Bak, ↓Bcl-2	60–120 mg/kg of mice, p.o.	[164]
		fluoride-exposed model	↓iROS, ↓TBARS, ↑GSH/GSSG level, ↑SOD, ↑CAT, ↑GPx, ↑GST ↓p-JNK, ↓p-c-Jun, ↑Bcl-2/Bax	0.5–1 g/kg of carp, diet	[165]
		DOX-treated model	↓iROS level, ↓MDA content ↑SOD, ↑CAT, ↑GPx	20–40 mg/kg of rat, i.g.	[166]
		6-OHDA model	↓iROS level, ↓MDA content, ↑SOD	20 mg/kg of rat, p.o.	[167]
		LPS-treated model	↑SOD, ↓MDA content	10 mg/kg of rat, p.o.	[168]
		LPS-treated model	↑GSH/GSSG level, ↓MDA content ↑SOD, ↑CAT, ↑Nrf2	100 mg/kg of mice, p.o.	[169]
		DSS-induced colitis	↓iROS level, ↑GSH/GSSG level, ↓MDA content, ↑SOD, ↑Nrf2, ↓Keap1, ↑HO-1, ↑NQO1, ↑GCLC, ↑GCLM, ↑GR, ↑p-AKT, ↑p-ERK1/2	50–100 mg/kg of mice, i.g.	[113]
		cisplatin-injured model	↓MDA content, ↑SOD, ↑Nrf2 ↓nitrate/nitrite ratio	5 mg/kg of rat, p.o.	[170]

Table 2. Cont.

Lignan	Source	Model	Target	Dose, Road	Ref.
		adult <i>Drosophila</i>	↑Nrf2/Cnc	2 mg/mL, diet	[171]
Syringaresinol	<i>Panax ginseng</i> C.A. Meyer	Sod1 ^{-/-} double-mutant model	↓iROS level, ↓8-isoprostane level ↓FoxO3a, ↓MMP-2	50 mg/kg of mice, p.o.	[172]
	<i>Sargentodoxa cuneata</i>	STZ-induced diabetes	↑Nrf2, ↑NQO-1, ↑HO-1, ↓Keap1, ↑SOD, ↑Bcl-2/Bax	25 mg/kg of mice, p.o.	[116]

6-OHDA, 6-hydroxydopamine; 8-OHG, 8-hydroxy-2-deoxyguanosine; α -TOC, α -tocopherol; A β , amyloid β ; ALIOS model, American lifestyle-induced obesity syndrome model; AMI, acute myocardial infarction; Ang, angiotensin; BaP, benzo[a]pyrene; BLM, bleomycin; CLP, cecal ligation and puncture; Cnc, *Drosophila* Nrf2 orthologue; DOX, doxorubicin; DSS, dextran sulfate sodium; e.v.p., ex vivo pretreatment; HFD, high fat diet; i.c.v., intracerebroventricular administration; i.g., intragastric administration; i.p., intraperitoneal injection; i.v., intravenous injection; JEV, Japanese encephalitis virus; LMI, learning and memory impairment; LPO, lipid peroxidation; MCAO, middle cerebral artery occlusion model; MCT, monocrotaline; miR-101, microRNA 101a; MKP-1, protein-mitogen-activated protein kinase phosphatase 1; NAG, N-acetyl- β -D-glucosaminidase; NRC, nerve root compression; p.o., oral administration; RTECs, renal tubular epithelial cells; s.c., subcutaneous injection; STZ, streptozotocin; WFST, weight-loaded forced swimming test. Downward-pointing red arrows reflect the downregulatory action, upward-pointing green arrows reflect the upregulatory action.

3.3. Dibenzocyclooctadiene Skeletons

3.3.1. Gomisins

Gomisin A ameliorated fibrogenesis and demonstrated hepatoprotective effect in the CCl₄-induced acute liver injury model by suppressing the oxidative stress and activation of NF- κ B. The treatment resulted in a decreased hepatic lipid peroxidation and increased SOD activity, as well as in the inhibition of pro-inflammatory mediators and iNOS [127]. Gomisin A protected against high glucose-induced oxidative stress in MC3T3 E1 cells via upregulation of potent antioxidant enzymes HO-1, copper-zinc SOD, manganese SOD and maintenance of mitochondrial homeostasis [36].

Gomisin N significantly increased the ROS level and potentiated tumor necrosis factor-related apoptosis-inducing ligand (TRAIL)-induced apoptosis of HeLa cells through ROS-mediated up-regulation of death receptor 4 and 5, thereby demonstrating its potency in the treatment of malignant tumors [37]. Gomisin N also exerted a protective effect against alcoholic liver disease by inhibiting hepatic steatosis, oxidative stress, and inflammation both in vitro in ethanol-treated male human Caucasian hepatocyte carcinoma (HepG2) cells and in vivo in ethanol-fed mice via the stimulation of hepatic sirtuin 1 (SIRT1)/AMP-activated protein kinase (AMPK) signaling. This was accompanied by downregulation of inflammation and lipogenesis, upregulation of fatty acid oxidation, and the suppression of cytochrome P450 2E1 (CYP2E1) followed by the enhancement of antioxidant genes and GSH levels in hepatic tissues [38].

3.3.2. Schisandrins

Schisandrin A attenuated the increased ROS generation and the production of thio-barbituric acid reactive substance (TBARS), as well as prevented lipid peroxidation and enhanced the CYP3A4 mRNA level and protein activity in CCl₄-treated HepG2 cells [39]. Different studies showed that schisandrin A inhibited NF- κ B, c-Jun N-terminal kinase (JNK)/p38 MAPK, PI3K/Akt signaling pathways and activated the antioxidant Nrf2/HO-1 pathway. Schisandrin A decreased NO and prostaglandin E2 (PGE₂) release, COX-2 and iNOS expression in a RAW 264.7 murine macrophage cell line, reduced plasma nitrite concentration in LPS-treated mice and attenuated xylene-induced ear edema and carrageenan-induced paw edema in vivo via the downregulation of the TLR4/NF- κ B signaling pathway [173,174]. Additionally, schisandrin A showed a protective effect against

LPS-induced inflammatory and oxidative responses in RAW 264.7 cells decreasing the expression of inflammatory mediators and cytokines, thereby diminishing the accumulation of iROS [40]. Schisandrin A protected the mitochondrial function in C2C12 skeletal muscle cells by eliminating the ROS under H₂O₂-induced oxidative stress [41]. Pre-treatment with schisandrin A protected human colorectal adenocarcinoma HT-29 cells against mycotoxin deoxynivalenol-induced cytotoxicity, oxidative stress and inflammation [42]. Schisandrin A suppressed the receptor activator of NF- κ B ligand (RANKL)-induced osteoclastogenesis in vitro and prevented an ovariectomy-induced osteoporosis bone loss in vivo by reducing ROS production [43].

Schisandrin B is known as the main bioactive compound of *Schisandra chinensis* (Chinese magnoliavine), the plant of traditional Chinese medicine. Schisandrin B produces a variety of effects from apoptosis induction to anti-inflammatory and antioxidant action. Schisandrin B was shown to inhibit mitogen-induced phosphorylation of extracellular signal-regulated kinase (ERK), MAPK/ERK kinase (MEK), JNK, and p38, suppress I κ B α degradation and nuclear translocation of NF- κ B. All positive effects of schisandrin B were significantly reduced by Nrf2 and HO-1 inhibitors, which suggests that its anti-inflammatory effect was mediated by Nrf2 modulation [46].

Under oxidative stress, schisandrin B enhanced myocardial glutathione antioxidant status, thereby protecting against ischemia-reperfusion (I/R)-induced myocardial damage in isolated perfused rat hearts [128]. The cardioprotective effect of schisandrin B was also shown on H9c2 cardiomyocytes (rat embryonic cardiomyoblasts) in myocardial ischemia-reperfusion injury (MIRI) model through attenuation of the oxidative stress and inflammatory response via the AMPK/Nrf2 signaling pathway. Mechanistically, schisandrin B pretreatment reversed hypoxia/reoxygenation (H/R)-induced iROS generation, higher MDA content, upregulation of Keap1 and decreased enzymatic activities of SOD and GPx but induced the downregulation of pro-inflammatory cytokines (IL-1 β , TNF- α and IL-8) and the upregulation of the anti-inflammatory cytokine IL-10 [50,51]. In another study, schisandrin B effectively protected the heart from injury caused by a doxorubicin analog pirarubicin by exerting strong antioxidant capacity [137].

In CCl₄-induced hepatotoxicity in mice, schisandrin B catalyzed by hepatic P-450 triggered the enhancement of hepatic mitochondrial glutathione antioxidant status and induced heat shock responses in the liver [129,130,175]. In the model of long-term ethanol-treated rats, the treatment by schisandrin B reversed the altered mitochondrial antioxidant parameters, plasma reactive oxygen metabolites levels and mtMDA production in various tissues [131]. Oral administration of schisandrin B in the diabetic nephropathy mouse model significantly alleviated hyperglycemia-induced renal injury via the suppression of inflammatory response and oxidative stress [135].

Schisandrin B increased the resistance of dopaminergic cells to paraquat-induced oxidative stress and protected BJ human fibroblasts against solar irradiation-induced oxidative injury through the reduction in the oxidant-induced GSH depletion rate and the enhancement of the subsequent GSH recovery [44,45]. Schisandrin B prevented cyclosporine A-induced oxidative stress in human immortalized proximal tubular epithelial HK-2 cells and protected human keratinocyte-derived HacaT cells against t-butyl hydroperoxide-induced oxidative stress via scavenging ROS, increasing levels of mitochondrial membrane potential and GSH, promoting Nrf2 translocation into the nucleus followed by the target gene expression [48,49]. Schisandrin B treatment attenuated the vascular injury and fibrosis mediated by the endothelial to mesenchymal transition in vitro and in vivo [176]. Moreover, schisandrin B reduced epithelial cell injury in a model of colitis by modulating pyroptosis through AMPK/Nrf2/NLRP3 inflammasome pathways [177] as well as regulated STAT3-dependent Th17 cell differentiation and IL-17A cytokine release [178].

The neuroprotective potential of schisandrin B has been demonstrated in a number of experiments. It was found to protect nerve cells from apoptosis [47]. Another study presented schisandrin B as a neuroprotector for rats in a model of amyloid beta peptide (A β)-infused Alzheimer's disease (AD), and revealed the potential role of schisandrin B

for the cognitive improvement via the inhibition of the receptor for advanced glycation end products (RAGE)/NF- κ B/MAPK axis [132]. Schisandrin B oral administration rescued the oxidative stress damage in amygdale and anxiety-like symptoms in forced swimming-induced anxiety model by upregulating Nrf2 expression and down-regulating Keap1 protein levels, reversing the SOD activity and GSH content and decreasing MDA and ROS levels in serum and amygdale [136]. In traumatic spinal cord injury (SCI) model of adult rats, schisandrin B also reversed the activation of injury-associated pathways, cancelling reduced SOD activity, increased MDA level and the activation of NF- κ B p65 and TNF- α [133].

Schisandrin B potently suppressed lymphocyte activation, proliferation, and cytokine secretion in vitro, ex vivo and in vivo via alteration of cellular redox status. Schisandrin B enhanced the basal ROS levels, altered the GSH/GSSG ratio, induced nuclear translocation of Nrf2, and increased the transcription of corresponding genes in intact lymphocytes [46]. In another study, schisandrin B demonstrated anti-inflammatory and antioxidative effects in rat hind limb I/R skeletal muscle injury model [134]. Additionally, schisandrin B mitigated chondrocytes inflammation and ameliorated cartilage degeneration and osteoarthritis and attenuated hypoxia-induced inflammation, apoptosis and the progression of heart remodeling after myocardial infarction [179,180].

Importantly, schisandrin B can significantly reduce the viability of various cell lines in vitro at the concentrations of 40–100 μ M [180,181] and cause hepatotoxicity in mice starting at a dose of 125 mg/kg [182], but was considered safe enough for animal treatment, since a dose of 80 mg/kg did not cause toxic effects [46].

Schisandrin C enhanced the resistance of cultured human fibroblasts to the solar irradiation-induced oxidative damage by eliciting the glutathione antioxidant response [45]. Orally administered schisandrin C ameliorated Ang II-induced oxidative stress in rat aortic endothelium cells (RAECs) by specifically binding to Keap1 and allowing for the Nrf2 translocation into the nucleus to promote the expression of its downstream antioxidant genes [138]. Schisandrin C also exhibited anti-inflammatory and antioxidant effects in human dental pulp cells (HDPCs). The effects were mediated by the upregulation of p-Akt-mediated Nrf2 pathway, the increase of the expression of PGC-1 α and mitochondrial biogenesis. The MAPK pathway was downregulated, which was accompanied by the blocked NF- κ B translocation to the nucleus and decreased production of ROS, NO, matrix metalloproteinase (MMP)-2/9, IL-1 β , TNF- α , intracellular adhesion molecule-1 (ICAM-1) and vascular cell adhesion molecule-1 [52].

3.3.3. Schisantherin A

Schisantherin A was shown to effectively inhibit lipid peroxidation and the production of TBARS, prevent the increased ROS generation and enhance the CYP3A4 mRNA level and protein activity in CCl₄-treated HepG2 cells [39]. Generally, schisantherin A downregulated the expression of Keap1, Bax and caspase-3 and upregulated the expression of Nrf2, HO-1 and Bcl-2 which resulted in the increased level of GSH and decreased level of MDA [140,141]. Intracerebroventricular (i.c.v.) administration of schisantherin A significantly attenuated A β -induced cognitive deficits, oxidative stress and neurodegeneration in the hippocampus and cerebral cortex which allows schisantherin A to be considered as a potential agent in the treatment of AD [139]. In another study, schisantherin A exerted neuroprotective effects and alleviated the symptoms of ischemic stroke, oxidative stress and inflammation responses in parietal cortex of rats after middle cerebral artery occlusion and reperfusion (MCAO/R) injury via the modulation of TLR4, NOX4, Trx1/Prx and C5aR1 signaling pathways [142]. Schisantherin A demonstrated antioxidative and anti-neuroinflammatory effects in LPS-activated BV-2 microglial cells [54] and could improve the learning and memory abilities of chronic fatigue mice and D-galactose treated mice [140,141]. Schisantherin A exerted a protective effect in human renal tubular epithelial cells subjected to H/R (model of renal I/R injury) [53] and also mitigated LPS-induced kidney inflammation via Nrf2-mediated NF- κ B inhibition in rat tubular cells [55].

Table 3. Anti-inflammatory activity of lignans in vitro.

Lignan	Source	In Vitro Model	Target	Concentration	Ref.
Arylnaphthalene structure group					
Sevanol	<i>Thymus armeniacus</i>	HEO of <i>X. laevis</i>	↓hASIC3	IC ₅₀ 353 ± 23 µM	[119]
			↓rASIC1a	IC ₅₀ 2.2 ± 0.6 mM	
	Synthetic	HEO of <i>X. laevis</i>	↓rASIC3	IC ₅₀ 175 ± 18 µM	[120,121]
↓rASIC1a			IC ₅₀ 227.5 ± 37.4 µM		
		RA-treated SH-SY5Y cells	↓hASIC1a	300 µM	[118]
Aryltetralin structure group					
(+)-Isolariciresinol 3a-O-β-D-glucopyranoside	<i>Carissa spinarum</i> Linn.	COX-2 assay	↓COX-2	IC ₅₀ 0.3 µM	[30]
Sauchinone	<i>Saururus chinensis</i>	LPS-stimulated RAW264.7	↓NO production	IC ₅₀ 4.08 µM	[124]
			↓iNOS, ↓TNF-α, ↓COX-2	1–30 µM	[125]
	Synthetic	AngII-induced mesangial cells	↓TGF-β,	0.1–1 µM	[35]
↓NLRP3, ↓ICAM-1, ↓MCP-1, ↓IL-1β, ↓NF-κB p65			1 µM		
Dibenzocyclooctadiene structure group					
Schisandrin A	<i>Schisandra chinensis</i> (Turcz.) Baill.	LPS-stimulated RAW 264.7 macrophages	↓NO level, ↓iNOS, ↓PGE ₂ , ↓COX-2, ↓NF-κB, ↑IκBα, ↓p-JNK, ↓p-p38 MAPK	25–100 µM	[173]
			LPS-stimulated RAW 264.7 macrophages	↓iNOS, ↓COX-2, ↓TNF-α, ↓IL-1β, ↑IκB-α, ↓p-JNK, ↓p-p38 MAPK, ↓p-ERK, ↓p-PI3K, ↓p-Akt	200 µM
	Synthetic	DON-induced cytotoxicity in HT-29 cells	↓PGE ₂ , ↓COX-2, ↓NF-κB, ↓IL8, ↓p-p38, ↓p-ERK	2.5–10 µM	[42]
		RANKL-induced osteoclast differentiation	↓PGE ₂ , ↓COX-2, ↓NF-κB, ↓IL8, ↓p-p38, ↓p-ERK	50–200 µM	[43]
Schisandrin B	Synthetic	Con A-induced lymphocytes	↓NF-κB, ↓p-MEK, ↓p-p38, ↓p-ERK, ↓p-JNK, ↑IκBα, ↓IL-2, ↓IL-4, ↓IL-6, ↓IFN-γ	25–50 µM	[46]

Table 3. Cont.

Lignan	Source	In Vitro Model	Target	Concentration	Ref.
		Ang II/TNF- α /ROS-induced HUVECs	\downarrow NF- κ B, TNF- α , \downarrow p-Smad2/3, \downarrow vimentin, \downarrow α -SMA, \downarrow Snail/slug, \downarrow TGF- β , \downarrow Twist, \uparrow VE-cadherin	10 μ M	[176]
		TH17 cell differentiation	\downarrow p-STAT3	1 μ M	[178]
		H/R-induced H9c2 cell injury	\downarrow IL-1 β , \downarrow TNF- α , \downarrow IL-6, \downarrow IL-8, \downarrow TGF- β , \uparrow IL-10	20 μ M	[50,51]
		LPS+ATP-treated intestinal epithelial cells	\downarrow TNF- α , \downarrow IL-6, \downarrow IL-18, \downarrow IL-1 β , \downarrow NLRP3, \uparrow p-AMPK	40 μ M	[177]
Schisandrin C	Synthetic	LPS-stimulated HDPCs	\downarrow NO level, \downarrow p-ERK1/2, \downarrow p-SAPK/JNK, \downarrow p-p38, \downarrow NF- κ B	10–20 μ M	[52]
		H/R-induced HK-2 cells	\downarrow TNF- α , \downarrow IL-1 β , \downarrow IL-6	5–20 μ M	[53]
Schisantherin A	<i>Schisandra chinensis</i> (Turcz.) Baill.	LPS-stimulated BV-2 microglial cells	\downarrow NF- κ B, \downarrow IKK, \uparrow I κ B, \downarrow TNF- α , \downarrow IL-6, \downarrow IL-1 β , \uparrow IL-10, \downarrow iNOS, \downarrow COX-2, \downarrow p-p38, \uparrow p-ERK, \downarrow p-JNK, \downarrow p-Akt	50 μ M	[54]
	Synthetic	LPS-stimulated NRK-52E cells	\downarrow NF- κ B, \downarrow TNF- α , \downarrow Rantes	25–50 μ M	[55]
Dibenzylbutane structure group					
Nordihydroguaiaretic acid	Synthetic	IL-1 β -induced PC12 cells	\downarrow APP secretion and processing	10 μ M	[183]
		IFN- γ -induced rat brain astrocytes/C6 cells	\downarrow IRF-1, \downarrow IP-10 \downarrow p-STAT1, \downarrow p-STAT3, \downarrow p-JAK2	5–20 μ M	[184]
		RANKL-induced bone marrow-derived macrophage/RAW-D cells	\downarrow osteoclast differentiation, \downarrow RANKL-induced signal cascade \downarrow NFATc1, \downarrow p-ERK	1–10 μ M	[185]
Secoisolariciresinol diglucoside	<i>Linum usitatissimum</i> Linn.	iron treated H9c2 cells	\downarrow TNF- α , \uparrow IL-10	500 μ M	[73]
		CdCl ₂ -injured model	\downarrow MPO, \downarrow NO level	10 mg/kg of rat	[148]
	Synthetic (LGM2605)	asbestos-exposed MFs	\downarrow iNOS, \downarrow IL-1 β , \downarrow IL-6, \downarrow IL-18, \downarrow TNF α	50–100 μ M	[74,75]

Table 3. Cont.

Lignan	Source	In Vitro Model	Target	Concentration	Ref.
Dibenzylbutyrolactone structure group					
	<i>Forsythia fructus</i>	pro-inflammatory enzyme assays	↓PLA2, ↓COX-1, ↓COX-2, ↓5-LOX	100 μM	[186]
	<i>Arctium lappa</i> Linn.	bone marrow-derived MDSCs	↑Arg-1, ↑iNOS	10–20 μM	[187]
		LPS-treated Raw264.7 cells	↓iNOS, ↓p-STAT, ↓IL-1β, ↓IL-6, ↓MCP-1, ↓p-JAK2	5–50 μM	[78]
		TGF-β1-induced HK-2 cells	↓NF-κB p65, ↓MCP-1	0.5–1 μM	[83]
		OA-treated WRL68 hepatocytes	↓ICAM-1, ↓IL-1β, ↓IL-6, ↓IL-7, ↓IL-8, ↓TNFα	50 μM	[85]
		LPS-treated RAW264.7 cells	↓TNF-α, ↓IFN-γ, ↓IL-17, ↓IL-1β, ↓CXCL10, ↑TGF-β1, ↑IL-4	10–100 μM	[188]
Arctigenin	Synthetic	LPS-treated RAW264.7 cells	↓TNF-α, ↓IFN-γ, ↓IL-17, ↓IL-1β, ↓CXCL10, ↑TGF-β1, ↑IL-4	10–100 μM	[188]
		IL-1β-stimulated human chondrocytes	↓TNF-α, ↓COX-2, ↓iNOS, ↓IL-6, ↓PGE ₂ , ↓NO, ↑IκBα, ↓p65, ↓PI3K, ↓Akt	10–50 μM	[189]
		scintillation proximity assay	↓PDE4	IC ₅₀ 3.76 ± 0.28 μM	[190]
		LPS-stimulated human PBMCs	↓TNF-α	IC ₅₀ 35.18 ± 6.01 μM	
		LPS-treated RAW264.7 cells	↓TNF-α, ↑p-CREB, ↓PDE4	100 μM	
		OGD-injured H9c2 cardiomyocytes	↓NF-κB, ↑IκBα, ↓TNF-α, ↓IL-1β, ↓IL-6	50–200 μM	[87]
		silica-injured RAW 264.7 macrophages	↓iNOS, ↓Arg-1, ↓TLR-4, ↓NLRP3, ↓TGF-β	1 μM	[88]
Hinokinin	<i>Aristolochia indica</i> L.	LPS-stimulated THP-1 cells	↓IL-6, ↓TNF-α	20.5 ± 0.5 μM 77.5 ± 27.5 μM	[191]
		naive CD4 ⁺ T cells	↓p-p38, ↓p-ERK, ↓ROR-γt	20 μM	[192]
Matairesinol	Synthetic	LPS-stimulated NSC-34 neurons and BV2 microglia	↓TNF-α, ↓IL-1β, ↓IL-6, ↓IFN-γ, ↓IL-8, ↓MCP1, ↓MAPK, ↓JNK, ↓NF-κB	5–20 μM	[93]

Table 3. Cont.

Lignan	Source	In Vitro Model	Target	Concentration	Ref.
Matairesinol-7'-hydroxyl	<i>Piceaabies</i>	TNF- α -induced HAEC	\downarrow ICAM-1, \downarrow VCAM-1, \downarrow monocyte adhesion	0.1–100 μ M	[193]
			\downarrow p-NF- κ B	10–100 μ M	
			\downarrow p-ERK	100 μ M	
Nortrachelogenin	Synthetic	LPS-stimulated J774 macrophages	\downarrow PGE ₂ , \downarrow NO, \downarrow iNOS	1–30 μ M	[194]
			\downarrow MCP-1, \downarrow IL-6	3–30 μ M	
			\downarrow mPGES-1	30 μ M	
Furanoid structure group					
(–)-Olivil	<i>Osmanthus fragrans</i> var. <i>aurantiacus</i>	LPS-activated RAW264.7 cells	\downarrow NO level	IC ₅₀ 85.6 \pm 1.49 μ M	[195]
Taxiresinol	<i>Osmanthus fragrans</i> var. <i>aurantiacus</i>	LPS-activated RAW264.7 cells	\downarrow NO level	IC ₅₀ 58.1 \pm 1.42 μ M	[195]
	<i>Perovskiaatriplicifolia</i> Benth	RBL-1 leukemia cells	\downarrow leukotriene C4 release	IC ₅₀ 3.4 \pm 0.09 μ M	[196]
Furofuranoid structure group					
Dendranlignan A	<i>Dendranthema morifolium</i> (Ramat.)	LPS-induced H9c2 cells	\downarrow TNF- α , \downarrow IL-6, \downarrow IFN- γ \downarrow p-cJUN, \downarrow p-P65, \downarrow p-IRF3	10 μ M	[103]
(+)–Diayangambin	<i>Piper fimbriulatum</i>	human mononuclear cells	\downarrow proliferation	1.5 μ M	[197]
		LPS-stimulated RAW264.7 macrophages	\downarrow PGE ₂	10 μ M	
Fargesin	<i>Magnolia fargesii</i>	PMA-stimulated THP-1	\downarrow iNOS, \downarrow COX-2, \downarrow IL-1 β , \downarrow TNF- α , \downarrow AP-1, \downarrow NF- κ B, \downarrow JNK	5–20 μ M	[198]
	<i>Magnolia</i> sp.	LPS-stimulated RAW264.7	\downarrow iNOS, \downarrow COX-2, \downarrow NF- κ B	25 μ M	[199]
Koreanaside A	<i>Forsythia koreana</i>	LPS-stimulated RAW 264.7 macrophages	\downarrow iNOS, \downarrow COX-2, \downarrow IL-6, \downarrow TNF- α , \downarrow p-I κ B α , \downarrow p-TAK1	20–80 μ M	[200]
			\downarrow AP-1, \downarrow p-c-Fos, \downarrow p-p65, \downarrow NF- κ B, \downarrow p-IKK α / β , \downarrow p-STAT1, \downarrow p-STAT3, \downarrow p-JAK1, \downarrow p-JAK2	40–80 μ M	
Phillygenin	<i>Forsythia koreana</i>	RAW 264.7 cells	\downarrow PGE ₂ , \downarrow NO, \downarrow iNOS, \downarrow NF- κ B	1–100 μ M	[201]
Pinoresinol	Synthetic	IL-1 β -stimulated Caco-2 cells	\downarrow PGE ₂ , \downarrow MCP-1, \downarrow NF- κ B	50–100 μ M	[202]
			\downarrow IL-6	10–100 μ M	

Table 3. Cont.

Lignan	Source	In Vitro Model	Target	Concentration	Ref.
Pinoresinol diglucoside	<i>Eucommia ulmoides</i>	oxLDL-induced HUVEC cytotoxicity	↓eNOS, ↓p-p38MAPK, ↓p-NF-κB p65	1 μM	[109]
		oxLDL-induced HUVECs cytotoxicity	↓NF-κB, ↓IL-8	12.5–100 μM	[110]
Sesamin	<i>Sesamum indicum</i> Linn.	FPR-transfected ETFR cells, THP1 cells	↓cell migration, ↓NF-κB activation, ↓ERK1/2 phosphorylation	6.25–50 μM	[203]
		KA-induced PC12 and BV-2 cells	↓ERK1/2, ↓p38 MAPK, ↓COX-2	10–50 μM	[111]
		RPMC	↓histamine release		
		HMC-1	↓TNF-α, ↓IL-6, ↓p38 MAPK, ↓NF-κB	25–100 μM	[204]
		Synthetic	RLE-6TN and L2 cells	↑A20, ↑TAX1BP1	10 μM
<i>epi</i> -Sesamin	<i>Asarum sieboldii</i>	HUVEC	↓EPCR shedding	1–10 μM	[206]
Syringaresinol	<i>Peroovskiaatriplicifolia</i> Benth	RBL-1 leukemia cells	↓leukotriene C4 release	IC ₅₀ 7.9 ± 0.04 μM	[196]
		LPS-stimulated RAW 264.7 cells	↓iNOS, ↓COX-2, ↓TNF-α, ↓IL-1β, ↓IL-6, ↓PGE ₂ , ↓ERK1/2, ↓JNK, ↓p38 MAPK	25, 50, 100 μM	[207]
	<i>Rubia philippinensis</i>	High glucose-treated NRVM	↓TNF-α, ↓IL-6, ↓IL-1β, ↓TGF-β, ↓p-Smad2/3	50, 100 μM	[116]
		LPS+ ATP-treated H9c2 cells	↓IL-1β, ↓IL-18, ↑SIRT1 expression, ↓NLRP3 inflammasome activation	100 μM	[208]
<i>Albiziae cortex</i>	BV2 microglia cells	↓TNF-α, ↓IL-6, ↓IL-1β, ↓COX-2, ↓NO, ↑M2 phenotype, ↓NF-κB	25, 50, 100 μM	[209]	

AKT, protein kinase B; APP, amyloid precursor protein; ASIC 1/3 h/r, acid-sensing ion channel isoform 1/3 type human/rat; BV-2 cells, murine microglial cell line; COX-2, cyclooxygenase-2; CREB, cAMP-response element binding protein; DON, trichothecene toxin deoxynivalenol; EPCR, endothelial protein C receptor; ERK, extracellular signal-regulated kinase; ETFR, epitope-tagged human FPR cell; FPR, formyl peptide receptor; H9c2 cells, embryonic rat heart derived cell line; HAEC, human aortic endothelial cells; HDPCs, human dental pulp cells; HEO of *X. laevis*, heterologously expressing oocytes of *Xenopus laevis* frog; HK-2, human renal tubular epithelial cells; HMC-1, human mast cell line 1; H/R, hypoxia/reoxygenation; HUVECs, human umbilical vein endothelial cells; IκBα, inhibitor of κB; IKKα/β, IκB kinase; IL, interleukin; iNOS, inducible nitric oxide synthase; IP-10, inducible protein-10; IRF-1, interferon regulatory factor-1; JAK2, Janus kinase 2/signal transducer; JNK, c-Jun N-terminal kinase; KA, kainic acid; LPS, lipopolysaccharide; MAPK, mitogen-activated protein kinase; mPGES-1, microsomal prostaglandin E synthase-1; MPO, myeloperoxidase; NF-κB, nuclear factor-κB; NLRP3, nod-like receptor family pyrin domain containing 3; NRK-52E cells, normal rat kidney cell line; NRVM, neonatal rat ventricular myocytes; OA, oleic acid; OGD, oxygen glucose deprivation; oxLDL, oxidized low-density lipoprotein; PBMCs, human peripheral blood mononuclear cells; PC12 cells, rat pheochromocytoma cell line; PDE, phosphodiesterase; PGE2, prostaglandin E2; PMA, phorbol-12-myristate-13-acetate; PPAR, peroxisome proliferator-activated receptor; RA, retinoic acid; RANKL, receptor activator of NF-κB ligand; RLE-6TN, rat lung epithelial-6-T-antigen negative cell line;

ROR- γ t, retinoid-related orphan receptor- γ t; RPMC, rat peritoneal mast cell; SH-SY5Y, human neuroblastoma cell line; SIRT1, NAD-dependent deacetylase sirtuin-1; STAT3, signal transducer and activator of transcription 3; TAK1, TGF- β -activated kinase 1; TGF- β , transforming growth factor- β ; TNF- α , tumor necrosis factor α . Downward-pointing red arrows reflect the downregulatory action, upward-pointing green arrows reflect the upregulatory action.

3.4. Dibenzylbutane Skeletons

3.4.1. Nordihydroguaiaretic Acid (NDGA) and Its Derivatives

NDGA, found in leaves and twigs of the evergreen desert shrub *Larrea tridentata* (Sesse and Moc. ex DC) Coville (creosote bush), is the best known lignan with lipoxygenase-inhibitory activity [210]. However, many studies also demonstrate its antioxidant and anti-inflammatory properties. NDGA showed potent antioxidant activity against iROS in HL-60 cells [59]. It was shown that NDGA scavenges efficiently at least two hydroxyl radicals (HO \bullet) generated by the Fenton reaction [63]. NDGA also demonstrated scavenging effects against ONOO $^-$ peroxynitrite anion as efficiently as uric acid; against $^1\text{O}_2$ singlet oxygen more efficiently than dimethyl thiourea, lipoic acid, N-acetyl-cysteine (NAC) and glutathione; against OH \bullet hydroxyl radicals more efficiently than dimethyl thiourea, uric acid, Trolox, dimethyl sulfoxide and mannitol; against O $_2^{\bullet-}$ superoxide anion more efficiently than NAC, glutathione, tempol and deferoxamine; against HOCl hypochlorous acid as efficiently as lipoic acid and NAC; and was unable to scavenge H $_2\text{O}_2$. It should be noted that NDGA exerted protective effects not only by scavenging ROS but also by inducing the expression of cytoprotective genes. NDGA prevented iROS accumulation and mitochondrial depolarization in Keap1-independent manner via the inhibitory phosphorylation of glycogen synthase kinase-3 (GSK-3) and the activation of ERK1/2, p38, JNK, and PI3K pathways with a subsequent nuclear localization of Nrf2 and activation of the ARE regulatory sequence and the increase in HO-1 protein levels [65].

In an in vivo study in rats, NDGA was able to prevent ozone-induced tyrosine nitration in lungs [61]. NDGA treatment ameliorated oxidative and nitrosative stress and showed renoprotective effect in a K $_2\text{Cr}_2\text{O}_7$ -induced nephrotoxicity model in rats [143]. NDGA protected cerebellar granule neurons against H $_2\text{O}_2$ - or 3-nitropropionic acid-induced neurotoxicity [62]. In kidney-derived LLC-PK1 and HEK293T cells and in wild-type mouse embryo fibroblasts (MEFs), NDGA prevented H $_2\text{O}_2$ -induced cell death [65]. NDGA attenuated toxicity, ROS production and the oxidative stress-induced decrease of CD33 (a myeloid cell-specific type I transmembrane glycoprotein) expression in the iodoacetate- or H $_2\text{O}_2$ -treated human acute monocytic leukemia (THP-1) cell line [66].

Dietary administration of NDGA to obese mice improved the metabolic dysregulation by upregulating PPAR α , hepatic antioxidant enzymes, GPx4, mitochondrion-specific antioxidant peroxiredoxin 3, and expression of key genes involved in fatty acid oxidation together with downregulating the key lipogenic enzymes, apoptosis and ER stress signaling pathways [144].

In the model of mouse skin treated by stage I tumor promoting agent, 12-O-tetradecanoylphorbol-13-acetate, NDGA pretreatment mitigated cutaneous lipid peroxidation, inhibited H $_2\text{O}_2$ production, restored reduced GSH level and activated antioxidant enzymes, lowered the elevated activities of myeloperoxidase (MPO), xanthine oxidase and skin edema formation, thereby demonstrating antioxidative and anti-inflammatory properties and chemopreventive potential against skin cancer [64].

Furthermore, NDGA inhibited the inflammatory response after SCI by decreasing MPO, IL-1 β and TNF- α levels and the number of macrophages/microglia, thereby limiting secondary damage and demonstrating neuroprotective potential [211]. In cultured rat brain astrocytes, NDGA suppressed IFN- γ -induced inflammatory responses by inhibiting JAK/STAT activation and downregulating the inflammatory mediators IRF-1 and IP-10 [184]. NDGA inhibited the IL-1 β -increased maturation, processing and secretion of amyloid precursor protein in PC12 cells, thereby indirectly contributing to the attenuation of the amyloid plaque formation in AD [183].

NDGA showed ameliorating potential on inflammatory bone destruction mediated by osteoclasts via the inhibition of calcium oscillation followed by the downregulation of a key transcription factor for osteoclastogenesis NFATc1 and inhibition of RANKL-induced osteoclastogenesis in cultures of murine osteoclast precursor cell line RAW-D and primary bone marrow-derived macrophages [185]. Dietary supplementation with NDGA ameliorated dyslipidemia and hepatic steatosis in *ob/ob* mice via PPAR α -dependent and PPAR α -independent lipid pathways and AMPK signaling [212]. In cecal ligation and double puncture (CLP)-induced abdominal sepsis model in rats, NDGA treatment improved oxygenation, decreased lactate, lowered lung injury and mitigated lung edema, thereby demonstrating its anti-inflammatory potential in the modulation of organ injury [213].

Aside its protective effects, NDGA has also shown cytotoxic effects in several studies. NDGA treatment led to the increase in oxidative processes, phosphorylation and activation of the MAP kinases ERK, JNK and p38, causing apoptosis of murine pro-B lymphocytes (FL5.12 cells) [60], and evoked cell death inducing oxidative damage of proteins in the medulloblastoma-derived Daoy cell line [67]. Thus, NDGA is not a safe compound. The Food and Drug Administration (FDA) removed NDGA from the FDA's list of Generally Regarded as Safe (GRAS) agents as early as 1968. NDGA was shown to cause cystic nephropathy in rats and skin hypersensitivity in humans, and high doses of *L. tridentata* were associated with kidney disease and hepatotoxicity in humans [214,215]. The LD₅₀ of NDGA was found to be 75 mg/kg (i.p. administration in mice) with higher NDGA doses (100 and 500 mg/kg) causing 100% mortality within 30 h [214].

3.4.2. Meso-Dihydroguaiaretic Acid

Meso-dihydroguaiaretic acid showed hepatoprotective activity for rat hepatocytes that manifested in a significant decrease of GPT level released into the medium from the primary culture. It also preserved the GSH/GSSG and MDA levels, and SOD, GPx, CAT activities [24]. Meso-dihydroguaiaretic acid demonstrated strong free radical scavenging activity in various cell-free assays, modulated MAPKs/Akt signal pathways in G-protein coupled receptor agonists-induced human neutrophils, and reduced ROS generation. In a murine model of LPS-induced acute respiratory distress syndrome, the lignan application showed anti-neutrophilic inflammatory effects [58].

3.4.3. Secoisolariciresinol and Its Derivatives

Secoisolariciresinol exhibited strong scavenging activity against the stable free radical DPPH [56,68,70,71] and potently scavenged superoxide and peroxy radicals, being more effective than two generally accepted standards: butylated hydroxyanisole (BHA) and Trolox [69]. Secoisolariciresinol also showed strong protection against AAPH peroxy radical that is capable to initiate plasmid DNA nicking and phosphatidylcholine liposome lipid peroxidation [71]. 7-Hydroxy-Secoisolariciresinol also showed significant but weaker DPPH radical scavenging activity than secoisolariciresinol [70].

Secoisolariciresinol diglucoside (SDG) exerted high in vitro antioxidant potency to DPPH and AAPH scavenging similar to unglucosylated secoisolariciresinol [71,72]. In various models of pathological states, SDG showed cytoprotective effect by reversing AMPK and mitogen-activated protein kinase phosphatase 1 (MKP-1) expression that restored the activity of antioxidant enzymes (SOD, CAT, GPx, GR, and peroxidase (POX)). It decreased pro-apoptotic protein levels, suppressed pro-inflammatory signaling (p-p38 MAPK, p-ERK, NF- κ B) and the expression of inflammatory mediators (TNF- α , IL-10, interferon γ (IF- γ), MMP-2/9) [149,150]. SDG showed cytoprotective effect in cardiac iron overload-induced redox-inflammatory damage condition suggesting the cardioprotective role for this flaxseed lignan [73].

SDG improved ovarian aging by inhibiting oxidative stress and scavenging slowly accumulated ROS in ovarian tissues [150]. In in vivo models of CCl₄ and benzo[a]pyrene intoxication, SDG attenuated oxidative damage in liver and kidney tissues [72]. Additionally, SDG protected kidneys from cadmium-induced oxidative damage by restoring antioxidant

enzymes activity and decreasing lipid peroxidation [148,149]. SDG showed protective effect against oxidative stress in rats with metabolic syndrome by preventing lipids from oxidative damage, improving enzymatic antioxidant defenses and GSH level [145]. Pre-treatment with SDG provided protection in a monocrotaline-induced model of pulmonary arterial hypertension by decreasing right ventricle hypertrophy, ROS levels, lipid peroxidation, plasma levels of alanine transaminase and aspartate transaminase [146].

A number of studies have been carried out on LGM2605 that is a chemically synthesized SDG by a proprietary route. It was shown that LGM2605 treatment reduced 8-hydroxy-2-deoxyguanosine (8-OHdG), attributed to ROS-specific nuclear damage, and nitrotyrosine in DRG and spinal neurons of rats after a painful nerve root compression [147]. As it was shown in human ventricular cardiomyocyte-derived cell line AC16 treated with LPS and CLP mouse model of peritonitis-induced sepsis, LGM2605 alleviated oxidative stress, increased mitochondrial respiration, and restored cardiac systolic function by directly decreasing ROS accumulation not via affecting the expression of antioxidant genes but preventing the activation of NF- κ B [76]. LGM2605 treatment significantly mitigated asbestos-induced cytotoxicity, inflammation, and oxidative damage by reducing ROS generation and nitrosative stress, decreasing levels of MDA and 8-iso Prostaglandin F $_{2\alpha}$ (8-isoP) (markers of lipid peroxidation), enhancing Nrf2 activation and the expression of phase II antioxidant enzymes, HO-1 and Nqo1, as well as reducing levels of IL-1 β , IL-18, IL-6, and TNF α in both WT and Nrf2 $^{-/-}$ murine peritoneal macrophages, supporting its possible use as a chemoprevention agent in the development of asbestos-induced malignant mesothelioma [74,75].

Table 4. Anti-inflammatory activity of lignans ex vivo and in vivo.

Lignan	Source	Model	Target	Dose, Road	Ref.
Arylnaphthalene structure group					
Sevanol	<i>Thymus armeniacus</i>	CFA-induced thermal hyperalgesia	↑ withdrawal latency of inflamed hind paw	1–10 mg/kg of mice, i.v.	[119]
	Synthetic	CFA-induced paw edema	↓ paw edema	0.1–1 mg/kg of mice, i.m., i.n., p.o.	[120,121]
Aryltetralin structure group					
Podophyllotoxin	Synthetic (G-003M)	TGR-exposed model	↑ survival, ↓ NO, ↓ IL-6, ↓ TNF- α , ↓ TGF- β 1	5 mg/kg of mice, i.m.	[122]
	Synthetic, conjugated with PAA dendrimer	HCC-induced model	↓ IL-6, ↓ NF- κ B, ↓ α -SMA, ↓ TGF- β	10, 20 mg/kg of mice, p.o.	[123]
Sauchinone	<i>Saururus chinensis</i>	OVA-induced asthma model	↓ neutrophil, lymphocyte, eosinophil infiltration in BALF, ↓ IL-5, ↓ IL-13, ↓ Th2 cell development	10, 100 mg/kg of mice, i.p.	[126]
Dibenzocyclooctadiene structure group					
Gomisin A	<i>Schisandra chinensis</i> Baill.	CCl $_4$ -induced hepatotoxicity	↓ TNF- α , ↓ IL-1 β , ↓ iNOS, ↓ NF- κ B, ↓ p-I κ B	50–100 mg/kg of rat, i.p.	[127]
Gomisin N	<i>Schisandra chinensis</i> Baill.	ethanol-induced liver injury	↓ NF- κ B p65, ↑ I κ B, ↓ TNF- α , ↓ IL-6, ↓ MCP-1	5–20 mg/kg of mice, p.o.	[38]

Table 4. Cont.

Lignan	Source	Model	Target	Dose, Road	Ref.
Schisandrin A	<i>Schisandra chinensis</i> (Turcz.) Baill.	LPS-treated model	↓NO level	100–200 mg/kg of mice, i.p.	[173]
		carrageenan-induced paw edema	↓paw edema volume		
		xylene-induced ear edema	↓ear edema degree	25–50 mg/kg of mice, p.o.	
		carrageenan-induced paw edema	↓paw edema volume ↓TNF- α , ↓IL-1 β , ↓MPO, ↓p-p65NF- κ B, ↓p-I κ B, ↓TLR4	25–50 mg/kg of mice, p.o.	[174]
Schisandrin B	Synthetic	Con A-induced lymphocytes	↓IL-2, ↓IL-4, ↓IL-6, ↓IFN- γ	80 mg/kg of mice, i.p.	[46]
		myocardial infarction model	↓in left ventricular end-systolic and end-diastolic diameter, ↓heart weight/body weight ratio, ↓infarct size, ↓NF- κ B, ↓TGF- β 1, ↓TNF- α	80 mg/kg of mice, i.g.	[179]
		A β -infused model	↓COX-2, ↓iNOS, ↓TNF- α , ↓IL-1 β , ↓IL-6	25–50 mg/kg of rat, i.g.	[132]
		I/R injury model	↓IL-1 β , ↓TNF- α , ↓p-p38MAPK, ↓p-ERK1/2, ↓NF- κ B p65	80 mg/kg of rat, p.o.	[134]
		TSCI model	↓NF- κ B p65, ↓TNF- α	50 mg/kg of rat, p.o.	[133]
		IL-1 β -induced rat chondrocytes	↓IL-6, ↓iNOS, ↓MMP3, ↓MMP13, ↓NF- κ B, ↓MAPK	50 μ M, i.a.	[180]
		STZ-induced diabetes	↑I κ B α , ↓VCAM-1, ↓TNF- α	20 mg/kg of mice, p.o.	[135]
		Ang II-induced vascular injury model	↓ α -SMA, ↓p-Smad2/3, ↑VE-cadherin	20 mg/kg of mice, p.o.	[176]
		DSS induced colitis	↓TNF- α , ↓IL-6, ↓IL-18, ↓IL-1 β , ↓NLRP3, ↑p-AMPK	10 mg/kg of mice, i.p.	[177]
		Schisantherin A	Synthetic	MCAO/R-induced brain injury model	↓IL-1 β , ↓IL-6, ↓p-I κ B α , ↓NF- κ B, ↓p-ERK, ↓p-JNK, ↓p-p38, ↓TLR4, ↓C5aR1

Table 4. Cont.

Lignan	Source	Model	Target	Dose, Road	Ref.
		LPS-induced acute kidney injury	↓accumulation neutrophils and T-lymphocytes, ↓NF-κB, ↓TNF-α, ↓Rantes	40 mg/kg of mice, i.p.	[55]
Dibenzylbutane structure group					
Meso-dihydroguaiaretic acid	<i>Machilus philippinensis</i> Merr.	LPS-induced ARDS model	↓MPO, ↓4-HNE, ↓elastase accumulation	30 mg/kg of mice, i.p.	[58]
		TPA-treated model	↓LPO level, ↓XOD, ↓MPO	15–25 μM, shaved area of dorsal skin	[64]
		spinal cord injury	↓MPO, ↓TNF-α, ↓IL-1β	30 mg/kg of rat, i.p.	[211]
Nordihydroguaiaretic acid	Synthetic	leptin-deficient (<i>ob/ob</i>) mice	↑PPARα, ↑p-AMPK, ↑fatty acid oxidation pathway	0.83 g/kg, 2.5 g/kg, diet	[212]
		CLP-induced sepsis	↓lung edema, ↓lactate, ↓blood urea nitrogen, ↓histologic lung injury	20 mg/kg of rat, i.p.	[213]
		CLP-induced sepsis	↓p-IκBα, ↓NF-κB	100 mg/kg of mice, i.p.	[76]
Secoisolariciresinol diglucoside	Synthetic	BaP-injured model	↓MPO, ↓NO level, ↓TNF-α, ↓IL-6, ↓IL-1β, ↓NF-κB	100 mg/kg of mice, i.g.	[149]
Dibenzylbutyrolactone structure group					
		OVA-induced asthma model	↓PDE	10–100 μM	
		48/80-induced RPMCs	↓histamine release	10 μM	
		IgE-rich mouse serum-induced PCA skin model	↓amount of Evans blue leakage	15–45 mg/kg of rat, p.o.	
Arctigenin	<i>Forsythia fructus</i>	anti-rat rabbit serum antibody-induced RCA skin model	↓skin edema		[186]
		SRBC-induced Arthus reaction model	↓footpad thickness, ↓hemolysis tier, ↓hemagglutinin titer, ↓plaque-forming cells	15–45 mg/kg of mice, p.o.	
		SRBC-induced DTH model	↓footpad thickness, ↓rosette-forming cells		
		DNFB/PC-induced contact dermatitis	↓ear edema	0.1–1 mg/ear of mice	

Table 4. Cont.

Lignan	Source	Model	Target	Dose, Road	Ref.
<i>Arctium lappa</i> Linn.		LPS-/PGN-stimulated peritoneal macrophages	↓IL-6, ↓TNF- α , ↓IL-1 β , ↑IL-10, ↑CD204, ↓p-PI3K, ↓p-Akt, ↓p-p65, ↓p-IKK β	10–20 μ M	
		LPS-/PGN-induced model	↓TNF- α , ↓IL-1 β	5 mg/kg of mice, i.p.	[216]
		TNBS-induced colitic model	↓IL-6, ↓TNF- α , ↓IL-1 β , ↓MPO, ↑IL-10, ↓p-PI3K, ↓p-Akt, ↓p-p65	30–60 mg/kg of mice, p.o.	
		acetic acid-induced chronic ulcer model	↓TNF- α , ↓IL-6, ↑IL-10, ↓CRP	0.05–0.45 mg/kg of rat, p.o.	[151]
		LPS-induced acute inflammation model	↓CD86, ↓IL-6, ↓IL-12, ↓TNF- α , ↓IL-1 β , ↑IL-10, ↑G-MDSCs, ↓M-MDSCs, ↓IRF8, ↑miR-127-5p, ↓M1 macrophage polarization, ↑Arg-1, ↑iNOS	50 mg/kg of mice, i.p.	[187]
Synthetic		JEV-infected model	↓iNOS, ↓TNF- α , ↓IFN- γ , ↓MCP-1, ↓IL-6, ↓p-p38 MAPK, ↓p-c-Jun ↓p-ERK-1/2, ↑p-Akt	10 mg/kg of mice, i.p.	[152]
		LPS-injured model	↓nitrate/nitrite ratio, ↓iNOS, ↓TNF- α , ↓IL-6, ↓MIP-2, ↓p-ERK1/2, ↓p-JNK, ↓p-p38	50 mg/kg of mice, i.p.	[153]
		EAE model	↓IFN- γ , ↓T-bet, ↓IL-17, ↓ROR- γ t, ↓Th1, ↓Th17	5–10 mg/kg of mice, i.p.	[217]
		ConA-induced acute hepatitis	↑IL-4, ↓F4/80, ↓CD49b, ↓CD4 T cells	5–10 mg/kg of mice, i.p.	[188]
		AMI model	↓iNOS, ↓COX-2, ↓IL-1 β , ↓IL-6, ↓p-ERK1/2	100–200 μ mol/kg of rat	[155]
	BLM-induced skin fibrosis model	↓TGF- β 1, ↓IL-1 β , ↓IL-4, ↓IL-6, ↓TNF- α , ↓MCP-1	3 mg/kg of mice, i.p.	[156]	
	DMM model	↓cartilage erosion, ↓hypocellularity, ↓proteoglycan loss	30 mg/kg of mice, p.o.	[189]	

Table 4. Cont.

Lignan	Source	Model	Target	Dose, Road	Ref.
		imiquimod-induced murine psoriasis model	↑p-CREB, ↑cAMP, ↑IL-10, ↓TNF- α , IFN- γ , ↓COX-2, ↓iNOS, ↓IL-2, ↓IL-6, ↓IL-12, ↓IL-17, ↓IL-22, ↓IL-23, ↓IL-27	5% cream	[190]
		silicosis model	↓TGF- β , ↓TLR-4	30–60 mg/kg of rat, i.g.	[88]
		cadmium-intoxicated model	↓NF- κ B p65, ↓TNF- α , ↓IL-1 β	80 mg/kg of rat, i.g.	[157]
Hinokinin	Synthetic	high-fat diet/STZ-induced type 2 diabetic	↓TLR 4, ↓MYD88, ↓NF- κ B p65, ↑IKB α , ↓TNF- α , ↓IL-1 β , ↓p38, ↓ERK 1/2, ↓JNK, ↓MEK	20–40 mg/kg of mice, p.o.	[158]
		IRBP/CFA-induced EAU model	↓T17 cells, ↓IL-17A, ↓IL-17F, ↓IL-21, ↓GM-CSF, ↓IRF-4, ↓Hif1, ↓Batf, ↓ROR- γ t, ↓TNF- α	1 mg/kg of mice, i.p.	[192]
Matairesinol	Synthetic	CLP-induced sepsis	↓TNF- α , ↓IL-1 β , ↓IL-6, ↓IFN- γ , ↓IL-8, ↓MCP1, ↓MAPK, ↓JNK, ↓NF- κ B	5–20 mg/kg of rat, p.o.	[93]
Nortrachelogenin	Synthetic	carrageenan-induced paw edema	↓paw edema volume	100 mg/kg of mice, i.p.	[194]
Furanoid structure group					
Nectandrin B	<i>Guaiacum officinale</i> L.	IL-1 β -treated rat hepatocytes	↓NO level	IC ₅₀ 43.4 μ M	[218]
Taxiresinol	<i>Taxus baccata</i> Linn.	carrageenan-induced paw edema	↓paw edema volume	100 mg/kg of mice, p.o.	[219]
Furofuranoid structure group					
Acanthoside B	<i>Salicornia europaea</i> Linn.	Amnesic AD-like model	↓iNOS, ↓COX-2, ↓TNF- α , ↓IL-1 β , ↓IL-6, ↑IL-10	10, 20 mg/kg of mice, p.o.	[220]
(+)-Diayangambin	<i>Piper fimbriulatum</i>	carrageenan-induced paw edema	↓paw volume, ↓prostaglandin E2	40 mg/kg of mice, p.o.	[197]
Fargesin	<i>Magnolia</i> sp.	DSS-induced colitis	↓inflammatory infiltration, ↓MPO, ↓TNF- α , ↓NO, ↑IKB α , ↓NF- κ B	50 mg/kg of mice, p.o.	[199]

Table 4. Cont.

Lignan	Source	Model	Target	Dose, Road	Ref.
	Synthetic	ApoE ^{-/-} model	↓macrophage infiltration, ↑M2 phenotype polarization, ↓TNF-α, ↓IL-1β, ↓IL-6, ↓MCP-1, ↑IL-10	50 mg/kg of mice, p.o.	[221]
Isoeucommin A	<i>Eucommia ulmoides</i> Oliv.	STZ-induced diabetic nephropathy	↓immune infiltration, ↓TNF-α, ↓IL-1β, ↓IL-6	2.5–10 mg/kg of rat, i.v.	[104]
Koreanaside A	<i>Forsythia koreana</i>	DSS-induced acute colitis	↓iNOS, ↓COX-2, ↓IL-6, ↓TNF-α, ↓p-c-Fos, ↓p-p65, ↓p-STAT1, ↓p-STAT3	5–20 mg/kg of mice, i.p.	[200]
Phillygenin	<i>Forsythia koreana</i>	carrageenan-induced paw edema	↓paw volume	12.5–100 mg/kg of mice, i.p.	[201]
	<i>Forsythia fructus</i>	CCl ₄ -induced liver fibrosis	↓LPS, ↓MIP-1, ↓TNF-α, ↓IL-1β, ↓IL-6, ↓immune infiltration	20, 40 mg/kg of mice, i.g.	[222]
Pinoresinol diglucoside	Synthetic	Aβ-infused model	↓TLR4, ↓NF-κB p65, ↓TNF-α, ↓IL-1β	5–10 mg/kg of mice, i.g.	[160]
		MCAO model	↓TNF-α, ↓IL-1β, ↓IL-6, ↓p-IKKβ, ↓p-IκBα, ↑cNF-κB p65, ↓p-p65	5–10 mg/kg of mice, i.v.	[161]
Sesamin	<i>Sesamum indicum</i> Linn.	fMLF-induced inflammation in a murine air-pouch model	↓leukocyte infiltration	12 mg/kg of mice, i.p.	[203]
		PCA model	↓PCA reaction	50–200 mg/kg of rat, p.o.	[204]
		LPS-treated model	↓TNF-α, ↓MCP-1, ↓IL-1β	10 mg/kg of rat, p.o.	[168]
		LPS-treated model	↓NF-κB, ↓TLR4, ↓Cox2, ↓TNF-α, ↓IL-6	100 mg/kg of mice, p.o.	[169]
		DSS-induced colitis model	↓IL-6, ↓IL-1β, ↓TNF-α	50–100 mg/kg of mice, i.g.	[113]
		cisplatin-injured model	↓TNF-α, ↓IL-1β, ↓TGF-β1, ↓MPO	5 mg/kg of rat, p.o.	[170]
	Synthetic	CCl ₄ -induced hepatotoxicity model	↓TNF-α	60–120 mg/kg of mice, p.o.	[164]

Table 4. Cont.

Lignan	Source	Model	Target	Dose, Road	Ref.
Syringaresinol		carrageenan-induced lung inflammation	↑A20, ↑TAX1BP1, ↓IL-6, ↓IL-8, ↓IL-1β, ↓TNF-α, ↓MIP-2, ↓MPO, ↓β-glucuronidase, ↓p-p65, ↓TRAF6	50–100 mg/kg of rat, p.o.	[205]
		fluoride-exposed model	↓TNF-α	0.5–1 g/kg of carp, diet	[165]
	<i>Rubia philippinensis</i>	carrageenan-induced paw edema model	↓paw edema volume	50 mg/kg of mice, p.o.	[207]
		CLP-induced sepsis	↓TNF-α, ↓IL-6, ↓IL-18, ↓IL-1β	50 mg/kg of mice, p.o.	[208]
		STZ-induced type 1 diabetic model	↓macrophage, monocyte, neutrophil infiltration in myocardium, ↓TNF-α, ↓IL-6, ↓IL-1β	25 mg/kg of mice, p.o.	[116]
	<i>Albiziae cortex</i>	LPS-treated model	↓IL-6, ↓IL-1β, ↓TNF-α, ↓COX-2, ↓iNOS, ↓microglia activation	60 mg/kg of mice, p.o.	[209]

4-HNE, 4-hydroxy-2-nonenal; AD, Alzheimer's disease; Ang, angiotensin; ARDS, acute respiratory distress syndrome; BALF, bronchoalveolar lavage fluid; Batf, basic leucine zipper transcriptional factor ATF-like; CFA, Complete Freund's Adjuvant; CLP, cecal ligation and puncture; ConA, concanavalin A; CRP, C-reactive protein; DTH, delayed type hypersensitivity; DMM, destabilization of the medial meniscus; DNFB, 2,4-dinitro-1-fluorobenzene; DSS, dextran sulfate sodium; EAE, experimental autoimmune encephalomyelitis; EAU, experimental autoimmune uveitis; fMLF, N-Formyl-Met-Leu-Phe; G-003M, formulation of synthetic podophyllotoxin with rutin; GM-CSF, granulocyte-macrophage colony-stimulating factor; HCC, hepatocellular carcinoma; Hif1, hypoxia-inducible factor-1; i.a., intra-articular injection; i.g., intragastric administration; i.m., intramuscular injection; i.n., intranasal administration; i.p., intraperitoneal injection; i.v., intravenous injection; IRBP, inter photoreceptor binding protein; IRF-4/8, interferon regulatory factor 4/8; JEV, Japanese encephalitis virus; MCAO, middle cerebral artery occlusion model; MDSCs-G/M, myeloid-derived suppressor cells granulocytic/monocytic; MIP, macrophage inflammatory protein; OVA, ovalbumin; PAA, polyamidoamine; PC, picryl chloride; PCA, passive cutaneous anaphylaxis; PGN, peptidoglycan; p.o., oral administration; RCA, reversed cutaneous anaphylaxis; ROR-γt, retinoic-acid-receptor-related orphan nuclear receptor gamma; SRBC, sheep red blood cell; STZ, streptozotocin; TGR, thoracic gamma radiation; Th2, T-helper 2; TLR4, Toll-like receptor 4; TNBS, 2,4,6-trinitrobenzene sulfonic acid; TPA, 12-O-tetradecanoylphorbol-13-acetate; XOD, xanthine oxidase. Downward-pointing red arrows reflect the downregulatory action, upward-pointing green arrows reflect the upregulatory action.

3.5. Dibenzylbutyrolactone and Dibenzylbutyrolactol Skeletons

3.5.1. Arctigenin

Arctigenin showed strong DPPH radical scavenging activity in vitro and in vivo, improved survival of *C. elegans* under oxidative stress [84]. Arctigenin had multiple effects in various cellular and animal models, inhibiting ROS-induced activation of ERK1/2, PI3K/Akt, IKKβ, and NF-κB signaling pathways, followed by the suppression of pro-inflammatory enzymes such as COX, LOX, phospholipase A2 (PLA2) and phosphodiesterase (PDE), decrease in production of TGF-β1 and inflammatory cytokines (IL-1β, IL-4, IL-6, TNF-α, MCP-1). At the same time, additional activation of the AMPK and Nrf2 signaling pathways by arctigenin increased the expression of genes associated with antioxidants, including SOD, GR, GPx, Trx, HO-1, CAT, uncoupling protein 2 (UCP2), and promoted the secretion of IL-10 [80,83,155–157,186,216]. Arctigenin also inhibited ROS production in H₂O₂-treated rat primary astrocytes [82], scavenged free radicals and reduced the level

of cellular peroxide in glutamate-injured rat cortical neurons by directly binding to kainic acid receptors [77], thereby demonstrating its neuroprotective potential.

Arctigenin protected against LPS-induced lung inflammatory and oxidative damage [153], and, in IL-1 β -induced human osteoarthritis (OA) chondrocytes and mouse OA model, the lignan effectively decreased the level of pro-inflammatory mediators attenuating the progression of OA [189]. Arctigenin inhibited allergic inflammation type I as heterologous passive cutaneous anaphylaxis, type II as reversed cutaneous anaphylaxis, type III as the sheep red blood cell-induced Arthus reaction and contact dermatitis (type IV hypersensitive inflammation) in vivo as well as suppressed pro-inflammatory enzymes, such as COX, LOX, phospholipase A2 (PLA₂), and phosphodiesterase (PDE), in vitro [186]. Arctigenin possessed anti-inflammatory and immunosuppressive properties by inhibiting Th17 cell differentiation and proliferation in a model of experimental autoimmune encephalomyelitis (EAE), which indicates its therapeutic potential for multiple sclerosis treatment [217].

In another study, arctigenin showed anti-inflammatory effects in peptidoglycan- or LPS-induced peritoneal macrophages in vitro, LPS-induced systemic inflammation in vivo, and 2,4,6-trinitrobenzene sulfonic acid-induced colitis model [216]. Arctigenin also ameliorated LPS-induced inflammation in vitro and in vivo by enhancing the accumulation of granulocytic myeloid-derived suppressor cells (G-MDSCs) through miR-127-5p/IRF8 axis and the immunosuppressive role of MDSCs through the upregulation of Arg-1 and iNOS, thereby protecting from acute lung injury [187]. Arctigenin inhibited pro-inflammatory cytokines and chemokines in LPS-induced RAW264.7 murine macrophage-like cells in vitro as well as in vivo, remarkably reduced the congestion and necroinflammation of liver, decreased the infiltration of CD4 T and NKT cells and macrophages into the liver and suppressed T lymphocyte proliferation in a murine model of concanavalin A-induced acute hepatitis [188]. In LPS-primed human PBMCs and murine RAW264.7 cells in vitro and in imiquimod-induced murine psoriasis model in vivo, arctigenin inhibited activity of PDE4 and activated the cAMP-dependent protein kinase A/cAMP-response element binding protein (PKA/CREB) signaling, ameliorated psoriatic manifestations by decreasing the adhesion and chemotaxis of inflammatory cells, rectifying the immune dysfunction and hyperactivation of keratinocytes in the inflamed skin microenvironments, reducing the production of inflammatory cytokines and promoting the secretion of IL-10 [78,190].

In mice infected by Japanese encephalitis virus, arctigenin demonstrated a marked decrease in the levels of stress-associated signalling molecules, ROS/RNS and pro-inflammatory cytokine production, thereby reducing neuronal death, secondary inflammation and oxidative stress resulting from microglial activation [152]. Arctigenin protected against TGF- β 1-induced upregulation of a key mediator of tubulointerstitial inflammation MCP-1 and the resulting epithelial–mesenchymal transition-like phenotypic changes, thereby declaring arctigenin as therapeutic agent to treat renal tubulointerstitial fibrosis [83]. In bleomycin-induced skin fibrosis murine model, arctigenin reduced inflammation and oxidative stress, inhibited the transformation of fibroblasts into myofibroblasts, also showing antifibrotic potential [156]. In addition, arctigenin ameliorated silicosis-associated oxidative stress, immune-related inflammatory reaction, and fibrosis both in vitro and in vivo by inhibiting TLR-4/NLRP3/TGF- β signal transduction and increasing the mitochondrial membrane potential, which in turn inhibited the production of ROS, the polarization of macrophages, and the differentiation of myofibroblasts [88].

Arctigenin demonstrated anti-ulcer activity by reducing oxidative and inflammatory damage in the ethanol- and acetic acid-induced ulcerogenic models via the decrease in the levels of MDA, TNF- α , IL-6, IL-10, and C-reactive protein and the increase in the level of SOD in serum [151]. Arctigenin showed antiarrhythmic protective effect via the attenuation of myocardial ischemia/reperfusion (MI/R) injury by increasing the activities of antioxidant enzymes and reducing the level of MDA [154]. Arctigenin also attenuated apoptosis, inflammation, and oxidative stress in oxygen glucose deprivation-treated cardiomyocytes, improved the heart functions and decreased the infarct size in the acute MI/R-rats [87,155]. On the normal WRL68 hepatocytes exposed to oleic acid accumulation,

arctigenin demonstrated a protective effect on cell survival, lipid metabolism, oxidation stress, and inflammation [85]. Arctigenin mitigated cadmium-induced nephrotoxicity in rats by increasing GSH level and antioxidant enzyme activity providing protection against oxidative DNA damage [157].

A number of studies have suggested arctigenin as a potential chemotherapeutic agent against various premalignant and malignant cells. For example, arctigenin was shown to promote glucose-starved tumor cells to undergo necrosis by elevating the iROS level and inhibiting mitochondrial respiration and cellular energy metabolism in general [79]. Arctigenin also induced apoptosis of human breast cancer MDA-MB-231 cells via the triggering of the mitochondrial caspase-independent ROS/p38 MAPK pathway and epigenetic Bcl-2 downregulation [81]. In another study, arctigenin promoted apoptosis in human hepatocellular carcinoma-related Hep G2 cells via the enhancement of the ROS-mediated mitochondrial dysfunction, p38 and JNK and MAPK pathways activation as well as CYP450 and Bax upregulation [86].

The potential toxicity of arctigenin was demonstrated in a toxicological study of the subchronic toxicity profile for 28 days, where even the lowest dose of 12 mg/kg caused significant side effects in rats, including accumulation of arctigenin in organs and irreversible side effects in several tissues (focal necrosis, lymphocytic infiltration in the renal cortex, liver lobules and prostate) [223].

3.5.2. Carissanol

Carissanol showed moderate DPPH free radical scavenging activity three times weaker than a well-known antioxidant quercetin [96], although in another study (–)-carissanol showed almost equal potential like that of Trolox [224].

3.5.3. Hinokinin

Hinokinin exerted a significant antioxidant effect by inhibiting the accumulation of H₂O₂ produced by *Trypanosoma cruzi* mitochondria in the presence of the pro-oxidant compound, tert-butyl hydroperoxide, showed a protective effect against the chromosome damage induced by the free radicals generated by doxorubicin [89]. In another study, hinokinin inhibited the secretion of TNF- α and IL-6 in LPS-stimulated human leukemia monocytic (THP-1) cell line [191]. In the high fat diet/streptozotocin-induced cardiac injury model of type 2 diabetes, hinokinin significantly protected against oxidative stress, inflammation, and apoptosis via the modulation of Nrf2/Keap1/ARE pathway, MAPKs (JNK, p38 and ERK1/2) and TLR4/MyD88/NF- κ B mediated inflammatory pathways and mitochondrial-dependent (intrinsic) apoptosis pathway [158].

3.5.4. Matairesinol and Its Derivatives

Matairesinol showed strong superoxide, peroxy, and DPPH radical scavenging activity and improved survival of *C. elegans* under oxidative stress [69,70,84,90,91]. Matairesinol suppressed mitochondrial ROS generation and decreased hypoxia-inducible factor-1 α (HIF-1 α) in hypoxic HeLa cells, inhibited proliferation of human umbilical vein endothelial cells [92]. In another study, matairesinol in vitro inhibited Th17 cell differentiation via MAPK/ROR- γ t signaling pathway and in vivo restrained an interphotoreceptor retinoid-binding protein-specific Th17 proliferation, infiltration and cytokine production, alleviated intraocular inflammation in the eye in the model of experimental autoimmune uveitis [192]. In rat sepsis model by CLP and the model of LPS-induced neuronal damage, matairesinol exerted neuronal protection, anti-inflammatory and anti-oxidative stress effects by upregulating AMPK and Nrf2/HO-1 pathways and inactivating the MAPK and NF- κ B pathways, thereby ameliorating sepsis-mediated brain injury [93].

7'-hydroxymatairesinol showed antioxidative potency and peroxy radical scavenging capacity similar to that of Trolox [69] and also exhibited excellent scavenging of DPPH radicals reacting at the level of ascorbic acid and surpassing 2,6-di-tert-butyl-4-methylphenol (BHP) in activity [70,94]. In addition, 7'-hydroxymatairesinol demonstrated significant

anti-inflammatory effects by inhibiting NF- κ B and ERK phosphorylation in human aortic endothelial cells [193].

3.5.5. Nortrachelogenin

(-)-Notrachelogenin showed strong antioxidative potency and DPPH free radical, superoxide, and peroxy radical scavenging activity, more effective than both BHA and Trolox [56,69,70,90,96,97]. Nortrachelogenin was also able to reduce the basal level of peroxides in Jurkat cells as well as counteracted peroxide increase induced by BHP treatment [97]. In another study, (+)-notrachelogenin showed moderate anti-DPPH free radical activity 4.5 times weaker than a well-known antioxidant L-ascorbic acid [95]. The anti-inflammatory effect of notrachelogenin was demonstrated in mouse carrageenan-induced paw inflammation model and on LPS-activated murine J774 macrophages [194].

3.6. Furanoid Skeletons

3.6.1. Lariciresinol

(+)-Lariciresinol possessed significant antioxidant potential in various in vitro models. Lariciresinol revealed very strong DPPH-, ABTS-, superoxide-, and hydroxyl-radical scavenging activity, exhibited strong lipid peroxidation inhibition as well as ferric- and cupric-reducing power [26,27,69,70,98,99]. Lariciresinol inhibited ROS generation in HL-60, AAPH-treated and intact RAW 264.7 cells. Also, it increased transcriptional and translational levels of detoxifying antioxidant enzymes via Nrf2-p38 signaling [26,99].

3.6.2. Nectandrin B

Nectandrin B reduced senescence of cells by reducing cellular oxidative stress via the direct radical scavenging or indirectly via the induction of antioxidant enzymes through the activation of AMPK. Nectandrin B exerted DPPH radical scavenging equal to the well-known antioxidants Tempo and NAC, significantly reduced H₂O₂- and palmitic acid-induced iROS production in both young and old human diploid fibroblasts (HDFs), stimulated the expression of SOD I and II in old HDFs, increased activation of PI3K and Akt, and reversed the activity of ERK1/2 and p38 [100]. In another study, nectandrin B showed an anti-inflammatory effect by inhibiting NO production in IL-1 β -stimulated rat hepatocytes [218].

3.6.3. Olivil

(-)-Olivil showed moderate anti-DPPH free radical activity [56] and also possessed moderate anti-NO production activity in LPS-activated RAW264.7 cells [195].

3.6.4. Taxiresinol

Taxiresinol possessed strong DPPH radical scavenging activity (IC₅₀ 18.4 μ M), superior to that of a well-known antioxidant caffeic acid (IC₅₀ 25.5 μ M), and comparable to the activity of ascorbic acid (IC₅₀ 12.6 μ M) [68]. Taxiresinol exhibited strong anti-inflammatory potential by inhibiting the release of leukotriene C₄ (LTC₄) in rat basophilic leukemia (RBL-1) cells [196], showed moderate inhibitory activity of NO production in LPS-activated RAW264.7 cells [195]. Taxiresinol weakened the carrageenan-induced inflammatory process by reducing the swelling thickness of the hind paw by 27% [219].

3.7. Furofuran Skeletons

3.7.1. Acanthoside B

Acanthoside B isolated from *Salicornia europaea* substantially attenuated AD-like amnesic traits in mice by restoring the cholinergic activity, endogenous antioxidant status, and suppressing neuroinflammation [220].

3.7.2. Dendranlignan A

A bisepoxylic lignan dendranlignan A, isolated from the flowers of *Dendranthema morifolium* (Ramat.), was found to inhibit the ROS formation and decrease the levels of inflammatory cytokines and the nuclear localization of c-JUN, p65 and IRF3 in LPS-induced H9c2 cells, thereby suggesting that the lignan inhibits TLR4 signaling. Although no effect on TLR4 production was shown, it was predicted by molecular docking that dendranlignan A can occupy the ligand-binding sites of TLR4 receptor [103].

3.7.3. Diayangambin

(+)-Diayangambin showed immunosuppressive and anti-inflammatory activity in vitro and in vivo. Diayangambin inhibited human mononuclear cell proliferation and reduced the level of PGE₂ in stimulated RAW 264.7 macrophages. When administered orally, diayangambin reduced ear swelling in mice treated by 2,4-dinitrofluorobenzene. Also, in a model of carrageenan paw edema, this lignan significantly decreased inflamed paw volume and PGE₂ levels [197].

3.7.4. Fargesin

Fargesin was found in several species of Magnolia. It demonstrated anti-inflammatory properties via the suppression of PKC pathway, including downstream JNK, nuclear factors AP-1, and NF-κB [198]. In another study, fargesin ameliorated chemically induced inflammatory bowel disease in mice, reducing inflammatory infiltration, production of NO and cytokines. The effects were shown to be associated with NF-κB signaling suppression [199]. Fargesin also inhibited atherosclerosis in experimental mice by reducing inflammatory response via TLR4/NF-κB pathway [221]. In a rat MI/R injury model, it was shown that fargesin also had antioxidant properties by reducing the level of ROS and MDA and increasing the level of antioxidant enzymes [159].

3.7.5. Isoeucemmin A

Isoeucemmin A, a lignan compound from *Eucommia ulmoides* Oliv, showed protective effects in diabetic nephropathy and alleviated kidney injury by reducing inflammation and oxidative stress in vitro and in vivo [104].

3.7.6. Koreanaside A

Koreanaside A showed high radical scavenging activity with oxygen radical absorbance capacity (ORAC) values of 0.97 ± 0.01 and inhibited TNF-α-induced vascular cell adhesion molecule-1 (VCAM-1) expression in mouse vascular smooth muscle (MOVAS) cells [105]. Koreanaside A inhibited the activation of activator protein-1 (AP-1), NF-κB, and JAK/STAT pathways and the subsequent induction of pro-inflammatory mediators in LPS-stimulated RAW 264.7 macrophages and dextran sulfate sodium (DSS)-induced colitis mice models, thus demonstrating a potential in the treatment of inflammatory bowel disease [200].

3.7.7. Phylligenin

Phylligenin demonstrated anti-inflammatory activity in vitro and in vivo by reducing the production of PGE₂ and NO, suppressing NK-κB activation, and inhibiting carrageenan-induced paw edema in mice. Phylligenin also attenuated liver fibrosis partly via the modulation of inflammation and gut microbiota [201,222].

3.7.8. Pinoresinol and Its Derivatives

Pinoresinol exhibited a significant antioxidant potential in hydroxyl and DPPH radical scavenging assays [27,56,70,97] with ORAC comparable to Trolox [105]. Pinoresinol showed moderate inhibitory activity against lipid peroxidation induced by non-enzymic Fe(II)-ascorbic acid system in rat liver microsomes [107] and 1.8 times stronger inhibitory activity to Cu²⁺-induced low-density lipoprotein (LDL) oxidation over probucol [106]. In intact

human lung epithelial Beas-2B cells, pinoreesinol promoted the nuclear translocation and stabilization of Nrf2 followed by the activation of downstream cytoprotective genes, NQO1 and γ -GCS. Furthermore, pinoreesinol treatment protected human lung epithelial cells against sodium arsenite-induced oxidative insults by increasing the intracellular GSH level and inhibiting ROS production via Nrf2-mediated antioxidant response [108]. Pinoreesinol also demonstrated anti-inflammatory properties by decreasing the secretion of PGE₂, IL-6, and MCP-1 (but not IL-8) and inhibiting the NF- κ B activation in IL-1 β -treated human colon adenocarcinoma (Caco-2) cells [202].

4-Ketopinoreesinol has been shown to possess a significant antioxidant potential. 4-Ketopinoreesinol displayed strong DPPH free radical scavenging activity and the ability to reduce the basal level of peroxides in Jurkat cells, counteracted BHP-induced peroxide increase [97,101]. 4-Ketopinoreesinol protected against H₂O₂-induced cell injury, oxidative stress-induced DNA damage and cell death via scavenging ROS directly and increasing Akt phosphorylation with the following nuclear translocation of Nrf2 for the expression of ARE-dependent cytoprotective genes [102].

Pinoreesinol diglucoside (PDG) inhibited oxidized low-density lipoprotein, (oxLDL)-induced upregulation of the ROS production and lipid peroxidation, relieved the inhibition of SOD activity, and inhibited p38MAPK/NF- κ B activation in human umbilical vein endothelial cells (HUVECs) [109]. Intragastric administration of PDG ameliorated memory dysfunction and attenuated neuroinflammation, neuronal apoptosis and oxidative stress through the TLR4/NF- κ B and Nrf2/HO-1 pathways in the model of A β -infused mice. Mechanistically, PDG restrained the release of pro-inflammatory cytokines (TNF- α and IL-1 β), ROS, and MDA, promoted the activity of the antioxidant enzymes (SOD and CAT), Nrf2 and HO-1 expression, upregulated the ratio of Bcl-2/Bax and downregulated cytochrome C as well as significantly reduced the expression of TLR4 and the activation of NF- κ B p65 [160]. PDG also alleviated inflammation and oxidative stress developing during the MCAO-induced neurological dysfunction of the mice, reducing the infarct volume, brain water content, and neuron injury [161].

3.7.9. Sesamin

Sesamin, an abundant lignan in sesame seeds and oil, ameliorated oxLDL-mediated vascular endothelial dysfunction and showed the antiatherogenic action through its ability to counteract the ROS generation, the impairment of antioxidant enzymes, and the activation of the expression of IL-8 and NF- κ B [110]. As an important component of the immune reaction, the response of human leukocytes to chemoattractants can also be regulated by sesamin. Sesamin significantly attenuated bacterial chemotactic peptide fMLF-induced leukocyte chemotaxis and inhibited ERK1/2 phosphorylation and NF- κ B activation in ETFR cells expressing fMLF-specific receptor FPR in vitro and, in a murine air-pouch model in vivo, suppressed leukocyte infiltration induced by fMLF [203].

In addition, sesamin attenuated allergic responses mediated by mast cells in vivo and in vitro. Sesamin inhibited IgE-induced anaphylactic reactions by blocking histamine release and pro-inflammatory cytokine expression [204]. In aortic tissue of diabetic rats, sesamin attenuated oxidative stress by reversing the increased MDA content and the reduced activity of SOD [162]. Sesamin protected the femoral head from osteonecrosis by inhibiting the ROS-induced osteoblast apoptosis [112]. Sesamin protected against ulcerative colitis in colorectal adenocarcinoma Caco-2 cells injured by H₂O₂-induced oxidative stress [113]. Sesamin feeding protected adult *Drosophila* against oxidative damage [171].

The neuroprotective potential of sesamin has been demonstrated in several studies. Sesamin showed reversal effect in unilateral striatal 6-hydroxydopamine (6-OHDA) model of Parkinson's disease (PD), which included attenuation of oxidative stress via lowering striatal level of MDA and ROS and improving SOD activity [167]. In the kainic acid-induced status epilepticus brain injury model, sesamin demonstrated anti-inflammatory and antioxidative effects via decreasing MDA content and ROS level as well as reducing PGE₂ production [111]. Sesamin also demonstrated neuroprotective effects in H₂O₂-treated

human neuroblastoma (SH-SY5Y) through the expression of the antioxidant enzymes leading to the elimination of the excessive ROS production, activation of SIRT1-SIRT3-FOXO3a expression and upregulation of anti-apoptotic Bcl-2 [114].

Sesamin decreased oxidative stress and injury in the liver and kidneys of doxorubicin-treated rats [166]. Sesamin significantly prevented nickel-induced hepatotoxicity. Sesamin reversed the elevation of ROS production and depletion of the intracellular GSH level, restored the activities of antioxidant enzymes and decreased 8-OHdG levels (marker of oxidative DNA damage), increased expression levels of PI3K and phosphorylated Akt, which in turn led to the inactivation of pro-apoptotic signaling events in the liver of nickel-treated mice [163]. Sesamin also mitigated CCl₄-induced hepatotoxicity by suppressing the elevation of the ROS production, oxidative stress, and apoptosis in mouse liver [164]. Orally supplemented sesamin acted as a protective agent against LPS-induced lipid peroxidation in both serum and liver by restoring the loss of SOD (but not CAT and GR) activity and reducing serum levels of TNF- α , MCP-1, and IL-1 β [168]. In another study, sesamin attenuated carrageenan-induced lung inflammation and injury in rats by indirectly inhibiting NF- κ B pathway through the upregulation of A20 and TAX1BP1 [205]. It also abrogated LPS-induced acute kidney injury via the attenuation of renal oxidative stress, inflammation, and apoptosis, and returning the renal oxidative stress-related parameters [169], thereby demonstrating potential against injuries in septic conditions. Sesamin possessed mitigative action on cisplatin (CP) nephrotoxicity in rats by reversing the CP-induced oxidative stress and inflammation [170]. In addition, sesamin significantly alleviated fluoride-induced renal oxidative stress and apoptosis of carp *Cyprinus carpio* [165].

Epi-sesamin induced potent inhibition of endothelial protein C receptor shedding induced by PMA, TNF- α , IL-1b, and CLP operation, which affected the regulation of blood coagulation [206].

3.7.10. Syringaresinol

Syringaresinol (also known as liriouresinol B) exhibited potent antioxidant activities in hydroxyl and DPPH radical scavenging assays [27,101]. In a cardiomyocyte model of I/R injury following H/R, syringaresinol decreased the levels of ROS, increased the expression of antioxidant genes, and also stimulated the nuclear localization and activity of FOXO3 followed by the degradation of HIF-1 α that provided a protective effect against cellular damage and death [115]. Syringaresinol oral administration lowered the levels of lipid peroxide marker 8-isoprostane and iROS in cultured primary fibroblasts from the skin of Sod1^{-/-} mice as well as regulated the FOXO3/MMP-2 axis in oxidative-damaged skin and exhibited beneficial effects on age-related skin involution [172].

Anti-inflammatory efficacy of syringaresinol was demonstrated in various in vitro and in vivo experiments. In LPS-stimulated RAW 264.7 cells and in a carrageenan-induced hind paw edema assay, syringaresinol downregulated NF- κ B expression by interfering with JNK and p38 phosphorylation followed by the decrease in mRNA levels of iNOS, COX-2, TNF- α , IL-1 β , and IL-6, thus suggesting its significant therapeutic potential [207]. Syringaresinol inhibited the release of LTC₄ in RBL-1 cells [196].

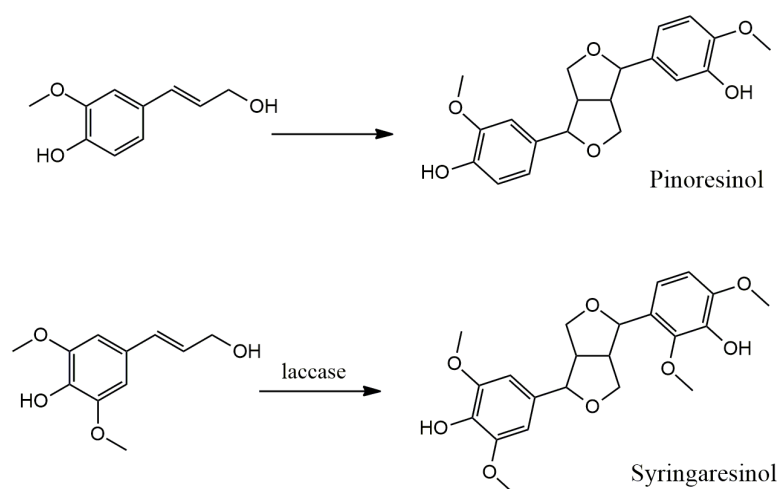
Syringaresinol also played a protective role against sepsis-induced cardiac inflammation and LPS-induced cardiomyocyte damage, suggesting its possible role in alleviating cardiac dysfunction. Levels of inflammatory cytokines were significantly reversed by the administration of the lignan after the increase elicited by CLP operation. The activation of estrogen receptor was shown to be essential for the cardioprotective function of syringaresinol [208]. On streptozotocin-induced type 1 diabetic mice and high glucose-injured neonatal cardiomyocytes, syringaresinol demonstrated anti-inflammatory, anti-fibrotic, and anti-oxidant effects through Keap1/Nrf2 system and TGF- β /Smad signaling pathway [116]. Thus, the above series of studies allows syringaresinol to be considered as a therapeutic agent for the treatment of cardiomyopathy. In addition, syringaresinol demonstrated anti-neuroinflammatory effects in microglia cells and wild-type mice. Estrogen receptor β was found to be implied in the anti-inflammatory activity of the lignan in BV2 microglia [209].

4. Main Approaches for Lignan Synthesis

Reviews over the past decades describe a huge variety of different approaches for the racemic or enantioselective synthesis of plant lignans. Overall, the key step is the dimerization of two monomers that are derivatives of coniferyl alcohol. The difference among chemical strategies for obtaining lignans depends on the skeleton peculiarities provided by natural biosynthesis. Wide varieties of elegant methods to obtain these compounds have been already published. Classical pathways include oxidative dimerization, the Diels-Alder reaction, aldol reaction, and the Stobbe condensation [225,226].

4.1. Oxidative Dimerization

The first attempts to synthesize lignans by oxidative dimerization of cinnamon derivatives included the oxidative coupling of phenols and their esters in the presence of various enzymes. Thus, synthetic analogs of pinoresinol and syringaresinol, respectively, were obtained from cinnamic alcohol derivatives under the catalytic action of enzymes isolated from *Caldariomyces fumago* [227] and other fungi [228], respectively (Scheme 1). The final compounds were obtained as a racemic mixture of isomers, and there was an overall low yield due to the side products formation.



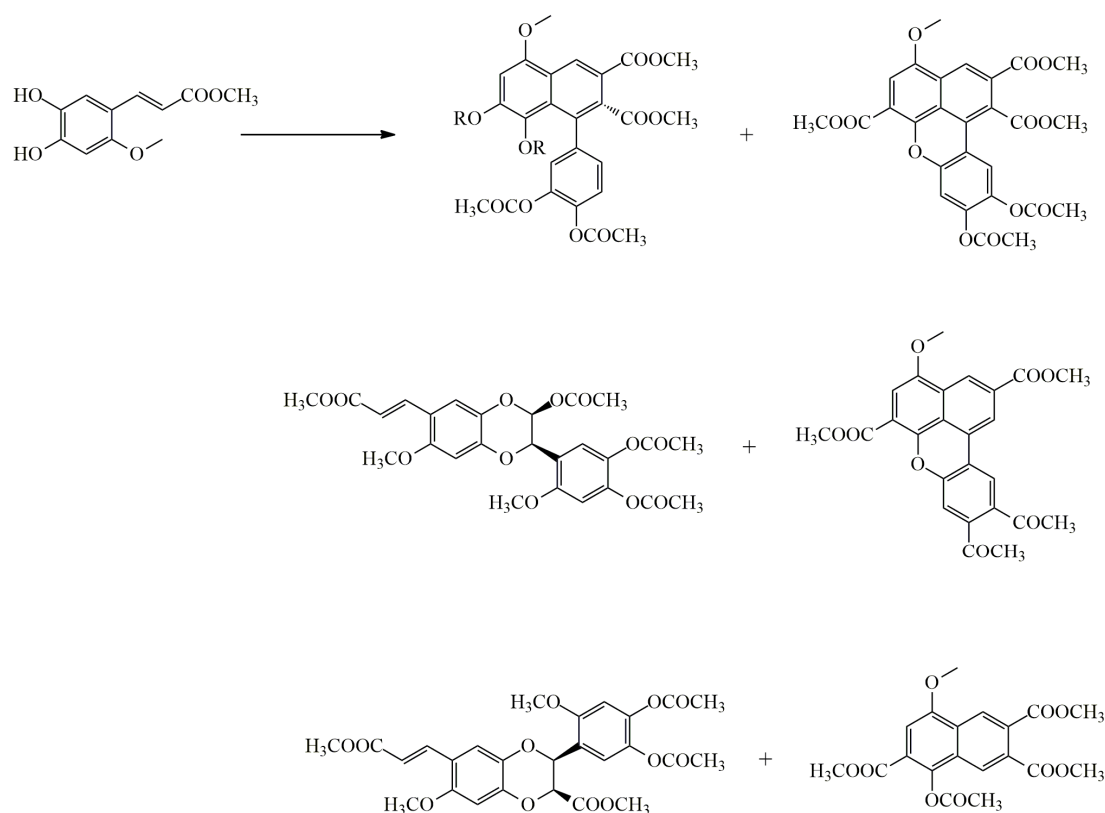
Scheme 1. Biomimetic pathway to obtain lignans from natural sources.

The method of oxidative dimerization of cinnamic acid esters derivatives with the use of inorganic compounds as catalysts emerged as the most effective from a practical point of view. The use of oxidizing agents such as FeCl_3 , $\text{K}_3[\text{Fe}(\text{CN})_6]$, Ag_2O , MnO_2 , H_2O_2 , $\text{Pb}(\text{C}_2\text{H}_3\text{O}_2)_4$ and various peroxidases is common in the developing of synthetic methods for obtaining analogs of natural lignans [225].

Nowadays, a large number of papers are devoted to investigation of an oxidizing agent effect on the oxidative coupling reaction efficiency. Thus, in the work of Maeda et al., their influence on dimerization of methyl (E)-3-(4,5-dihydroxy-2-methoxyphenyl) propionate was studied [229]. By-products predominantly were formed when Ag_2O was used in a benzene–acetone mixture at room temperature, and the yield of the target dihydronaphthalene derivative was quite low (28%). The obtained compounds were subjected to acylation reaction in the presence of pyridine for a more accurate separation by column chromatography. Scheme 2 describes in more detail possible by-products of the oxidative dimerization carried out in the presence of Ag_2O .

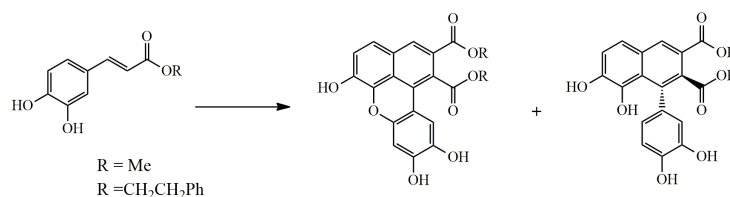
Further attempts to use this method for phenylpropanoid dimerization confirmed negative role of Ag_2O leading to the formation of a complex mixture that makes it difficult to separate the target product. Thus, attempt of dimerization in methylene chloride with two equivalents of silver oxide at room temperature led to the predominant formation of neolignans instead of lignans. The yield of 1,2-dihydronaphthalene derivative was less

than 1%. The shift of this reaction towards neolignans formation was also confirmed by Lemierre et al. [230].



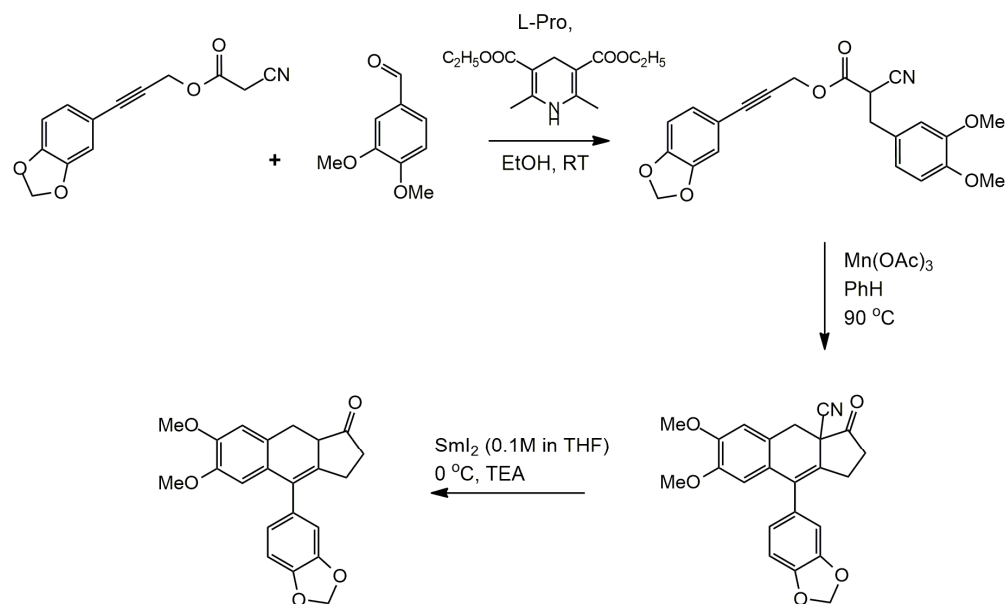
Scheme 2. Possible products of oxidative dimerization reaction when Ag_2O used as an oxidizing agent.

In the same work, it was found that the presence of Mn^{2+} ions shift the dimerization towards the formation of benzoxanthine derivatives. Thus, Dakino et al. performed the oxidative coupling reaction of caffeic acid phenethyl ester in methylene chloride in the presence of 10 equivalents of MnO_2 for 4 h at room temperature. Further analysis of the reaction mixture by HPLC-UV revealed two main products: dihydronaphthalene derivative and benzoxanthine (Scheme 3). After purification on silica gel using column chromatography, the total yield of 16.5% for the first compound and 48% for the second one was achieved. When the solvent was changed to chloroform, the ratio of the obtained substances changed in favor to the benzoxanthine derivative (51%), while only 7% of the aryl dihydronaphthalene lignan was formed. The use of $\text{Mn}(\text{acac})_2$ instead of MnO_2 led to a similar result, and dihydrobenzofuran neolignans were not observed in the reaction mixture. To shift the reaction direction towards benzoxanthine lignans, 4 equivalents of $\text{Mn}(\text{OAc})_3$ in chloroform were used. A larger amount of oxidizing agent led to tarring of the reaction mixture and the yield reduction. As a result, 71% of benzoxanthine lignan and 22% of aryl dihydronaphthalene derivative were formed (Scheme 3) [231].



Scheme 3. Oxidative dimerization reaction in the presence of $\text{MnO}_2/\text{CH}_2\text{Cl}_2$ or CHCl_3 and in the presence of $\text{Mn}(\text{OAc})_3/\text{CHCl}_3$ at room temperature for 4–6 h lead to two main compound formation.

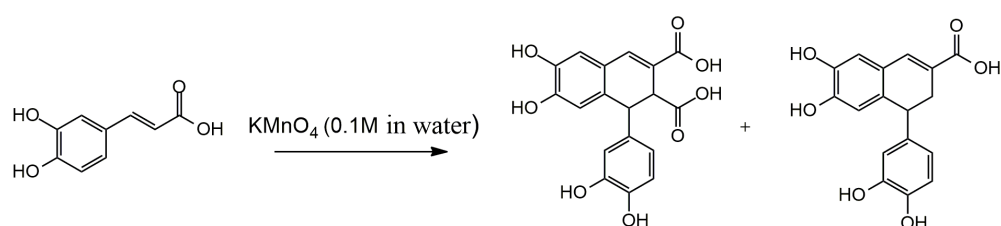
In 2015, a synthesis of three aryl naphthalene derivatives (retrojusticidin B, justicidin E, and helloxanthin) was published using $\text{Mn}(\text{OAc})_3$ as an oxidizing reagent [232]. In this publication, dimerization of carbonitrile was obtained by Knoevenagel condensation of α -cyanoether and an aldehyde with the yield of 67%. Next, the intermediate obtained as a result of dimerization was reduced to the final lignan (Scheme 4).



Retrojusticidin B

Scheme 4. Synthesis of retrojusticidin B using $\text{Mn}(\text{OAc})_3$ as an oxidizing agent at carbonitrile dimerization.

An aqueous solution of 0.1 M KMnO_4 was also tested as an oxidizing agent. In this case, the oxidative coupling was performed from caffeic acid in distilled water in the presence of 0.2 equivalents of potassium permanganate. A 1,2-dihydronaphthalene compound was formed as a by-product in the reaction with the loss of one carboxyl group. The yields observed in this reaction were quite low [233] (Scheme 5).

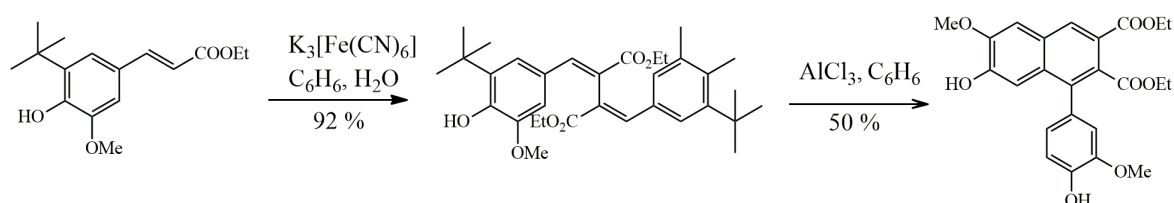


Scheme 5. Dimerization of caffeic acid in the presence of KMnO_4 as an oxidizing agent.

In Maeda's study the selection of potassium hexacyanoferrate $\text{K}_3[\text{Fe}(\text{CN})_6]$ as an oxidizing agent was also studied. Oxidative coupling in the presence of 1.2 equivalents of $\text{K}_3[\text{Fe}(\text{CN})_6]$ and 5 equivalents of sodium carbonate made it possible to obtain 20% of the aryl dihydronaphthalene derivative and 2% of benzoxanthine derivatives as by-products. At the same time, only 13% of the aryl dihydronaphthalene derivative was isolated when using a similar amount of potassium hexacyanoferrate and 1.5 equivalents of 1% sodium carbonate in chloroform solution at room temperature. Benzoxanthine and naphthalene derivatives emerged as by-products [229] (Scheme 6).

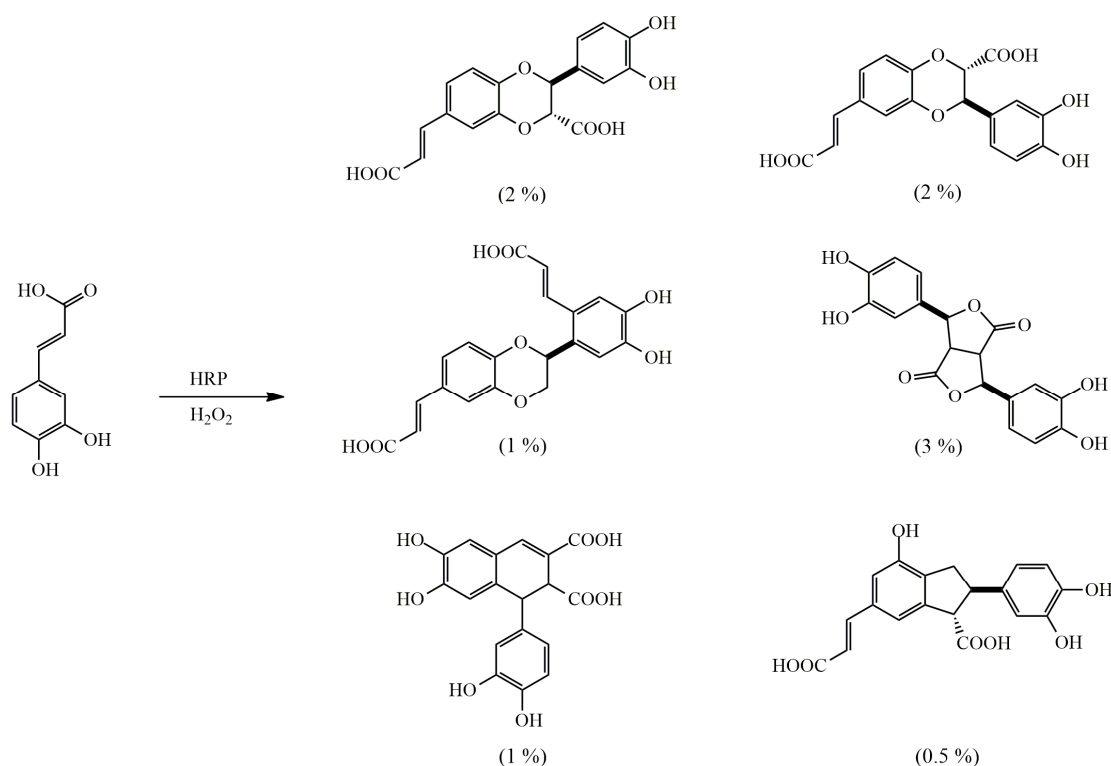
Potassium hexacyanoferrate was also used in the scheme for the preparation of synthetic lignans to obtain neolignans and further transformation into an aryl dihydronaphthalene product by the Friedel–Crafts reaction in the presence of AlCl_3 [234]. The resulting product could be further modified in order to synthesize the necessary analogs of natural

compounds with biological activity. Scheme 6 shows the synthetic pathway for the formation of dimeric products. The oxidative coupling of the protected phenylpropanoid derivative was carried out in a two-phase benzene-water system in the presence of 5.5 equivalents of KOH and 2.5 equivalents of $K_3[Fe(CN)_6]$ in an inert atmosphere at room temperature for 30 min. The yield was 92%.



Scheme 6. Application of the Friedel-Craftz method for the synthesis of natural lignans.

Hydrogen peroxide and horseradish peroxidase (HRP) are also known as catalysts for oxidative dimerization. In 2002, a group of Japanese scientists obtained americanol A and isoamericanol A [235]. Caffeic acid derivatives were used as the starting material, which reacted at room temperature in the presence of H_2O_2 in phosphate buffer (0.1 M, pH 6.0) with 18% dioxane and HRP as a catalyst. The main reaction products were benzodioxane derivatives, which were the target natural lignans. Aryl dihydronaphthalene derivatives were found only as by-products in minor amounts (Scheme 7). Later publications confirmed the possibilities of HRP use as a catalyst in the presence of hydrogen peroxide for the synthesis of other lignans [236].

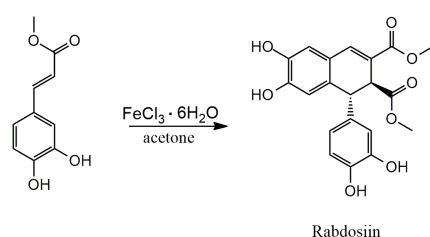


Scheme 7. Products of the oxidative coupling reaction of caffeic acid with horseradish peroxidase (HRP) and H_2O_2 .

Another alternative method of oxidative dimerization is the oxidation of caffeic acid with oxygen at pH~8.5 [237]. The described products obtained by this method were identical to the dimerization method described above using HRP (Scheme 7). The exact yield for obtained compounds was not published. However, such method had a rather

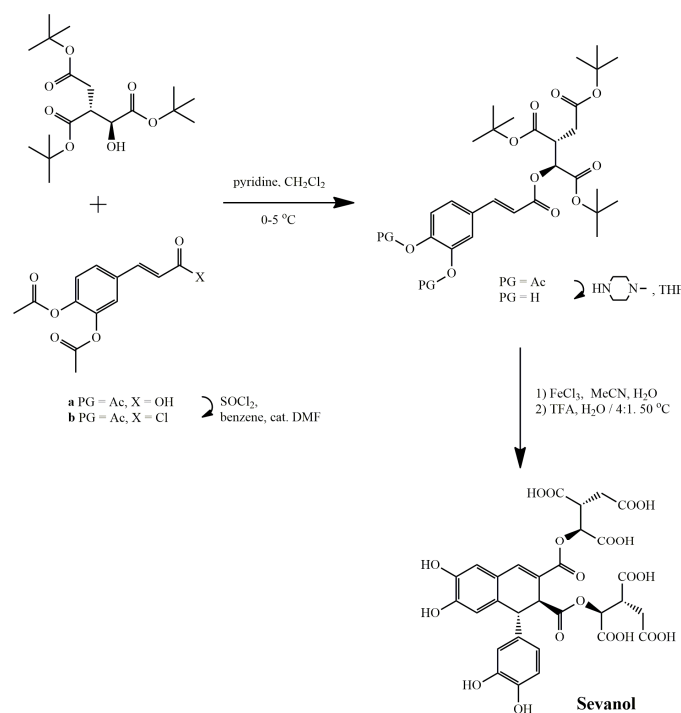
low selectivity and was not suitable for the targeted preparation of a desired product by oxidative coupling reaction.

The most common method for the synthesis of aryldihydronaphthalene derivatives is oxidative dimerization in the presence of FeCl_3 . In 1989, rabdosiin was obtained for the first time in the form of a racemic mixture [238]. Methyl caffeate was used as the starting material (Scheme 8). Next, the oxidative coupling was carried out in acetone at room temperature in the presence of $\text{FeCl}_3 \cdot 6\text{H}_2\text{O}$. The yield was 28%. Later, Boguki et al. conducted a study on the production of rabdosiin under varied conditions (changed solvents, the amount of FeCl_3) [239]. The most optimal conditions for dimerization were a mixture of acetone-water in a ratio of 2:1 and 2.2 equivalents of FeCl_3 . At the same time, the use of THF as a solvent led to decreased selectivity and reaction rate. In the course of the reaction, aryldihydronaphthalene derivatives were formed as a mixture of diastereomers as the main reaction products and benzoxyfuran derivatives as minor products.



Scheme 8. Synthesis of rabdosiin by dimerization of methyl caffeate in the presence of $\text{FeCl}_3 \cdot 6\text{H}_2\text{O}$.

In 2021, Belozerova et al. successfully applied the method of oxidative dimerization using FeCl_3 as an oxidative reagent to produce aryldihydronaphthalene lignan sevanol [121]. Crucial coupling step of isocitrate of caffeic acid was applied using optimal reaction medium carefully selected before [240]. The sevanol molecule was obtained in thirteen synthetic steps from malic acid with a 3% overall yield (Scheme 9). The construction of a dihydronaphthalene ring by oxidative dimerization of a protected dihydroxycinnamic acid ester was carefully researched.

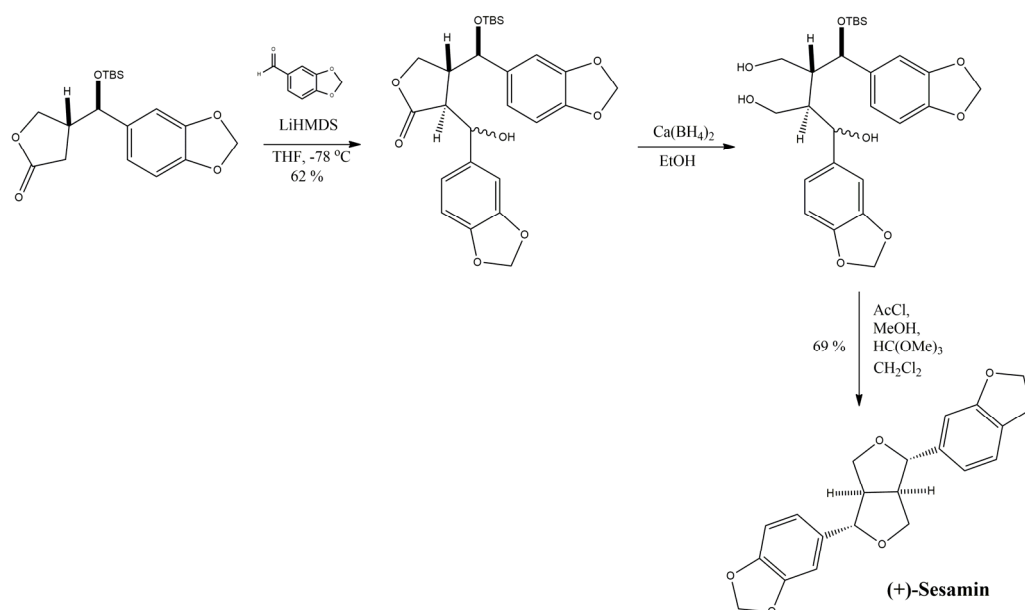


Scheme 9. The synthesis of sevanol (principal reactions).

4.2. Classical Cyclization and Non-Phenolic Oxidative Dimerization

The classical approach to the cyclization of phenylpropanoid subunits by dimerization in the presence of oxidizing agents is often accompanied by low yields due to the formation of a large amount of by-products as discussed above. Undesired by-products formation hampered isolating the target compound from the complex reaction mixture. This problem could be avoided with the use of alternative methods for lignans production via condensation or cyclization. Also, similar methods are used as intermediate stages in order to obtain varied analogues of natural compounds [234,241].

In 2014, Ishikawa et al. showed the complete synthesis of (+)-sesamin using aldol reactions to form the key lactone intermediate [242]. After reduction of lactone and subsequent treatment with HCl in situ, using AcCl in the presence of MeOH, Ishikawa et al. could obtain the desired furofuran ring of (+)-sesamin (Scheme 10).



Scheme 10. The synthesis of (+)-sesamin.

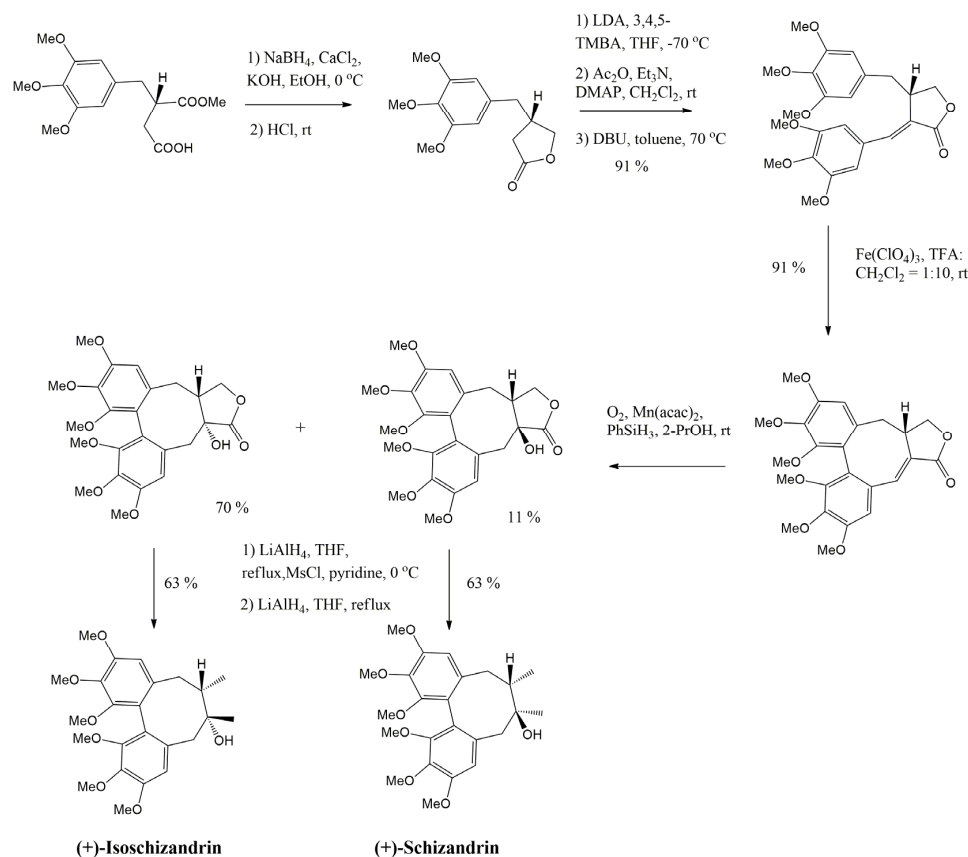
In 1995, Tanaka et al. developed a method for the total synthesis of (+)-schizandrin, (+)-gomisin A and (+)-isoschizandrin, as well as their further optimization, which enabled obtaining similar dibenzoylbutyrolactone lignans with good yield [243]. The demonstrated method includes the use of both oxidative coupling and classical cyclization approaches. The authors obtained a key lactone using aldol condensation, which subsequently underwent oxidative dimerization in the presence of iron (III) perchlorate in trifluoroacetic acid and dichloromethane. Further successive transformations made it possible to obtain (+)-schisandrin, (+)-isoschizandrin and gomisin A (Scheme 11).

A similar synthesis strategy allowed Tanaka et al. to obtain other dibenzocyclooctane lignans, namely, gomisin N, J, schizandrin B, (-)-deoxyschizandrin, wuweizisu C, kadsurin (Scheme 12) [244].

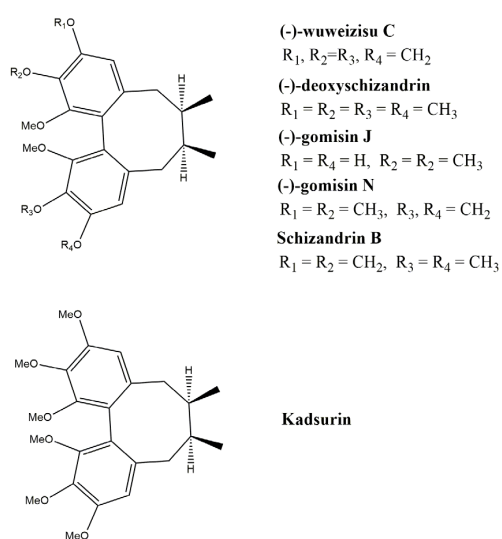
Fischer et al. demonstrated another example of aldol condensation followed by domino radical reaction in order to build the desired skeleton of lignans which were supposed to be (-)-arctgenin and (-)-matairesinol and its analogues [245]. Thus, they could develop and optimize an elegant approach that helped to produce similar dibenzoylbutyrolactones in a good yield (Scheme 13).

One of the classical cyclization methods is the Stobbe condensation that is used in the most of cases in order to build the basic skeleton of a desired lignan. In 2010, an efficient route of nordihydroguaiaretic acid synthesis (NGDA), (-)-saururenin and their analogues was described by Xia et al. [246]. The synthetic pathway was based on a unified synthetic strategy involving the Stobbe reaction and subsequent alkylation to construct

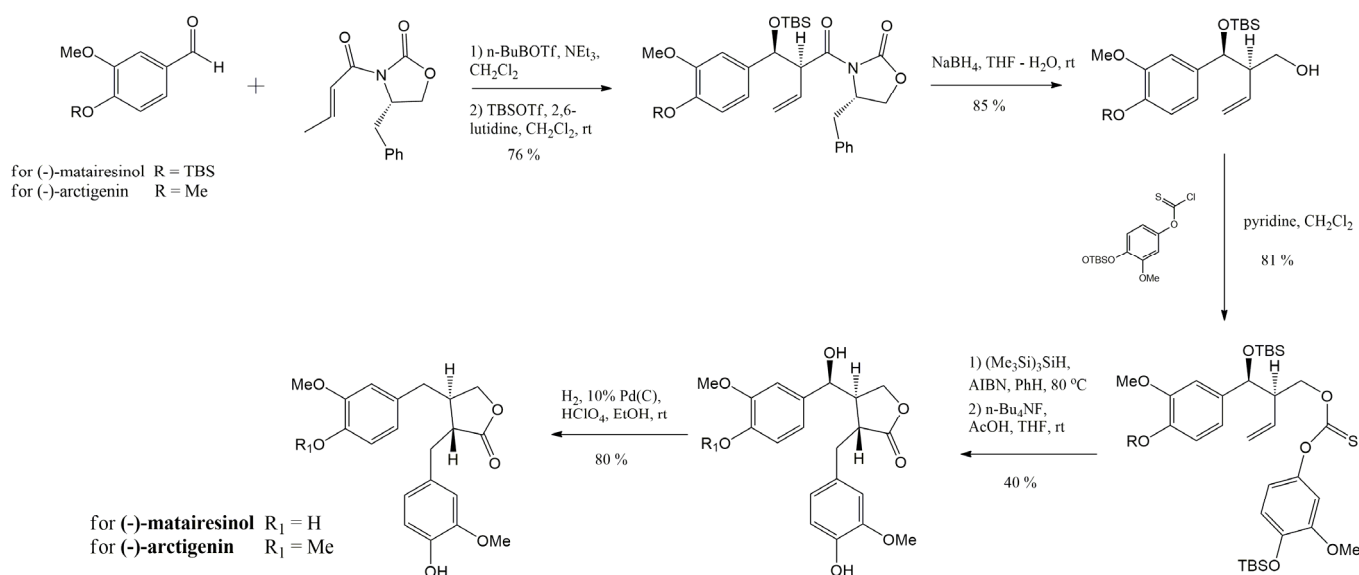
lignan skeletons. The corresponding aldehyde was chosen as a starting molecules for the condensation reaction with diethyl succinate followed by treatment with LDA and 3,4-methylenedioxybenzyl bromide to give the desired diester as a product of condensation. Next, after the subsequent transformation of key intermediates, it became possible to prepare the target dibenzylbutane lignans (Scheme 14).



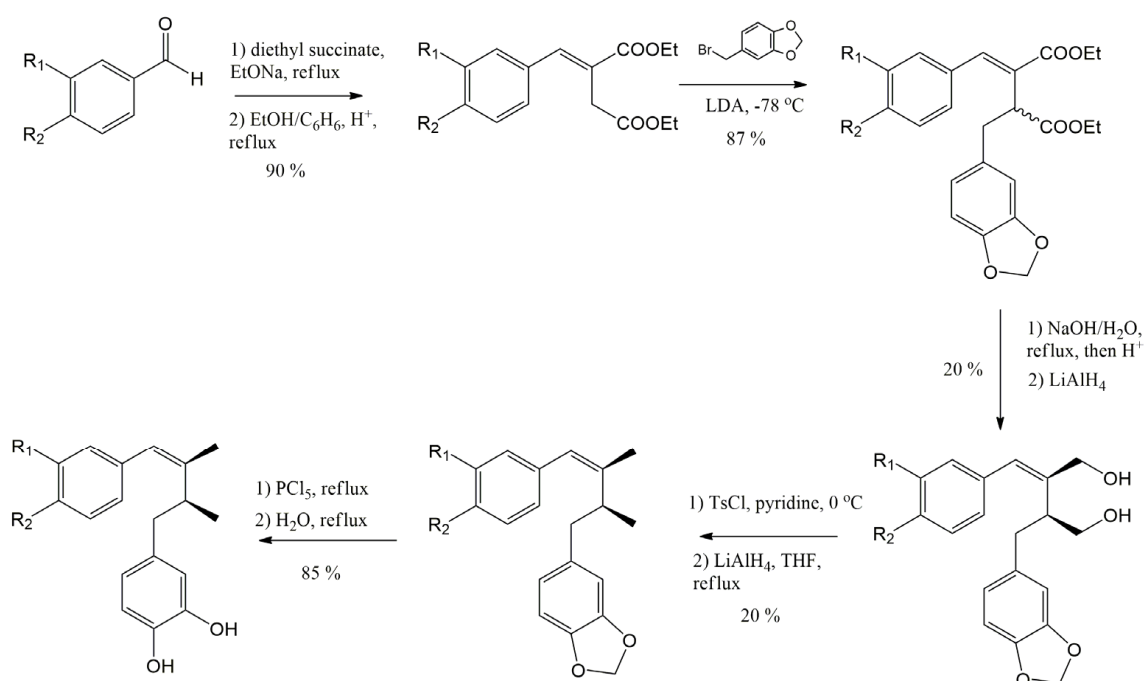
Scheme 11. The synthesis of (+)-schizandrin and (+)-isochizandrin.



Scheme 12. Dibenzocyclooctane lignans synthesized as described by Tanaka et al. [244], using a combination of classic cyclization and oxidative coupling.



Scheme 13. The synthesis of (-)-matairesinol and (-)-arctigenin.



NGDA (nordihydroguaiaretic acid)

Scheme 14. The synthesis of *meso*-Nordihydroguaiaretic acid.

The Diels-Alder reaction is used to synthesize aryl-naphthalene and aryl-tetralin lignans. This technique included the cyclization of acetylenic anhydride and was used for the synthesis of taiwanin C and dehydrotoobain in the 60–70s [247,248]. Scheme 15 shows an example of Diels-Alder reaction use to obtain lignans.

In 2019, Chi et al. used Diels-Alder reaction in order to build the key scaffold of podophyllotoxin [249]. Tricyclic Diels-Alder adducts were prepared from cyclobutanol derivative lacking the aryl group in moderate yields. After careful and complicated search, authors could develop an interesting C-H bond arylation strategy that helped to synthesize the target compound podophyllotoxin (Scheme 16).

direction of the reaction in relation to the synthetic production of one or another class of natural lignans.

5. Conclusions

Plant lignans are attractive molecules for the drug development. They bear evolutionary optimized pharmacophores and are available for the production by chemical synthesis. In a plethora of studies, lignans have been shown to exert antioxidant, anti-inflammatory, neuroprotective, anti-cancer, and chemopreventive activities. Interestingly, some representatives combine all these activities (arctigenin, NDGA, schisandrin B, sesamin). The antioxidant properties of the most common lignans largely determine their functionality. Thus, the ability of lignans to regulate the ROS/ROS-sensitive proteins ratio makes it possible to switch intracellular signaling pathways. As a rule, antioxidant lignans inhibit ROS-induced activation of the NF- κ B pathway, which ultimately leads to a decreased expression of inflammatory cytokines (IL-1 β , IL-4, IL-6, TNF- α , MCP-1), TGF- β 1 and pro-inflammatory enzymes (COX, LOX, PLA₂ and PDE). Simultaneous activation of the AMPK and Nrf2 pathways increases the expression of antioxidant-related genes (SOD, GR, GPx, Trx, HO-1, CAT) and promotes secretion of the anti-inflammatory interleukin IL-10. This imbalance in cellular response may be crucial in various pathological conditions, mainly associated with a cell death. In contrast, the imbalance in the intracellular signaling can cause the death of the cells with already impaired signalling, such as cancer cells.

However, an unpleasant fact is the toxic effect of antioxidant lignans on liver and kidneys. These severe side effects can greatly diminish the importance of such compounds as therapeutic agents. The toxicity of most lignans has not been thoroughly studied. One of the most actively and widely studied lignans, NDGA, was banned for topical use in humans due to skin hypersensitivity and was prohibited as a food preservative due to its ability to induce cystic nephropathy in rats [214,250]. Also, chronic administration of arctigenin can lead to significant damage to liver and kidneys [223]. Therefore, the high antioxidant potential of a compound is not equally beneficial to different tissues and organs, and such compounds may impair their vital functions.

More intriguing are the lignans, that have been shown to act directly on specific molecular targets. For example, some lignans with antioxidant properties, such as cobusin and eudesmin, can directly activate CFTR and CaCCgic chloride channels and inhibit ANO1/CaCC channels in addition to radical scavenging activity [251]. Another known lignan sevanol from *Thymus armenicaus* inhibited acid-sensing ion channels ASIC1a and ASIC3 and demonstrated a significant anti-inflammatory effect in rodents [119–121]. ASIC channels are known as an important pharmacological target for the treatment of inflammatory and neurodegenerative diseases [252]. Completely diverse compounds isolated from plants are able to modulate these channels [253]. Some of these ligands can act as pH-independent ASIC3 activators [254], yet effectively inhibit ASIC1a channels, and possess anti-inflammatory effect [255,256]. And the fact that sevanol acts on the target that is an ion channel located on the cell surface may explain the relatively low doses (0.1–1 mg/kg) in which this lignan shows anti-inflammatory effects. The example of sevanol shows that lignans can be not only antioxidant compounds, but also rather specific inhibitors of channels important for drug development.

Funding: This research was funded by the Russian Science Foundation, grant No. 21-15-00322.

Institutional Review Board Statement: Not applicable.

Informed Consent Statement: Not applicable.

Data Availability Statement: Not applicable.

Conflicts of Interest: The authors declare no conflict of interest.

References

1. Dewick, P.M. *Medicinal Natural Products: A Biosynthetic Approach*, 3rd ed.; John Wiley & Sons, Ltd.: Chichester, UK, 2009; pp. 1–539. ISBN 9780470741689.
2. Lee, K.H.; Xiao, Z. Lignans in treatment of cancer and other diseases. *Phytochem. Rev.* **2003**, *2*, 341–362. [[CrossRef](#)]
3. Sies, H. Oxidative stress: A concept in redox biology and medicine. *Redox Biol.* **2015**, *4*, 180–183. [[CrossRef](#)] [[PubMed](#)]
4. Medzhitov, R. Origin and physiological roles of inflammation. *Nature* **2008**, *454*, 428–435. [[CrossRef](#)] [[PubMed](#)]
5. Fleshner, M.; Crane, C.R. Exosomes, DAMPs and miRNA: Features of Stress Physiology and Immune Homeostasis. *Trends Immunol.* **2017**, *38*, 768–776. [[CrossRef](#)] [[PubMed](#)]
6. Tang, D.; Kang, R.; Coyne, C.B.; Zeh, H.J.; Lotze, M.T. PAMPs and DAMPs: Signal 0s that spur autophagy and immunity. *Immunol. Rev.* **2012**, *249*, 158–175. [[CrossRef](#)] [[PubMed](#)]
7. Karin, M.; Delhase, M. The I κ B kinase (IKK) and NF- κ B: Key elements of proinflammatory signalling. *Semin. Immunol.* **2000**, *12*, 85–98. [[CrossRef](#)]
8. Liu, T.; Zhang, L.; Joo, D.; Sun, S.-C. NF- κ B signaling in inflammation. *Signal Transduct. Target. Ther.* **2017**, *2*, 17023. [[CrossRef](#)]
9. Sun, S.C. The noncanonical NF- κ B pathway. *Immunol. Rev.* **2012**, *246*, 125–140. [[CrossRef](#)]
10. He, Y.; Hara, H.; Núñez, G. Mechanism and Regulation of NLRP3 Inflammasome Activation. *Trends Biochem. Sci.* **2016**, *41*, 1012–1021. [[CrossRef](#)]
11. Zhang, M.; An, C.; Gao, Y.; Leak, R.K.; Chen, J.; Zhang, F. Emerging roles of Nrf2 and phase II antioxidant enzymes in neuroprotection. *Prog. Neurobiol.* **2013**, *100*, 30–47. [[CrossRef](#)]
12. Vomund, S.; Schäfer, A.; Parnham, M.J.; Brüne, B.; Von Knethen, A. Nrf2, the master regulator of anti-oxidative responses. *Int. J. Mol. Sci.* **2017**, *18*, 2772. [[CrossRef](#)] [[PubMed](#)]
13. Checa, J.; Aran, J.M. Reactive oxygen species: Drivers of physiological and pathological processes. *J. Inflamm. Res.* **2020**, *13*, 1057–1073. [[CrossRef](#)] [[PubMed](#)]
14. Soares, M.P.; Seldon, M.P.; Gregoire, I.P.; Vassilevskaia, T.; Berberat, P.O.; Yu, J.; Tsui, T.-Y.; Bach, F.H. Heme Oxygenase-1 Modulates the Expression of Adhesion Molecules Associated with Endothelial Cell Activation. *J. Immunol.* **2004**, *172*, 3553–3563. [[CrossRef](#)] [[PubMed](#)]
15. Kobayashi, E.H.; Suzuki, T.; Funayama, R.; Nagashima, T.; Hayashi, M.; Sekine, H.; Tanaka, N.; Moriguchi, T.; Motohashi, H.; Nakayama, K.; et al. Nrf2 suppresses macrophage inflammatory response by blocking proinflammatory cytokine transcription. *Nat. Commun.* **2016**, *7*, 11624. [[CrossRef](#)]
16. Ganesh Yerra, V.; Negi, G.; Sharma, S.S.; Kumar, A. Potential therapeutic effects of the simultaneous targeting of the Nrf2 and NF- κ B pathways in diabetic neuropathy. *Redox Biol.* **2013**, *1*, 394–397. [[CrossRef](#)]
17. Liu, G.-H.; Qu, J.; Shen, X. NF- κ B/p65 antagonizes Nrf2-ARE pathway by depriving CBP from Nrf2 and facilitating recruitment of HDAC3 to MafK. *Biochim. Biophys. Acta Mol. Cell Res.* **2008**, *1783*, 713–727. [[CrossRef](#)]
18. Sun, S.; Zhang, H.; Xue, B.; Wu, Y.; Wang, J.; Yin, Z.; Luo, L. Protective effect of glutathione against lipopolysaccharide-induced inflammation and mortality in rats. *Inflamm. Res.* **2006**, *55*, 504–510. [[CrossRef](#)]
19. Vinogradov, A.D.; Grivennikova, V.G. Oxidation of NADH and ROS production by respiratory complex i. *Biochim. Biophys. Acta Bioenerg.* **2016**, *1857*, 863–871. [[CrossRef](#)]
20. Rabinovitch, R.C.; Samborska, B.; Faubert, B.; Ma, E.H.; Gravel, S.P.; Andrzejewski, S.; Raissi, T.C.; Pause, A.; St-Pierre, J.; Jones, R.G. AMPK Maintains Cellular Metabolic Homeostasis through Regulation of Mitochondrial Reactive Oxygen Species. *Cell Rep.* **2017**, *21*, 1–9. [[CrossRef](#)]
21. Tebay, L.E.; Robertson, H.; Durant, S.T.; Vitale, S.R.; Penning, T.M.; Dinkova-Kostova, A.T.; Hayes, J.D. Mechanisms of activation of the transcription factor Nrf2 by redox stressors, nutrient cues, and energy status and the pathways through which it attenuates degenerative disease. *Free Radic. Biol. Med.* **2015**, *88*, 108–146. [[CrossRef](#)]
22. Aquilano, K.; Baldelli, S.; Pagliei, B.; Cannata, S.M.; Rotilio, G.; Ciriolo, M.R. P53 orchestrates the PGC-1 α -mediated antioxidant response upon mild redox and metabolic imbalance. *Antioxid. Redox Signal.* **2013**, *18*, 386–399. [[CrossRef](#)] [[PubMed](#)]
23. Birben, E.; Sahiner, U.M.; Sackesen, C.; Erzurum, S.; Kalayci, O. Oxidative stress and antioxidant defense. *World Allergy Organ. J.* **2012**, *5*, 9–19. [[CrossRef](#)] [[PubMed](#)]
24. Yu, Y.U.; Kang, S.Y.; Park, H.Y.; Sung, S.H.; Lee, E.J.; Kim, S.Y.; Kim, Y.C. Antioxidant Lignans from *Machilusthunbergii* Protect CCl₄-injured Primary Cultures of Rat Hepatocytes. *J. Pharm. Pharmacol.* **2000**, *52*, 1163–1169. [[CrossRef](#)] [[PubMed](#)]
25. Baderschneider, B.; Winterhalter, P. Isolation and characterization of novel benzoates, cinnamates, flavonoids, and lignans from Riesling wine and screening for antioxidant activity. *J. Agric. Food Chem.* **2001**, *49*, 2788–2798. [[CrossRef](#)]
26. Pullela, S.V.; Takamatsu, S.; Khan, S.I.; Khan, I.A. Isolation of lignans and biological activity studies of *Ephedra viridis*. *Planta Med.* **2005**, *71*, 789–791. [[CrossRef](#)]
27. Chin, Y.W.; Chai, H.B.; Keller, W.J.; Kinghorn, A.D. Lignans and other constituents of the fruits of *Euterpe oleracea* (Açai) with antioxidant and cytoprotective activities. *J. Agric. Food Chem.* **2008**, *56*, 7759–7764. [[CrossRef](#)]
28. Sampei, M.; Arai, M.A.; Ishibashi, M. Total syntheses of schizandriside, saracoside and (\pm)-isolariciresinol with antioxidant activities. *J. Nat. Med.* **2018**, *72*, 651–654. [[CrossRef](#)]
29. Sadhu, S.K.; Khatun, A.; Phattanawasin, P.; Ohtsuki, T.; Ishibashi, M. Lignan glycosides and flavonoids from *Saracaasoca* with antioxidant activity. *J. Nat. Med.* **2007**, *61*, 480–482. [[CrossRef](#)]

30. Liu, Y.; Zhang, Y.; Muema, F.W.; Kimutai, F.; Chen, G.; Guo, M. Phenolic compounds from carissa spinarum are characterized by their antioxidant, anti-inflammatory and hepatoprotective activities. *Antioxidants* **2021**, *10*, 652. [[CrossRef](#)]
31. Liu, L.T.; Liang, L.; Wang, W.; Yan, C.Q.; Zhang, J.; Xiao, Y.C.; Ye, L.; Zhao, M.X.; Huang, Q.S.; Bian, J.J.; et al. Isolariciresinol-9'-O- α -L-arabinofuranoside protects against hydrogen peroxide-induced apoptosis of human umbilical vein endothelial cells via a PI3K/Akt/Bad-dependent pathway. *Mol. Med. Rep.* **2018**, *17*, 488–494. [[CrossRef](#)]
32. Tomosaka, H.; Chin, Y.W.; Salim, A.A.; Keller, W.J.; Chai, H.; Kinghorn, A.D. Antioxidant and cytoprotective compounds from *Berberis vulgaris* (barberry). *Phyther. Res.* **2008**, *22*, 979–981. [[CrossRef](#)] [[PubMed](#)]
33. Kim, S.Y.; Yang, E.J.; Son, Y.K.; Yeo, J.H.; Song, K.S. Enhanced anti-oxidative effect of fermented Korean mistletoe is originated from an increase in the contents of caffeic acid and lyoniresinol. *Food Funct.* **2016**, *7*, 2270–2277. [[CrossRef](#)] [[PubMed](#)]
34. Thongphasuk, P.; Suttisri, R.; Bavovada, R.; Verpoorte, R. Antioxidant lignan glucosides from *Strychnosvanprukii*. *Fitoterapia* **2004**, *75*, 623–628. [[CrossRef](#)]
35. Yoon, J.J.; Lee, H.K.; Kim, H.Y.; Han, B.H.; Lee, H.S.; Lee, Y.J.; Kang, D.G. Sauchinone protects renal mesangial cell dysfunction against angiotensin ii by improving renal fibrosis and inflammation. *Int. J. Mol. Sci.* **2020**, *21*, 7003. [[CrossRef](#)] [[PubMed](#)]
36. Takanche, J.S.; Kim, J.-E.; Han, S.-H.; Yi, H.-K. Effect of gomisin A on osteoblast differentiation in high glucose-mediated oxidative stress. *Phytomedicine* **2020**, *66*, 153107. [[CrossRef](#)] [[PubMed](#)]
37. Inoue, H.; Waiwut, P.; Saiki, I.; Shimada, Y.; Sakurai, H. Gomisin N enhances TRAIL-induced apoptosis via reactive oxygen species-mediated up-regulation of death receptors 4 and 5. *Int. J. Oncol.* **2012**, *40*, 1058–1065. [[CrossRef](#)] [[PubMed](#)]
38. Nagappan, A.; Jung, D.; Kim, J.-H.; Lee, H.; Jung, M. Gomisin N Alleviates Ethanol-Induced Liver Injury through Ameliorating Lipid Metabolism and Oxidative Stress. *Int. J. Mol. Sci.* **2018**, *19*, 2601. [[CrossRef](#)]
39. Xie, Y.; Hao, H.; Wang, H.; Guo, C.; Kang, A.; Wang, G. Reversing effects of lignans on CCl4-induced hepatic CYP450 down regulation by attenuating oxidative stress. *J. Ethnopharmacol.* **2014**, *155*, 213–221. [[CrossRef](#)]
40. Kwon, D.H.; Cha, H.J.; Choi, E.O.; Leem, S.H.; Kim, G.Y.; Moon, S.K.; Chang, Y.C.; Yun, S.J.; Hwang, H.J.; Kim, B.W.; et al. Schisandrin A suppresses lipopolysaccharide-induced inflammation and oxidative stress in RAW 264.7 macrophages by suppressing the NF- κ B, MAPKs and PI3K/Akt pathways and activating Nrf2/HO-1 signaling. *Int. J. Mol. Med.* **2018**, *41*, 264–274. [[CrossRef](#)]
41. Choi, Y.H. Schisandrin A prevents oxidative stress-induced DNA damage and apoptosis by attenuating ROS generation in C2C12 cells. *Biomed. Pharmacother.* **2018**, *106*, 902–909. [[CrossRef](#)]
42. Wan, M.L.Y.; Turner, P.C.; Co, V.A.; Wang, M.F.; Amiri, K.M.A.; El-Nezami, H. Schisandrin A protects intestinal epithelial cells from deoxynivalenol-induced cytotoxicity, oxidative damage and inflammation. *Sci. Rep.* **2019**, *9*, 19173. [[CrossRef](#)]
43. Ni, S.; Qian, Z.; Yuan, Y.; Li, D.; Zhong, Z.; Ghorbani, F.; Zhang, X.; Zhang, F.; Zhang, Z.; Liu, Z.; et al. Schisandrin A restrains osteoclastogenesis by inhibiting reactive oxygen species and activating Nrf2 signalling. *Cell Prolif.* **2020**, *53*, e12882. [[CrossRef](#)] [[PubMed](#)]
44. Lam, P.Y.; Ming Ko, K. (–)Schisandrin B ameliorates paraquat-induced oxidative stress by suppressing glutathione depletion and enhancing glutathione recovery in differentiated PC12 cells. *BioFactors* **2011**, *37*, 51–57. [[CrossRef](#)] [[PubMed](#)]
45. Chiu, P.Y.; Lam, P.Y.; Yan, C.W.; Ko, K.M. Schisandrin B protects against solar irradiation-induced oxidative injury in BJ human fibroblasts. *Fitoterapia* **2011**, *82*, 682–691. [[CrossRef](#)] [[PubMed](#)]
46. Checker, R.; Patwardhan, R.S.; Sharma, D.; Menon, J.; Thoh, M.; Bhilwade, H.N.; Konishi, T.; Sandur, S.K. Schisandrin B exhibits anti-inflammatory activity through modulation of the redox-sensitive transcription factors Nrf2 and NF- κ B. *Free Radic. Biol. Med.* **2012**, *53*, 1421–1430. [[CrossRef](#)] [[PubMed](#)]
47. Jiang, E.-P.; Li, H.; Yu, C.-R.; Yu, C.-Y.; Jing, S.; Sun, H.-X.; Wang, C.-M.; Fan, X.-T.; Chen, J.-G.; Wang, S. Schisandrin B protects PC12 cells against oxidative stress of neurodegenerative diseases. *Neuroreport* **2015**, *26*, 360–366. [[CrossRef](#)] [[PubMed](#)]
48. Lai, Q.; Luo, Z.; Wu, C.; Lai, S.; Wei, H.; Li, T.; Wang, Q.; Yu, Y. Attenuation of cyclosporine A induced nephrotoxicity by schisandrin B through suppression of oxidative stress, apoptosis and autophagy. *Int. Immunopharmacol.* **2017**, *52*, 15–23. [[CrossRef](#)]
49. Ding, M.; Shu, P.; Gao, S.; Wang, F.; Gao, Y.; Chen, Y.; Deng, W.; He, G.; Hu, Z.; Li, T. Schisandrin B protects human keratinocyte-derived HaCaT cells from tert-butyl hydroperoxide-induced oxidative damage through activating the Nrf2 signaling pathway. *Int. J. Mol. Med.* **2018**, *42*, 3571–3581. [[CrossRef](#)]
50. Chiu, P.Y.; Chen, N.; Leong, P.K.; Leung, H.Y.; Ko, K.M. Schisandrin B elicits a glutathione antioxidant response and protects against apoptosis via the redox-sensitive ERK/Nrf2 pathway in H9c2 cells. *Mol. Cell. Biochem.* **2011**, *350*, 237–250. [[CrossRef](#)]
51. Zhao, B.; Li, G.-P.; Peng, J.-J.; Ren, L.-H.; Lei, L.-C.; Ye, H.-M.; Wang, Z.-Y.; Zhao, S. Schisandrin B attenuates hypoxia/reoxygenation injury in H9c2 cells by activating the AMPK/Nrf2 signaling pathway. *Exp. Ther. Med.* **2021**, *21*, 220. [[CrossRef](#)]
52. Takanche, J.S.; Lee, Y.-H.; Kim, J.-S.; Kim, J.-E.; Han, S.-H.; Lee, S.-W.; Yi, H.-K. Anti-inflammatory and antioxidant properties of Schisandrin C promote mitochondrial biogenesis in human dental pulp cells. *Int. Endod. J.* **2018**, *51*, 438–447. [[CrossRef](#)] [[PubMed](#)]
53. Gong, J.; Wang, X. Schisandrin A protects renal tubular epithelial cells from hypoxia/reoxygenation injury through the activation of PI3K/Akt signaling pathway. *J. Biochem. Mol. Toxicol.* **2018**, *32*, e22160. [[CrossRef](#)] [[PubMed](#)]
54. Li, C.; Chen, T.; Zhou, H.; Zhang, C.; Feng, Y.; Tang, F.; Hoi, M.P.M.; He, C.; Zheng, Y.; Lee, S.M.Y. Schisandrin A attenuates neuroinflammation in activated microglia: Role of Nrf2 activation through ERK phosphorylation. *Cell. Physiol. Biochem.* **2018**, *47*, 1769–1784. [[CrossRef](#)] [[PubMed](#)]
55. Gui, Y.; Yang, Y.; Xu, D.; Tao, S.; Li, J. Schisandrin A attenuates sepsis-induced acute kidney injury by suppressing inflammation via regulating the NRF2 pathway. *Life Sci.* **2020**, *258*, 118161. [[CrossRef](#)] [[PubMed](#)]
56. Wangteeraprasert, R.; Lipipun, V.; Gunaratnam, M.; Neidle, S.; Gibbons, S.; Likhitwitayawuid, K. Bioactive compounds from *Carissa spinarum*. *Phyther. Res.* **2012**, *26*, 1496–1499. [[CrossRef](#)]

57. Suryadevara, P.K.; Tatipaka, H.B.; Vidadala, R.S.R.; Tiwari, A.K.; Rao, J.M.; Babu, K.S. Novel C-9, 9'-O-acyl Esters of (-)-Carinol as Free-radical Scavengers and Xanthine Oxidase Enzyme Inhibitors: Synthesis and Biological Evaluation. *Med. Chem.* **2013**, *9*, 100–103. [[CrossRef](#)] [[PubMed](#)]
58. Lee, Y.T.; Chen, Y.L.; Wu, Y.H.; Chen, I.S.; Chang, H.S.; Wang, Y.H.; Chang, S.H.; Wu, Y.H.; Kao, T.I.; Yu, H.P.; et al. Meso-Dihydroguaiaretic Acid Ameliorates Acute Respiratory Distress Syndrome through Inhibiting Neutrophilic Inflammation and Scavenging Free Radical. *Antioxidants* **2022**, *11*, 123. [[CrossRef](#)]
59. Abou-Gazar, H.; Bedir, E.; Takamatsu, S.; Ferreira, D.; Khan, I.A. Antioxidant lignans from *Larrea tridentata*. *Phytochemistry* **2004**, *65*, 2499–2505. [[CrossRef](#)]
60. Deshpande, V.S.; Kehrer, J.P. Oxidative stress-driven mechanisms of nordihydroguaiaretic acid-induced apoptosis in FL5.12 cells. *Toxicol. Appl. Pharmacol.* **2006**, *214*, 230–236. [[CrossRef](#)]
61. Floriano-Sánchez, E.; Villanueva, C.; Noel Medina-Campos, O.; Rocha, D.; Javier Sánchez-González, D.; Cárdenas-Rodríguez, N.; Pedraza-Chaverri, J. Nordihydroguaiaretic acid is a potent in vitro scavenger of peroxyxynitrite, singlet oxygen, hydroxyl radical, superoxide anion and hypochlorous acid and prevents in vivo ozone-induced tyrosine nitration in lungs. *Free Radic. Res.* **2006**, *40*, 523–533. [[CrossRef](#)]
62. Guzmán-Beltrán, S.; Espada, S.; Orozco-Ibarra, M.; Pedraza-Chaverri, J.; Cuadrado, A. Nordihydroguaiaretic acid activates the antioxidant pathway Nrf2/HO-1 and protects cerebellar granule neurons against oxidative stress. *Neurosci. Lett.* **2008**, *447*, 167–171. [[CrossRef](#)] [[PubMed](#)]
63. Galano, A.; Macías-Ruvalcaba, N.A.; Medina Campos, O.N.; Pedraza-Chaverri, J. Mechanism of the OH Radical Scavenging Activity of Nordihydroguaiaretic Acid: A Combined Theoretical and Experimental Study. *J. Phys. Chem. B* **2010**, *114*, 6625–6635. [[CrossRef](#)]
64. Rahman, S.; Ansari, R.A.; Rehman, H.; Parvez, S.; Raisuddin, S. Nordihydroguaiaretic Acid from Creosote Bush (*Larrea tridentata*) Mitigates 12-O-Tetradecanoylphorbol-13-Acetate-Induced Inflammatory and Oxidative Stress Responses of Tumor Promotion Cascade in Mouse Skin. *Evid. Based Complement. Altern. Med.* **2011**, *2011*, 734785. [[CrossRef](#)] [[PubMed](#)]
65. Rojo, A.I.; Medina-Campos, O.N.; Rada, P.; Zúñiga-Toalá, A.; López-Gazcón, A.; Espada, S.; Pedraza-Chaverri, J.; Cuadrado, A. Signaling pathways activated by the phytochemical nordihydroguaiaretic acid contribute to a Keap1-independent regulation of Nrf2 stability: Role of glycogen synthase kinase-3. *Free Radic. Biol. Med.* **2012**, *52*, 473–487. [[CrossRef](#)] [[PubMed](#)]
66. Guzmán-Beltrán, S.; Pedraza-Chaverri, J.; Gonzalez-Reyes, S.; Hernández-Sánchez, F.; Juárez-Figueroa, U.E.; Gonzalez, Y.; Bobadilla, K.; Torres, M. Nordihydroguaiaretic Acid Attenuates the Oxidative Stress-Induced Decrease of CD33 Expression in Human Monocytes. *Oxid. Med. Cell. Longev.* **2013**, *2013*, 375893. [[CrossRef](#)]
67. Rojas-Ochoa, A.; Córdova, E.J.; Carrillo-García, A.; Lizano, M.; Pedraza-Chaverri, J.; Patiño, N.; Cruz-Gregorio, A.; Osnaya, N. The polyphenols α -mangostin and nordihydroguaiaretic acid induce oxidative stress, cell cycle arrest, and apoptosis in a cellular model of medulloblastoma. *Molecules* **2021**, *26*, 7230. [[CrossRef](#)]
68. Banskota, A.H.; Tezuka, Y.; Nguyen, N.T.; Awale, S.; Nobukawa, T.; Kadota, S. DPPH Radical Scavenging and Nitric Oxide Inhibitory Activities of the Constituents from the Wood of *Taxus yunnanensis*. *Planta Med.* **2003**, *69*, 500–505. [[CrossRef](#)]
69. Willför, S.M.; Ahotupa, M.O.; Hemming, J.E.; Reunanen, M.H.T.; Eklund, P.C.; Sjöholm, R.E.; Eckerman, C.S.E.; Pohjamo, S.P.; Holmbom, B.R. Antioxidant Activity of Knotwood Extractives and Phenolic Compounds of Selected Tree Species. *J. Agric. Food Chem.* **2003**, *51*, 7600–7606. [[CrossRef](#)]
70. Eklund, P.C.; Långvik, O.K.; Wärnå, J.P.; Salmi, T.O.; Willför, S.M.; Sjöholm, R.E. Chemical studies on antioxidant mechanisms and free radical scavenging properties of lignans. *Org. Biomol. Chem.* **2005**, *3*, 3336. [[CrossRef](#)]
71. Hu, C.; Yuan, Y.V.; Kitts, D.D. Antioxidant activities of the flaxseed lignan secoisolariciresinoldiglucoside, its aglycone secoisolariciresinol and the mammalian lignans enterodiol and enterolactone in vitro. *Food Chem. Toxicol.* **2007**, *45*, 2219–2227. [[CrossRef](#)]
72. Moree, S.S.; Rajesha, J. Investigation of in vitro and in vivo antioxidant potential of secoisolariciresinoldiglucoside. *Mol. Cell. Biochem.* **2013**, *373*, 179–187. [[CrossRef](#)] [[PubMed](#)]
73. Puukila, S.; Bryan, S.; Laakso, A.; Abdel-Malak, J.; Gurney, C.; Agostino, A.; Belló-Klein, A.; Prasad, K.; Khaper, N. Secoisolariciresinoldiglucoside Abrogates Oxidative Stress-Induced Damage in Cardiac Iron Overload Condition. *PLoS ONE* **2015**, *10*, e0122852. [[CrossRef](#)] [[PubMed](#)]
74. Pietrofesa, R.; Velapoulou, A.; Albelda, S.; Christofidou-Solomidou, M. Asbestos Induces Oxidative Stress and Activation of Nrf2 Signaling in Murine Macrophages: Chemopreventive Role of the Synthetic Lignan Secoisolariciresinoldiglucoside (LGM2605). *Int. J. Mol. Sci.* **2016**, *17*, 322. [[CrossRef](#)] [[PubMed](#)]
75. Pietrofesa, R.A.; Chatterjee, S.; Park, K.; Arguiri, E.; Albelda, S.M.; Christofidou-Solomidou, M. Synthetic lignan secoisolariciresinoldiglucoside (LGM2605) reduces asbestos-induced cytotoxicity in an Nrf2-dependent and -independent manner. *Antioxidants* **2018**, *7*, 38. [[CrossRef](#)]
76. Kokkinaki, D.; Hoffman, M.; Kalliora, C.; Kyriazis, I.D.; Maning, J.; Lucchese, A.M.; Shanmughapriya, S.; Tomar, D.; Park, J.Y.; Wang, H.; et al. Chemically synthesized Secoisolariciresinoldiglucoside (LGM2605) improves mitochondrial function in cardiac myocytes and alleviates septic cardiomyopathy. *J. Mol. Cell. Cardiol.* **2019**, *127*, 232–245. [[CrossRef](#)]
77. Jang, Y.P.; Kim, S.R.; Choi, Y.H.; Kim, J.; Kim, S.G.; Markelonis, G.J.; Oh, T.H.; Kim, Y.C. Arctigenin protects cultured cortical neurons from glutamate-induced neurodegeneration by binding to kainate receptor. *J. Neurosci. Res.* **2002**, *68*, 233–240. [[CrossRef](#)]
78. Kou, X.; Qi, S.; Dai, W.; Luo, L.; Yin, Z. Arctigenin inhibits lipopolysaccharide-induced iNOS expression in RAW264.7 cells through suppressing JAK-STAT signal pathway. *Int. Immunopharmacol.* **2011**, *11*, 1095–1102. [[CrossRef](#)]

79. Gu, Y.; Qi, C.; Sun, X.; Ma, X.; Zhang, H.; Hu, L.; Yuan, J.; Yu, Q. Arctigenin preferentially induces tumor cell death under glucose deprivation by inhibiting cellular energy metabolism. *Biochem. Pharmacol.* **2012**, *84*, 468–476. [[CrossRef](#)]
80. Wu, R.; Sun, Y.; Zhou, T.; Zhu, Z.; Zhuang, J.; Tang, X.; Chen, J.; Hu, L.; Shen, X. Arctigenin enhances swimming endurance of sedentary rats partially by regulation of antioxidant pathways. *Acta Pharmacol. Sin.* **2014**, *35*, 1274–1284. [[CrossRef](#)]
81. Hsieh, C.-J.; Kuo, P.-L.; Hsu, Y.-C.; Huang, Y.-F.; Tsai, E.-M.; Hsu, Y.-L. Arctigenin, a dietary phytoestrogen, induces apoptosis of estrogen receptor-negative breast cancer cells through the ROS/p38 MAPK pathway and epigenetic regulation. *Free Radic. Biol. Med.* **2014**, *67*, 159–170. [[CrossRef](#)]
82. Jeong, Y.-H.; Park, J.-S.; Kim, D.-H.; Kim, H.-S. Arctigenin Increases Hemeoxygenase-1 Gene Expression by Modulating PI3K/AKT Signaling Pathway in Rat Primary Astrocytes. *Biomol. Ther.* **2014**, *22*, 497–502. [[CrossRef](#)] [[PubMed](#)]
83. Li, A.; Wang, J.; Zhu, D.; Zhang, X.; Pan, R.; Wang, R. Arctigenin suppresses transforming growth factor- β 1-induced expression of monocyte chemoattractant protein-1 and the subsequent epithelial-mesenchymal transition through reactive oxygen species-dependent ERK/NF- κ B signaling pathway in renal tubular epithe. *Free Radic. Res.* **2015**, *49*, 1095–1113. [[CrossRef](#)] [[PubMed](#)]
84. Su, S.; Wink, M. Natural lignans from *Arctium lappa* as antiaging agents in *Caenorhabditis elegans*. *Phytochemistry* **2015**, *117*, 340–350. [[CrossRef](#)] [[PubMed](#)]
85. Chen, K.-Y.; Lin, J.-A.; Yao, H.-Y.; Hsu, A.-C.; Tai, Y.-T.; Chen, J.-T.; Hsieh, M.-C.; Shen, T.-L.; Hsu, R.-Y.; Wu, H.-T.; et al. Arctigenin protects against steatosis in WRL68 hepatocytes through activation of phosphoinositide 3-kinase/protein kinase B and AMP-activated protein kinase pathways. *Nutr. Res.* **2018**, *52*, 87–97. [[CrossRef](#)] [[PubMed](#)]
86. Lu, Z.; Zhou, H.; Zhang, S.; Dai, W.; Zhang, Y.; Hong, L.; Chen, F.; Cao, J. Activation of reactive oxygen species-mediated mitogen-activated protein kinases pathway regulates both extrinsic and intrinsic apoptosis induced by arctigenin in Hep G2. *J. Pharm. Pharmacol.* **2019**, *72*, 29–43. [[CrossRef](#)]
87. Liu, C.-Y.; Zhou, Y.; Chen, T.; Lei, J.-C.; Jiang, X.-J. AMPK/SIRT1 Pathway is Involved in Arctigenin-Mediated Protective Effects Against Myocardial Ischemia-Reperfusion Injury. *Front. Pharmacol.* **2021**, *11*, 2351. [[CrossRef](#)]
88. Liu, X.; Wang, J.; Dou, P.; Zhang, X.; Ran, X.; Liu, L.; Dou, D. The Ameliorative Effects of Arctiin and Arctigenin on the Oxidative Injury of Lung Induced by Silica via TLR-4/NLRP3/TGF- β Signaling Pathway. *Oxid. Med. Cell. Longev.* **2021**, *2021*, 1–18. [[CrossRef](#)]
89. Medola, J.F.; Cintra, V.P.; e Silva, P.P.; Royo, V.; da Silva, R.; Saraiva, J.; de Albuquerque, S.; Bastos, J.K.; e Silva, M.L.A.; Tavares, D.C. (–)-Hinokinin causes antigenotoxicity but not genotoxicity in peripheral blood of Wistar rats. *Food Chem. Toxicol.* **2007**, *45*, 638–642. [[CrossRef](#)]
90. Tiwari, A.K.; Srinivas, P.V.; Praveen Kumar, S.; Madhusudana Rao, J. Free radical scavenging active components from *Cedrus deodara*. *J. Agric. Food Chem.* **2001**, *49*, 4642–4645. [[CrossRef](#)]
91. Yamauchi, S.; Sugahara, T.; Nakashima, Y.; Okada, A.; Akiyama, K.; Kishida, T.; Maruyama, M.; Masuda, T. Radical and superoxide scavenging activities of matairesinol and oxidized matairesinol. *Biosci. Biotechnol. Biochem.* **2006**, *70*, 1934–1940. [[CrossRef](#)]
92. Lee, B.; Kim, K.H.; Jung, H.J.; Kwon, H.J. Matairesinol inhibits angiogenesis via suppression of mitochondrial reactive oxygen species. *Biochem. Biophys. Res. Commun.* **2012**, *421*, 76–80. [[CrossRef](#)] [[PubMed](#)]
93. Wu, Q.; Wang, Y.; Li, Q. Matairesinol exerts anti-inflammatory and antioxidant effects in sepsis-mediated brain injury by repressing the MAPK and NF- κ B pathways through up-regulating AMPK. *Aging* **2021**, *13*, 23780–23795. [[CrossRef](#)] [[PubMed](#)]
94. Moraux, T.; Dumarçay, S.; Gérardin, P.; Gérardin-Charbonnier, C. Derivatives of the Lignan 7'-Hydroxymatairesinol with Antioxidant Properties and Enhanced Lipophilicity. *J. Nat. Prod.* **2017**, *80*, 1783–1790. [[CrossRef](#)] [[PubMed](#)]
95. Wang, L.Y.; Unehara, N.; Kitanaka, S. Lignans from the Roots of *Wikstroemia indica* and their DPPH radical scavenging and nitric oxide inhibitory activities. *Chem. Pharm. Bull.* **2005**, *53*, 1348–1351. [[CrossRef](#)]
96. Wangteeraprasert, R.; Likhitwitayawuid, K. Lignans and a sesquiterpene glucoside from *Carissa carandas* stem. *Helv. Chim. Acta* **2009**, *92*, 1217–1223. [[CrossRef](#)]
97. Tebboub, O.; Cotugno, R.; Oke-Altuntas, F.; Bouheroum, M.; Demirtas, Í.; D'Ambola, M.; Malafronte, N.; Vassallo, A. Antioxidant potential of herbal preparations and components from galactites *elegans* (All.) nyman ex soldano. *Evid. Based Complement. Altern. Med.* **2018**, *2018*, 9294358. [[CrossRef](#)]
98. Zhang, Y.; Cichewicz, R.H.; Nair, M.G. Lipid peroxidation inhibitory compounds from daylily (*Hemerocallis fulva*) leaves. *Life Sci.* **2004**, *75*, 753–763. [[CrossRef](#)]
99. Bajpai, V.K.; Alam, M.B.; Quan, K.T.; Kwon, K.-R.; Ju, M.-K.; Choi, H.-J.; Lee, J.S.; Yoon, J.-I.; Majumder, R.; Rather, I.A.; et al. Antioxidant efficacy and the upregulation of Nrf2-mediated HO-1 expression by (+)-lariciresinol, a lignan isolated from *Rubia philippinensis*, through the activation of p38. *Sci. Rep.* **2017**, *7*, 46035. [[CrossRef](#)]
100. Jang, H.J.; Yang, K.E.; Oh, W.K.; Lee, S.I.; Hwang, I.H.; Ban, K.T.; Yoo, H.S.; Choi, J.S.; Yeo, E.J.; Jang, I.S. Nectandrin B-mediated activation of the AMPK pathway prevents cellular senescence in human diploid fibroblasts by reducing intracellular ROS levels. *Aging* **2019**, *11*, 3731–3749. [[CrossRef](#)]
101. Kuo, C.C.; Chiang, W.; Liu, G.P.; Chien, Y.L.; Chang, J.Y.; Lee, C.K.; Lo, J.M.; Huang, S.L.; Shih, M.C.; Kuo, Y.H. 2,2'-Diphenyl-1-picrylhydrazyl radical-scavenging active components from adlay (*Coixlachryma-jobi* L. var. *ma-yuen* Stapf) hulls. *J. Agric. Food Chem.* **2002**, *50*, 5850–5855. [[CrossRef](#)]
102. Chen, H.-H.; Chen, Y.-T.; Huang, Y.-W.; Tsai, H.-J.; Kuo, C.-C. 4-Ketopinoresinol, a novel naturally occurring ARE activator, induces the Nrf2/HO-1 axis and protects against oxidative stress-induced cell injury via activation of PI3K/AKT signaling. *Free Radic. Biol. Med.* **2012**, *52*, 1054–1066. [[CrossRef](#)] [[PubMed](#)]

103. Zeng, M.; Li, M.; Chen, Y.; Zhang, J.; Cao, Y.; Zhang, B.; Feng, W.; Zheng, X.; Yu, Z. A new bisepoxy lignandendranlignan A isolated from *Chrysanthemum* Flower inhibits the production of inflammatory mediators via the TLR4 pathway in LPS-induced H9c2 cardiomyocytes. *Arch. Biochem. Biophys.* **2020**, *690*, 108506. [[CrossRef](#)] [[PubMed](#)]
104. Huang, Q.; Ouyang, D.S.; Liu, Q. Isoeucumin A attenuates kidney injury in diabetic nephropathy through the Nrf2/HO-1 pathway. *FEBS Open Bio* **2021**, *11*, 2350–2363. [[CrossRef](#)] [[PubMed](#)]
105. Lee, Y.G.; Jang, S.A.; Seo, K.H.; Gwag, J.E.; Kim, H.G.; Ko, J.H.; Ji, S.A.; Kang, S.C.; Lee, D.Y.; Baek, N.I. New Lignans from the Flower of *Forsythia koreana* and Their Suppression Effect on VCAM-1 Expression in MOVAS Cells. *Chem. Biodivers.* **2018**, *15*, e1800026. [[CrossRef](#)] [[PubMed](#)]
106. Chen, C.-C.; Chen, H.-Y.; Shiao, M.-S.; Lin, Y.-L.; Kuo, Y.-H.; Ou, J.-C. Inhibition of Low Density Lipoprotein Oxidation by Tetrahydrofuran Lignans from *Forsythia suspensa* and *Magnolia coco*. *Planta Med.* **1999**, *65*, 709–711. [[CrossRef](#)] [[PubMed](#)]
107. Yun, B.S.; Lee, I.K.; Kim, J.P.; Chung, S.H.; Shim, G.S.; Yoo, I.D. Lipid peroxidation inhibitory activity of some constituents isolated from the stem bark of *Eucalyptus globulus*. *Arch. Pharm. Res.* **2000**, *23*, 147–150. [[CrossRef](#)]
108. Li, A.L.; Li, G.H.; Li, Y.R.; Wu, X.Y.; Ren, D.M.; Lou, H.X.; Wang, X.N.; Shen, T. Lignan and flavonoid support the prevention of cinnamon against oxidative stress related diseases. *Phytomedicine* **2019**, *53*, 143–153. [[CrossRef](#)]
109. Yao, J.; Zou, Z.; Wang, X.; Ji, X.; Yang, J. Pinoresinol Diglucoside Alleviates oxLDL-Induced Dysfunction in Human Umbilical Vein Endothelial Cells. *Evid. Based Complement. Altern. Med.* **2016**, *2016*, 3124519. [[CrossRef](#)]
110. Lee, W.-J.; Ou, H.-C.; Wu, C.-M.; Lee, I.-T.; Lin, S.-Y.; Lin, L.-Y.; Tsai, K.-L.; Lee, S.-D.; Sheu, W.H.-H. Sesamin mitigates inflammation and oxidative stress in endothelial cells exposed to oxidized low-density lipoprotein. *J. Agric. Food Chem.* **2009**, *57*, 11406–11417. [[CrossRef](#)]
111. Hsieh, P.F.; Hou, C.-W.; Yao, P.-W.; Wu, S.-P.; Peng, Y.-F.; Shen, M.-L.; Lin, C.-H.; Chao, Y.-Y.; Chang, M.-H.; Jeng, K.-C. Sesamin ameliorates oxidative stress and mortality in kainic acid-induced status epilepticus by inhibition of MAPK and COX-2 activation. *J. Neuroinflamm.* **2011**, *8*, 57. [[CrossRef](#)]
112. Deng, S.; Zhou, J.-L.; Fang, H.-S.; Nie, Z.-G.; Chen, S.; Peng, H. Sesamin Protects the Femoral Head from Osteonecrosis by Inhibiting ROS-Induced Osteoblast Apoptosis in Rat Model. *Front. Physiol.* **2018**, *9*, 1787. [[CrossRef](#)] [[PubMed](#)]
113. Bai, X.; Gou, X.; Cai, P.; Xu, C.; Cao, L.; Zhao, Z.; Huang, M.; Jin, J. Sesamin Enhances Nrf2-Mediated Protective Defense against Oxidative Stress and Inflammation in Colitis via AKT and ERK Activation. *Oxid. Med. Cell. Longev.* **2019**, *2019*, 2432416. [[CrossRef](#)]
114. Ruankham, W.; Suwanjang, W.; Wongchitrat, P.; Prachayasittikul, V.; Prachayasittikul, S.; Phopin, K. Sesamin and sesamol attenuate H₂O₂-induced oxidative stress on human neuronal cells via the SIRT1-SIRT3-FOXO3a signaling pathway. *Nutr. Neurosci.* **2021**, *24*, 90–101. [[CrossRef](#)]
115. Cho, S.; Cho, M.; Kim, J.; Kaerberlein, M.; Lee, S.J.; Suh, Y. Syringaresinol protects against hypoxia/reoxygenation-induced cardiomyocytes injury and death by destabilization of HIF-1 α in a FOXO3-dependent mechanism. *Oncotarget* **2015**, *6*, 43–55. [[CrossRef](#)] [[PubMed](#)]
116. Li, G.; Yang, L.; Feng, L.; Yang, J.; Li, Y.; An, J.; Li, D.; Xu, Y.; Gao, Y.; Li, J.; et al. Syringaresinol Protects against Type 1 Diabetic Cardiomyopathy by Alleviating Inflammation Responses, Cardiac Fibrosis, and Oxidative Stress. *Mol. Nutr. Food Res.* **2020**, *64*, 2000231. [[CrossRef](#)]
117. Osmakov, D.I.; Koshelev, S.G.; Belozerova, O.A.; Kublitski, V.S.; Andreev, Y.A.; Grishin, E.V.; Kozlov, S.A. Biological Activity of Sevanol and Its Analogues 1. *Russ. J. Bioorganic Chem.* **2015**, *41*, 543–547. [[CrossRef](#)] [[PubMed](#)]
118. Kalinovskii, A.P.; Osmakov, D.I.; Koshelev, S.G.; Lubova, K.I.; Korolkova, Y.V.; Kozlov, S.A.; Andreev, Y.A. Retinoic Acid-Differentiated Neuroblastoma SH-SY5Y Is an Accessible In Vitro Model to Study Native Human Acid-Sensing Ion Channels 1a (ASIC1a). *Biology* **2022**, *11*, 167. [[CrossRef](#)]
119. Dubinnyi, M.A.; Osmakov, D.I.; Koshelev, S.G.; Kozlov, S.A.; Andreev, Y.A.; Zakaryan, N.A.; Dyachenko, I.A.; Bondarenko, D.A.; Arseniev, A.S.; Grishin, E.V. Lignan from Thyme Possesses Inhibitory Effect on ASIC3 Channel Current. *J. Biol. Chem.* **2012**, *287*, 32993–33000. [[CrossRef](#)]
120. Andreev, Y.; Osmakov, D.; Koshelev, S.; Maleeva, E.; Logashina, Y.; Palikov, V.; Palikova, Y.; Dyachenko, I.; Kozlov, S. Analgesic Activity of Acid-Sensing Ion Channel 3 (ASIC3) Inhibitors: Sea Anemones Peptides Ugr9-1 and APETx2 versus Low Molecular Weight Compounds. *Mar. Drugs* **2018**, *16*, 500. [[CrossRef](#)]
121. Belozerova, O.A.; Osmakov, D.I.; Vladimirov, A.; Koshelev, S.G.; Chugunov, A.O.; Andreev, Y.A.; Palikov, V.A.; Palikova, Y.A.; Shaykhutdinova, E.R.; Gvozdz, A.N.; et al. Sevanol and Its Analogues: Chemical Synthesis, Biological Effects and Molecular Docking. *Pharmaceuticals* **2020**, *13*, 163. [[CrossRef](#)]
122. Verma, S.; Kalita, B.; Bajaj, S.; Prakash, H.; Singh, A.K.; Gupta, M.L. A combination of podophyllotoxin and rutin alleviates radiation-induced pneumonitis and fibrosis through modulation of lung inflammation in mice. *Front. Immunol.* **2017**, *8*, 658. [[CrossRef](#)] [[PubMed](#)]
123. Sharma, S.; Mehak; Chhimwal, J.; Patial, V.; Sk, U.H. Dendrimer-conjugated podophyllotoxin suppresses DENA-induced HCC progression by modulation of inflammatory and fibrogenic factors. *Toxicol. Res.* **2019**, *8*, 560–567. [[CrossRef](#)] [[PubMed](#)]
124. Hwang, B.Y.; Lee, J.H.; Jung, H.S.; Kim, K.S.; Nam, J.B.; Hong, Y.S.; Paik, S.G.; Lee, J.J. Sauchinone, a Lignan from *Saururus chinensis*, Suppresses iNOS Expression through the Inhibition of Transactivation Activity of RelA of NF- κ B. *Planta Med.* **2003**, *69*, 1096–1101. [[CrossRef](#)] [[PubMed](#)]
125. Lee, A.K.; Sung, S.H.; Kim, Y.C.; Kim, S.G. Inhibition of lipopolysaccharide-inducible nitric oxide synthase, TNF- α and COX-2 expression by sauchinone effects on I- κ B α phosphorylation, C/EBP and AP-1 activation. *Br. J. Pharmacol.* **2003**, *139*, 11–20. [[CrossRef](#)]

126. Min, H.J.; Won, H.Y.; Kim, Y.C.; Sung, S.H.; Byun, M.R.; Hwang, J.H.; Hong, J.H.; Hwang, E.S. Suppression of Th2-driven, allergen-induced airway inflammation by sauchinone. *Biochem. Biophys. Res. Commun.* **2009**, *385*, 204–209. [[CrossRef](#)]
127. Teraoka, R.; Shimada, T.; Aburada, M. The Molecular Mechanisms of the Hepatoprotective Effect of Gomisin A against Oxidative Stress and Inflammatory Response in Rats with Carbon Tetrachloride-Induced Acute Liver Injury. *Biol. Pharm. Bull.* **2012**, *35*, 171–177. [[CrossRef](#)]
128. Yim, T.K.; Ko, K.M. Schisandrin B protects against myocardial ischemia-reperfusion injury by enhancing myocardial glutathione antioxidant status. *Mol. Cell. Biochem.* **1999**, *196*, 151–156. [[CrossRef](#)]
129. Ip, S.P.; Ko, K.M. The crucial antioxidant action of schisandrin B in protecting against carbon tetrachloride hepatotoxicity in mice: A comparative study with butylated hydroxytoluene. *Biochem. Pharmacol.* **1996**, *52*, 1687–1693. [[CrossRef](#)]
130. Chiu, P.Y.; Tang, M.H.; Mak, D.H.F.; Poon, M.K.T.; Ko, K.M. Hepatoprotective mechanism of schisandrin B: Role of mitochondrial glutathione antioxidant status and heat shock proteins. *Free Radic. Biol. Med.* **2003**, *35*, 368–380. [[CrossRef](#)]
131. Lam, P.Y.; Chiu, P.Y.; Leung, H.Y.; Chen, N.; Leong, P.K.; Ko, K.M. Schisandrin B co-treatment ameliorates the impairment on mitochondrial antioxidant status in various tissues of long-term ethanol treated rats. *Fitoterapia* **2010**, *81*, 1239–1245. [[CrossRef](#)] [[PubMed](#)]
132. Giridharan, V.V.; Thandavarayan, R.A.; Arumugam, S.; Mizuno, M.; Nawa, H.; Suzuki, K.; Ko, K.M.; Krishnamurthy, P.; Watanabe, K.; Konishi, T.D. Schisandrin B ameliorates ICV-infused amyloid β induced oxidative stress and neuronal dysfunction through inhibiting RAGE/NF- κ B/MAPK and Up-regulating HSP/beclin expression. *PLoS ONE* **2015**, *10*, e0142483. [[CrossRef](#)] [[PubMed](#)]
133. Xin, D.Q.; Hu, Z.M.; Huo, H.J.; Yang, X.J.; Han, D.; Xing, W.H.; Zhao, Y.; Qiu, Q.H. Schisandrin B attenuates the inflammatory response, oxidative stress and apoptosis induced by traumatic spinal cord injury via inhibition of p53 signaling in adult rats. *Mol. Med. Rep.* **2017**, *16*, 533–538. [[CrossRef](#)] [[PubMed](#)]
134. Zhu, N.; Cai, C.; Zhou, A.; Zhao, X.; Xiang, Y.; Zeng, C. Schisandrin B Prevents Hind Limb from Ischemia-Reperfusion-Induced Oxidative Stress and Inflammation via MAPK/NF- κ B Pathways in Rats. *Biomed Res. Int.* **2017**, *2017*, 4237973. [[CrossRef](#)] [[PubMed](#)]
135. Mou, Z.; Feng, Z.; Xu, Z.; Zhuang, F.; Zheng, X.; Li, X.; Qian, J.; Liang, G. Schisandrin B alleviates diabetic nephropathy through suppressing excessive inflammation and oxidative stress. *Biochem. Biophys. Res. Commun.* **2019**, *508*, 243–249. [[CrossRef](#)]
136. Wu, Y.; Li, Z.; Yao, L.; Li, M.; Tang, M. Schisandrin B alleviates acute oxidative stress via modulation of the Nrf2/Keap1-mediated antioxidant pathway. *Appl. Physiol. Nutr. Metab.* **2019**, *44*, 1–6. [[CrossRef](#)]
137. Tang, H.; Zhao, J.; Feng, R.; Pu, P.; Wen, L. Reducing oxidative stress may be important for treating pirarubicin-induced cardiotoxicity with schisandrin B. *Exp. Ther. Med.* **2021**, *23*, 68. [[CrossRef](#)]
138. Han, J.; Shi, X.; Du, Y.; Shi, F.; Zhang, B.; Zheng, Z.; Xu, J.; Jiang, L. Schisandrin C targets Keap1 and attenuates oxidative stress by activating Nrf2 pathway in Ang II-challenged vascular endothelium. *Phyther. Res.* **2019**, *33*, 779–790. [[CrossRef](#)]
139. Li, X.; Zhao, X.; Xu, X.; Mao, X.; Liu, Z.; Li, H.; Guo, L.; Bi, K.; Jia, Y. Schisantherin A recovers A β -induced neurodegeneration with cognitive decline in mice. *Physiol. Behav.* **2014**, *132*, 10–16. [[CrossRef](#)]
140. Liu, C.; Sun, W.; Li, N.; Gao, J.; Yu, C.; Wang, C.; Sun, J.; Jing, S.; Chen, J.; Li, H. Schisantherin A Improves Learning and Memory of Mice with D-Galactose-Induced Learning and Memory Impairment Through Its Antioxidation and Regulation of p19/p53/p21/Cyclin D1/CDK4/RB Gene Expressions. *J. Med. Food* **2018**, *21*, 678–688. [[CrossRef](#)]
141. Lin, H.; Zhang, X.; Liu, J.; Yuan, L.; Liu, J.; Wang, C.; Sun, J.; Chen, J.; Jing, S.; Li, H. Schisantherin A improves learning and memory abilities partly through regulating the Nrf2/Keap1/ARE signaling pathway in chronic fatigue mice. *Exp. Ther. Med.* **2021**, *21*, 385. [[CrossRef](#)]
142. Shi, Y.W.; Zhang, X.C.; Chen, C.; Tang, M.; Wang, Z.W.; Liang, X.M.; Ding, F.; Wang, C.P. Schisantherin A attenuates ischemia/reperfusion-induced neuronal injury in rats via regulation of TLR4 and C5aR1 signaling pathways. *Brain. Behav. Immun.* **2017**, *66*, 244–256. [[CrossRef](#)]
143. Yam-Canul, P.; Chirino, Y.I.; Sánchez-González, D.J.; Martínez-Martínez, C.M.; Cruz, C.; Villanueva, C.; Pedraza-Chaverri, J. Nordihydroguaiaretic acid attenuates potassium dichromate-induced oxidative stress and nephrotoxicity. *Food Chem. Toxicol.* **2008**, *46*, 1089–1096. [[CrossRef](#)] [[PubMed](#)]
144. Chan, J.K.W.; Bittner, S.; Bittner, A.; Atwal, S.; Shen, W.J.; Inayathullah, M.; Rajada, J.; Nicolls, M.R.; Kraemer, F.B.; Azhar, S. Nordihydroguaiaretic acid, a lignan from *larrea tridentata* (Creosote bush), protects against American lifestyle-induced obesity syndrome diet-induced metabolic dysfunction in mice. *J. Pharmacol. Exp. Ther.* **2018**, *365*, 281–290. [[CrossRef](#)] [[PubMed](#)]
145. Pilar, B.; Güllich, A.; Oliveira, P.; Ströher, D.; Piccoli, J.; Manfredini, V. Protective Role of Flaxseed Oil and Flaxseed Lignan Secoisolariciresinoldiglucoside Against Oxidative Stress in Rats with Metabolic Syndrome. *J. Food Sci.* **2017**, *82*, 3029–3036. [[CrossRef](#)] [[PubMed](#)]
146. Puukila, S.; Fernandes, R.O.; Türck, P.; Carraro, C.C.; Bonetto, J.H.P.; de Lima-Seolin, B.G.; da Rosa Araujo, A.S.; Belló-Klein, A.; Boreham, D.; Khaper, N. Secoisolariciresinoldiglucoside attenuates cardiac hypertrophy and oxidative stress in monocrotaline-induced right heart dysfunction. *Mol. Cell. Biochem.* **2017**, *432*, 33–39. [[CrossRef](#)]
147. Kartha, S.; Weisshaar, C.L.; Pietrofesa, R.A.; Christofidou-Solomidou, M.; Winkelstein, B.A. Synthetic secoisolariciresinoldiglucoside attenuates established pain, oxidative stress and neuroinflammation in a rodent model of painful radiculopathy. *Antioxidants* **2020**, *9*, 1209. [[CrossRef](#)]
148. Aqeel, T.; Gurumallu, S.C.; Bhaskar, A.; Hashimi, S.M.; Javaraiah, R. Secoisolariciresinoldiglucoside protects against cadmium-induced oxidative stress-mediated renal toxicity in rats. *J. Trace Elem. Med. Biol.* **2020**, *61*, 126552. [[CrossRef](#)]
149. Ge, J.; Hao, R.; Rong, X.; Dou, Q.P.; Tan, X.; Li, G.; Li, F.; Li, D. Secoisolariciresinoldiglucoside mitigates benzo[a]pyrene-induced liver and kidney toxicity in mice via miR-101a/MKP-1-mediated p38 and ERK pathway. *Food Chem. Toxicol.* **2022**, *159*, 112733. [[CrossRef](#)]

150. He, X.; Wang, Y.; Wu, M.; Wei, J.; Sun, X.; Wang, A.; Hu, G.; Jia, J. Secoisolariciresinol Diglucoside Improves Ovarian Reserve in Aging Mouse by Inhibiting Oxidative Stress. *Front. Mol. Biosci.* **2022**, *8*, 806412. [[CrossRef](#)] [[PubMed](#)]
151. Li, X.-M.; Miao, Y.; Su, Q.-Y.; Yao, J.-C.; Li, H.-H.; Zhang, G.-M. Gastroprotective effects of arctigenin of *Arctium lappa* L. on a rat model of gastric ulcers. *Biomed. Rep.* **2016**, *5*, 589–594. [[CrossRef](#)]
152. Swarup, V.; Ghosh, J.; Mishra, M.K.; Basu, A. Novel strategy for treatment of Japanese encephalitis using arctigenin, a plant lignan. *J. Antimicrob. Chemother.* **2008**, *61*, 679–688. [[CrossRef](#)] [[PubMed](#)]
153. Zhang, W.; Jiang, Z.; He, B.; Liu, X. Arctigenin Protects against Lipopolysaccharide-Induced Pulmonary Oxidative Stress and Inflammation in a Mouse Model via Suppression of MAPK, HO-1, and iNOS Signaling. *Inflammation* **2015**, *38*, 1406–1414. [[CrossRef](#)] [[PubMed](#)]
154. Yang, J.; Yin, H.S.; Cao, Y.J.; Jiang, Z.A.; Li, Y.J.; Song, M.C.; Wang, Y.F.; Wang, Z.H.; Yang, R.; Jiang, Y.F.; et al. Arctigenin Attenuates Ischemia/Reperfusion Induced Ventricular Arrhythmias by Decreasing Oxidative Stress in Rats. *Cell. Physiol. Biochem.* **2018**, *49*, 728–742. [[CrossRef](#)] [[PubMed](#)]
155. Zhang, Y.; Yang, Y. Arctigenin exerts protective effects against myocardial infarction via regulation of iNOS, COX-2, ERK1/2 and HO-1 in rats. *Mol. Med. Rep.* **2018**, *17*, 4839–4845. [[CrossRef](#)]
156. Jiang, L.; Deng, Y.; Li, W.; Lu, Y. Arctigenin suppresses fibroblast activity and extracellular matrix deposition in hypertrophic scarring by reducing inflammation and oxidative stress. *Mol. Med. Rep.* **2020**, *22*, 4783–4791. [[CrossRef](#)]
157. Salama, S.A.; Mohamadin, A.M.; Abdel-Bakky, M.S. Arctigenin alleviates cadmium-induced nephrotoxicity: Targeting endoplasmic reticulum stress, Nrf2 signaling, and the associated inflammatory response. *Life Sci.* **2021**, *287*, 120121. [[CrossRef](#)]
158. Lu, Q.; Zheng, R.; Zhu, P.; Bian, J.; Liu, Z.; Du, J. Hinokinin alleviates high fat diet/streptozotocin-induced cardiac injury in mice through modulation in oxidative stress, inflammation and apoptosis. *Biomed. Pharmacother.* **2021**, *137*, 111361. [[CrossRef](#)]
159. Wang, X.; Cheng, Y.; Xue, H.; Yue, Y.; Zhang, W.; Li, X. Fargesin as a potential β 1 adrenergic receptor antagonist protects the hearts against ischemia/reperfusion injury in rats via attenuating oxidative stress and apoptosis. *Fitoterapia* **2015**, *105*, 16–25. [[CrossRef](#)]
160. Lei, S.; Wu, S.; Wang, G.; Li, B.; Liu, B.; Lei, X. Pinoresinoldiglucoside attenuates neuroinflammation, apoptosis and oxidative stress in a mice model with Alzheimer's disease. *Neuroreport* **2021**, *32*, 259–267. [[CrossRef](#)]
161. Zhang, Y.; Lei, Y.; Yao, X.; Yi, J.; Feng, G. Pinoresinoldiglucoside alleviates ischemia/reperfusion-induced brain injury by modulating neuroinflammation and oxidative stress. *Chem. Biol. Drug Des.* **2021**, *98*, 986–996. [[CrossRef](#)]
162. Baluchnejadmojarad, T.; Roghani, M.; Jalali Nadoushan, M.-R.; Vaez Mahdavi, M.-R.; Kalalian-Moghaddam, H.; Roghani-Dehkordi, F.; Dariani, S.; Raoufi, S. The sesame lignan sesamin attenuates vascular dysfunction in streptozotocin diabetic rats: Involvement of nitric oxide and oxidative stress. *Eur. J. Pharmacol.* **2013**, *698*, 316–321. [[CrossRef](#)]
163. Liu, C.-M.; Zheng, G.-H.; Ming, Q.-L.; Chao, C.; Sun, J.-M. Sesamin Protects Mouse Liver against Nickel-Induced Oxidative DNA Damage and Apoptosis by the PI3K-Akt Pathway. *J. Agric. Food Chem.* **2013**, *61*, 1146–1154. [[CrossRef](#)] [[PubMed](#)]
164. Ma, J.-Q.; Ding, J.; Zhang, L.; Liu, C.-M. Hepatoprotective properties of sesamin against CCl₄ induced oxidative stress-mediated apoptosis in mice via JNK pathway. *Food Chem. Toxicol.* **2014**, *64*, 41–48. [[CrossRef](#)] [[PubMed](#)]
165. Cao, J.; Chen, J.; Xie, L.; Wang, J.; Feng, C.; Song, J. Protective properties of sesamin against fluoride-induced oxidative stress and apoptosis in kidney of carp (*Cyprinus carpio*) via JNK signaling pathway. *Aquat. Toxicol.* **2015**, *167*, 180–190. [[CrossRef](#)]
166. Guo, H.; Liu, Y.; Wang, L.; Zhang, G.; Su, S.; Zhang, R.; Zhang, J.; Li, A.; Shang, C.; Bi, B.; et al. Alleviation of doxorubicin-induced hepatorenal toxicities with sesamin via the suppression of oxidative stress. *Hum. Exp. Toxicol.* **2016**, *35*, 1183–1193. [[CrossRef](#)]
167. Baluchnejadmojarad, T.; Mansouri, M.; Ghalami, J.; Mokhtari, Z.; Roghani, M. Sesamin imparts neuroprotection against intrastriatal 6-hydroxydopamine toxicity by inhibition of astroglial activation, apoptosis, and oxidative stress. *Biomed. Pharmacother.* **2017**, *88*, 754–761. [[CrossRef](#)] [[PubMed](#)]
168. Yashaswini, P.S.; Sadashivaiah, B.; Ramaprasad, T.R.; Singh, S.A. In vivo modulation of LPS induced leukotrienes generation and oxidative stress by sesame lignans. *J. Nutr. Biochem.* **2017**, *41*, 151–157. [[CrossRef](#)]
169. Rousta, A.-M.; Mirahmadi, S.-M.-S.; Shahmohammadi, A.; Nourabadi, D.; Khajevand-Khazaei, M.-R.; Baluchnejadmojarad, T.; Roghani, M. Protective effect of sesamin in lipopolysaccharide-induced mouse model of acute kidney injury via attenuation of oxidative stress, inflammation, and apoptosis. *Immunopharmacol. Immunotoxicol.* **2018**, *40*, 423–429. [[CrossRef](#)]
170. Ali, B.H.; Al Salam, S.; Al Suleimani, Y.; Al Za'abi, M.; Ashique, M.; Manoj, P.; Sudhadevi, M.; Al Tobi, M.; Nemmar, A. Ameliorative effect of sesamin in cisplatin-induced nephrotoxicity in rats by suppressing inflammation, oxidative/nitrosative stress, and cellular damage. *Physiol. Res.* **2020**, *69*, 61–72. [[CrossRef](#)]
171. Le, T.D.; Inoue, Y.H. Sesamin Activates Nrf2/Cnc-Dependent Transcription in the Absence of Oxidative Stress in *Drosophila* Adult Brains. *Antioxidants* **2021**, *10*, 924. [[CrossRef](#)]
172. Kim, J.; Toda, T.; Watanabe, K.; Shibuya, S.; Ozawa, Y.; Izuo, N.; Cho, S.; Seo, D.B.; Yokote, K.; Shimizu, T. Syringaresinol Reverses Age-Related Skin Atrophy by Suppressing FoxO3a-Mediated Matrix Metalloproteinase-2 Activation in Copper/Zinc Superoxide Dismutase-Deficient Mice. *J. Investig. Dermatol.* **2019**, *139*, 648–655. [[CrossRef](#)] [[PubMed](#)]
173. Guo, L.Y.; Hung, T.M.; Bae, K.H.; Shin, E.M.; Zhou, H.Y.; Hong, Y.N.; Kang, S.S.; Kim, H.P.; Kim, Y.S. Anti-inflammatory effects of schisandrin isolated from the fruit of *Schisandra chinensis* Baill. *Eur. J. Pharmacol.* **2008**, *591*, 293–299. [[CrossRef](#)] [[PubMed](#)]
174. Cui, L.; Zhu, W.; Yang, Z.; Song, X.; Xu, C.; Cui, Z.; Xiang, L. Evidence of anti-inflammatory activity of Schizandrin A in animal models of acute inflammation. *Naunyn. Schmiedebergs. Arch. Pharmacol.* **2020**, *393*, 2221–2229. [[CrossRef](#)] [[PubMed](#)]

175. Chiu, P.Y.; Mak, D.H.F.; Poon, M.K.T.; Ko, K.M. Role of cytochrome P-450 in schisandrin B-induced antioxidant and heat shock responses in mouse liver. *Life Sci.* **2005**, *77*, 2887–2895. [[CrossRef](#)]
176. You, S.; Qian, J.; Wu, G.; Qian, Y.; Wang, Z.; Chen, T.; Wang, J.; Huang, W.; Liang, G. Schisandrin B attenuates angiotensin II induced endothelial to mesenchymal transition in vascular endothelium by suppressing NF- κ B activation. *Phytomedicine* **2019**, *62*, 152955. [[CrossRef](#)]
177. Zhang, W.; Wang, W.; Shen, C.; Wang, X.; Pu, Z.; Yin, Q. Network pharmacology for systematic understanding of Schisandrin B reduces the epithelial cells injury of colitis through regulating pyroptosis by AMPK/Nrf2/NLRP3 inflammasome. *Aging* **2021**, *13*, 22193–22209. [[CrossRef](#)]
178. Ma, Z.; Xu, G.; Shen, Y.; Hu, S.; Lin, X.; Zhou, J.; Zhao, W.; Liu, J.; Wang, J.; Guo, J. Schisandrin B-mediated TH17 cell differentiation attenuates bowel inflammation. *Pharmacol. Res.* **2021**, *166*, 105459. [[CrossRef](#)]
179. Chen, P.; Pang, S.; Yang, N.; Meng, H.; Liu, J.; Zhou, N.; Zhang, M.; Xu, Z.; Gao, W.; Chen, B.; et al. Beneficial effects of schisandrin B on the cardiac function in mice model of myocardial infarction. *PLoS ONE* **2013**, *8*, e79418. [[CrossRef](#)]
180. Ran, J.; Ma, C.; Xu, K.; Xu, L.; He, Y.; Moqbel, S.A.A.; Hu, P.; Jiang, L.; Chen, W.; Bao, J.; et al. Schisandrin B ameliorated chondrocytes inflammation and osteoarthritis via suppression of NF- κ B and MAPK signal pathways. *Drug Des. Dev. Ther.* **2018**, *12*, 1195–1204. [[CrossRef](#)]
181. Zhang, Y.; Zhou, Z.W.; Jin, H.; Hu, C.; He, Z.X.; Yu, Z.L.; Ko, K.M.; Yang, T.; Zhang, X.; Pan, S.Y.; et al. Schisandrin B inhibits cell growth and induces cellular apoptosis and autophagy in mouse hepatocytes and macrophages: Implications for its hepatotoxicity. *Drug Des. Dev. Ther.* **2015**, *9*, 2001–2027. [[CrossRef](#)]
182. Zhang, Y.; Pan, S.Y.; Zhou, S.F.; Wang, X.Y.; Sun, N.; Zhu, P.L.; Chu, Z.S.; Yu, Z.L.; Ko, K.M. Time and dose relationships between schisandrin B- and schisandrae fructus oil-induced hepatotoxicity and the associated elevations in hepatic and serum triglyceride levels in mice. *Drug Des. Dev. Ther.* **2014**, *8*, 1429–1439. [[CrossRef](#)] [[PubMed](#)]
183. Dash, P.K.; Moore, A.N. Enhanced processing of APP induced by IL-1 β can be reduced by indomethacin and nordihydroguaiaretic acid. *Biochem. Biophys. Res. Commun.* **1995**, *208*, 542–548. [[CrossRef](#)] [[PubMed](#)]
184. Jeon, S.B.; Ji, K.A.; You, H.J.; Kim, J.H.; Jou, I.; Joe, E.H. Nordihydroguaiaretic acid inhibits IFN- γ -induced STAT tyrosine phosphorylation in rat brain astrocytes. *Biochem. Biophys. Res. Commun.* **2005**, *328*, 595–600. [[CrossRef](#)] [[PubMed](#)]
185. Li, Y.J.; Kukita, A.; Watanabe, T.; Takano, T.; Qu, P.; Sanematsu, K.; Ninomiya, Y.; Kukita, T. Nordihydroguaiaretic acid inhibition of NFATc1 suppresses osteoclastogenesis and arthritis bone destruction in rats. *Lab. Investig.* **2012**, *92*, 1777–1787. [[CrossRef](#)]
186. Lee, J.Y.; Kim, C.J. Arctigenin, a phenylpropanoid dibenzylbutyrolactone lignan, inhibits type I-IV allergic inflammation and pro-inflammatory enzymes. *Arch. Pharm. Res.* **2010**, *33*, 947–957. [[CrossRef](#)]
187. Shi, H.; Dong, G.; Yan, F.; Zhang, H.; Li, C.; Ma, Q.; Zhang, J.; Ning, Z.; Li, Z.; Dai, J.; et al. Arctigenin Ameliorates Inflammation by Regulating Accumulation and Functional Activity of MDSCs in Endotoxin Shock. *Inflammation* **2018**, *41*, 2090–2100. [[CrossRef](#)]
188. Cheng, X.; Wang, H.; Yang, J.; Cheng, Y.; Wang, D.; Yang, F.; Li, Y.; Zhou, D.; Wang, Y.; Xue, Z.; et al. Arctigenin protects against liver injury from acute hepatitis by suppressing immune cells in mice. *Biomed. Pharmacother.* **2018**, *102*, 464–471. [[CrossRef](#)]
189. Tang, S.; Zhou, W.; Zhong, X.; Xu, J.; Huang, H.; Zheng, X.; Zhang, J.; Yang, S.; Shang, P.; Tang, Q.; et al. Arctigenin prevents the progression of osteoarthritis by targeting PI3K/Akt/NF- κ B axis: In vitro and in vivo studies. *J. Cell. Mol. Med.* **2020**, *24*, 4183–4193. [[CrossRef](#)]
190. Li, H.; Zhang, X.; Xiang, C.; Feng, C.; Fan, C.; Liu, M.; Lu, H.; Su, H.; Zhou, Y.; Qi, Q.; et al. Identification of phosphodiesterase-4 as the therapeutic target of arctigenin in alleviating psoriatic skin inflammation. *J. Adv. Res.* **2021**, *33*, 241–251. [[CrossRef](#)]
191. Desai, D.C.; Jacob, J.; Almeida, A.; Kshirsagar, R.; Manju, S.L. Isolation, structural elucidation and anti-inflammatory activity of astragalol, (-)hinokinin, aristolactami and aristolochic acids (I & II) from *Aristolochia indica*. *Nat. Prod. Res.* **2014**, *28*, 1413–1417. [[CrossRef](#)]
192. Li, X.; Gao, Q.; Yang, L.; Han, M.; Zhou, C.; Mu, H. Matairesinol ameliorates experimental autoimmune uveitis by suppression of IRBP-specific Th17 cells. *J. Neuroimmunol.* **2020**, *345*, 577286. [[CrossRef](#)] [[PubMed](#)]
193. Spilioti, E.; Holmbom, B.; Papavassiliou, A.G.; Moutsatsou, P. Lignans 7-hydroxymatairesinol and 7-hydroxymatairesinol 2 exhibit anti-inflammatory activity in human aortic endothelial cells. *Mol. Nutr. Food Res.* **2014**, *58*, 749–759. [[CrossRef](#)] [[PubMed](#)]
194. Laavola, M.; Leppänen, T.; Eräsalo, H.; Hämäläinen, M.; Nieminen, R.; Moilanen, E. Anti-inflammatory Effects of Nortrachelogenin in Murine J774 Macrophages and in Carrageenan-Induced Paw Edema Model in the Mouse. *Planta Med.* **2017**, *83*, 519–526. [[CrossRef](#)] [[PubMed](#)]
195. Lee, D.G.; Lee, S.M.; Bang, M.H.; Park, H.J.; Lee, T.H.; Kim, Y.H.; Kim, J.Y.; Baek, N.I. Lignans from the flowers of *osmanthus fragrans* var. *aurantiacus* and their inhibition effect on NO production. *Arch. Pharm. Res.* **2011**, *34*, 2029–2035. [[CrossRef](#)] [[PubMed](#)]
196. Ahmad, I.; Fozia; Waheed, A.; Tahir, N.B.; Rais, A.K. Anti-inflammatory constituents from *Perovskia atriplicifolia*. *Pharm. Biol.* **2015**, *53*, 1628–1631. [[CrossRef](#)]
197. De León, E.J.; Olmedo, D.A.; Solís, P.N.; Gupta, M.P.; Terencio, M.C. Diayangambin exerts immunosuppressive and anti-inflammatory effects in vitro and in vivo. *Planta Med.* **2002**, *68*, 1128–1131. [[CrossRef](#)]
198. Pham, T.H.; Kim, M.S.; Le, M.Q.; Song, Y.S.; Bak, Y.; Ryu, H.W.; Oh, S.R.; Yoon, D.Y. Fargesin exerts anti-inflammatory effects in THP-1 monocytes by suppressing PKC-dependent AP-1 and NF- κ B signaling. *Phytomedicine* **2017**, *24*, 96–103. [[CrossRef](#)]
199. Yue, B.; Ren, Y.J.; Zhang, J.J.; Luo, X.P.; Yu, Z.L.; Ren, G.Y.; Sun, A.N.; Deng, C.; Wang, Z.T.; Dou, W. Anti-inflammatory effects of fargesin on chemically induced inflammatory bowel disease in mice. *Molecules* **2018**, *23*, 1380. [[CrossRef](#)]

200. Kim, T.W.; Shin, J.S.; Chung, K.S.; Lee, Y.G.; Baek, N.I.; Lee, K.T. Anti-Inflammatory Mechanisms of Koreanaside A, a Lignan Isolated from the Flower of *Forsythia koreana*, against LPS-Induced Macrophage Activation and DSS-Induced Colitis Mice: The Crucial Role of AP-1, NF- κ B, and JAK/STAT Signaling. *Cells* **2019**, *8*, 1163. [CrossRef]
201. Lim, H.; Lee, J.G.; Lee, S.H.; Kim, Y.S.; Kim, H.P. Anti-inflammatory activity of phylligenin, a lignan from the fruits of *Forsythia koreana*, and its cellular mechanism of action. *J. Ethnopharmacol.* **2008**, *118*, 113–117. [CrossRef]
202. During, A.; Debouche, C.; Raas, T.; Larondelle, Y. Among plant lignans, pinoresinol has the strongest antiinflammatory properties in human intestinal Caco-2 cells. *J. Nutr.* **2012**, *142*, 1798–1805. [CrossRef] [PubMed]
203. Cui, Y.; Hou, X.; Chen, J.; Xie, L.; Yang, L.; Le, Y. Sesamin inhibits bacterial formylpeptide-induced inflammatory responses in a murine air-pouch model and in THP-1 human monocytes. *J. Nutr.* **2010**, *140*, 377–381. [CrossRef]
204. Li, L.C.; Piao, H.M.; Zheng, M.Y.; Lin, Z.H.; Li, G.; Yan, G.H. Sesamin attenuates mast cell-mediated allergic responses by suppressing the activation of p38 and nuclear factor- κ B. *Mol. Med. Rep.* **2016**, *13*, 536–542. [CrossRef] [PubMed]
205. Ye, H.; Sun, L.; Li, J.; Wang, Y.; Bai, J.; Wu, L.; Han, Q.; Yang, Z.; Li, L. Sesamin attenuates carrageenan-induced lung inflammation through upregulation of A20 and TAX1BP1 in rats. *Int. Immunopharmacol.* **2020**, *88*, 107009. [CrossRef] [PubMed]
206. Ku, S.K.; Lee, W.; Yoo, H.; Han, C.K.; Bae, J.S. Inhibitory effects of epi-sesamin on endothelial protein C receptor shedding in vitro and in vivo. *Inflamm. Res.* **2013**, *62*, 895–902. [CrossRef]
207. Bajpai, V.K.; Alam, M.B.; Quan, K.T.; Ju, M.K.; Majumder, R.; Shukla, S.; Huh, Y.S.; Na, M.K.; Lee, S.H.; Han, Y.K. Attenuation of inflammatory responses by (+)-syringaresinol via MAP-Kinase-mediated suppression of NF- κ B signaling in vitro and in vivo. *Sci. Rep.* **2018**, *8*, 9216. [CrossRef]
208. Wei, A.; Liu, J.; Li, D.; Lu, Y.; Yang, L.; Zhuo, Y.; Tian, W.; Cong, H. Syringaresinol attenuates sepsis-induced cardiac dysfunction by inhibiting inflammation and pyroptosis in mice. *Eur. J. Pharmacol.* **2021**, *913*, 174644. [CrossRef]
209. Zhang, L.; Jiang, X.; Zhang, J.; Gao, H.; Yang, L.; Li, D.; Zhang, Q.; Wang, B.; Cui, L.; Wang, X. (–)-Syringaresinol suppressed LPS-induced microglia activation via downregulation of NF- κ B p65 signaling and interaction with ER β . *Int. Immunopharmacol.* **2021**, *99*, 107986. [CrossRef]
210. Manda, G.; Rojo, A.I.; Martínez-Klimova, E.; Pedraza-Chaverri, J.; Cuadrado, A. Nordihydroguaiaretic Acid: From Herbal Medicine to Clinical Development for Cancer and Chronic Diseases. *Front. Pharmacol.* **2020**, *11*, 151. [CrossRef]
211. Xue, H.; Zhang, X.Y.; Liu, J.M.; Song, Y.; Liu, T.T.; Chen, D. NDGA reduces secondary damage after spinal cord injury in rats via anti-inflammatory effects. *Brain Res.* **2013**, *1516*, 83–92. [CrossRef]
212. Zhang, H.; Shen, W.J.; Cortez, Y.; Kraemer, F.B.; Azhar, S. Nordihydroguaiaretic acid improves metabolic dysregulation and aberrant hepatic lipid metabolism in mice by both PPAR α -dependent and -independent pathways. *Am. J. Physiol. Gastrointest. Liver Physiol.* **2013**, *304*, G72–G86. [CrossRef] [PubMed]
213. Zubrow, M.E.; Margulies, S.S.; Yehya, N. Nordihydroguaiaretic acid reduces secondary organ injury in septic rats after cecal ligation and puncture. *PLoS ONE* **2020**, *15*, e0237613. [CrossRef] [PubMed]
214. Lambert, J.D.; Zhao, D.; Meyers, R.O.; Kuester, R.K.; Timmermann, B.N.; Dorr, R.T. Nordihydroguaiaretic acid: Hepatotoxicity and detoxification in the mouse. *Toxicol.* **2002**, *40*, 1701–1708. [CrossRef]
215. Lü, J.M.; Nurko, J.; Weakley, S.M.; Jiang, J.; Kougiaris, P.; Lin, P.H.; Yao, Q.; Chen, C. Molecular mechanisms and clinical applications of nordihydroguaiaretic acid (NDGA) and its derivatives: An update. *Med. Sci. Monit.* **2010**, *16*, RA93–RA100. [PubMed]
216. Hyam, S.R.; Lee, I.A.; Gu, W.; Kim, K.A.; Jeong, J.J.; Jang, S.E.; Han, M.J.; Kim, D.H. Arctigenin ameliorates inflammation in vitro and in vivo by inhibiting the PI3K/AKT pathway and polarizing M1 macrophages to M2-like macrophages. *Eur. J. Pharmacol.* **2013**, *708*, 21–29. [CrossRef] [PubMed]
217. Li, W.; Zhang, Z.; Zhang, K.; Xue, Z.; Li, Y.; Zhang, Z.; Zhang, L.; Gu, C.; Zhang, Q.; Hao, J.; et al. Arctigenin Suppress Th17 Cells and Ameliorates Experimental Autoimmune Encephalomyelitis Through AMPK and PPAR- γ /ROR- γ t Signaling. *Mol. Neurobiol.* **2016**, *53*, 5356–5366. [CrossRef]
218. Nakano, Y.; Nasu, M.; Kano, M.; Kameoka, H.; Okuyama, T.; Nishizawa, M.; Ikeya, Y. Lignans from guaiac resin decrease nitric oxide production in interleukin 1 β -treated hepatocytes. *J. Nat. Med.* **2017**, *71*, 190–197. [CrossRef]
219. Küpeli, E.; Erdemoğlu, N.; Yeşilada, E.; Şener, B. Anti-inflammatory and antinociceptive activity of taxoids and lignans from the heartwood of *Taxus baccata* L. *J. Ethnopharmacol.* **2003**, *89*, 265–270. [CrossRef]
220. Karthivashan, G.; Kweon, M.H.; Park, S.Y.; Kim, J.S.; Kim, D.H.; Ganesan, P.; Choi, D.K. Cognitive-enhancing and ameliorative effects of acanthoside B in a scopolamine-induced amnesic mouse model through regulation of oxidative/inflammatory/cholinergic systems and activation of the TrkB/CREB/BDNF pathway. *Food Chem. Toxicol.* **2019**, *129*, 444–457. [CrossRef]
221. Wang, G.; Gao, J.H.; He, L.H.; Yu, X.H.; Zhao, Z.W.; Zou, J.; Wen, F.J.; Zhou, L.; Wan, X.J.; Tang, C.K. Fargesin alleviates atherosclerosis by promoting reverse cholesterol transport and reducing inflammatory response. *Biochim. Biophys. Acta Mol. Cell Biol. Lipids* **2020**, *1865*, 158633. [CrossRef]
222. Wang, C.; Ma, C.; Fu, K.; Gong, L.H.; Zhang, Y.F.; Zhou, H.L.; Li, Y.X. Phylligenin Attenuates Carbon Tetrachloride-Induced Liver Fibrosis via Modulating Inflammation and Gut Microbiota. *Front. Pharmacol.* **2021**, *12*, 2537. [CrossRef] [PubMed]
223. Tan, Y.J.; Ren, Y.S.; Gao, L.; Li, L.F.; Cui, L.J.; Li, B.; Li, X.; Yang, J.; Wang, M.Z.; Lv, Y.Y.; et al. 28-Day Oral Chronic Toxicity Study of Arctigenin in Rats. *Front. Pharmacol.* **2018**, *9*, 1077. [CrossRef] [PubMed]
224. Rao, R.J.; Kumar, U.S.; Reddy, S.V.; Tiwari, A.K.; Rao, J.M. Antioxidants and a new germacrane sesquiterpene from *Carissa spinarum*. *Nat. Prod. Res.* **2005**, *19*, 763–769. [CrossRef] [PubMed]
225. Ward, R.S. The synthesis of lignans and neolignans. *Chem. Soc. Rev.* **1982**, *11*, 75–125. [CrossRef]

226. Fang, X.; Hu, X. Advances in the synthesis of lignan natural products. *Molecules* **2018**, *23*, 3385. [[CrossRef](#)]
227. Sih, C.J.; Ravikumar, P.R.; Huang, F.C.; Buckner, C.; Whitlock, H. Isolation and Synthesis of Pinoresinol Diglucoside, a Major Antihypertensive Principle of Tu-Chung (*Eucommia ulmoides*, Oliver). *J. Am. Chem. Soc.* **1976**, *98*, 5412–5413. [[CrossRef](#)]
228. Dickey, E.E. Liriodendrin, a New Lignan Diglucoside from the Inner Bark of Yellow Poplar (*Liriodendron tulipifera* L.). *J. Org. Chem.* **1958**, *23*, 179–184. [[CrossRef](#)]
229. Maeda, S.; Masuda, H.; Tokoroyama, T. Studies on the Preparation of Bioactive Lignans by Oxidative Coupling Reaction. II. Oxidative Coupling Reaction of Methyl (E)-3-(4,5-Dihydroxy-2-methoxyphenyl)propenoate and Lipid Peroxidation Inhibitory Effects of the Produced Lignans. *Chem. Pharm. Bull.* **1994**, *42*, 2506–2513. [[CrossRef](#)]
230. Lemièrre, G.; Gao, M.; De Groot, A.; Dommissie, R.; Lepoivre, J.; Pieters, L.; Buss, V. 3',4-Di-O-methylcedrusin: Synthesis, resolution and absolute configuration. *J. Chem. Soc. Perkin Trans.* **1995**, *13*, 1775–1779. [[CrossRef](#)]
231. Daquino, C.; Rescifina, A.; Spatafora, C.; Tringali, C. Biomimetic synthesis of natural and “unnatural” lignans by oxidative coupling of caffeic esters. *Eur. J. Org. Chem.* **2009**, *2009*, 6289–6300. [[CrossRef](#)]
232. Kao, T.T.; Lin, C.C.; Shia, K.S. The Total Synthesis of Retrojusticidin B, Justicidin E, and Helioxanthin. *J. Org. Chem.* **2015**, *80*, 6708–6714. [[CrossRef](#)] [[PubMed](#)]
233. Nahrstedt, A.; Albrecht, M.; Wray, V.; Gumbinger, H.G.; John Winterhoff, M.H.; Kemper, F.H. Structures of compounds with antigonadotropic activity obtained by in vitro oxidation of caffeic acid. *Planta Med.* **1990**, *56*, 395–398. [[CrossRef](#)] [[PubMed](#)]
234. Wang, Q.; Yang, Y.; Li, Y.; Yu, W.; Hou, Z.J. An efficient method for the synthesis of lignans. *Tetrahedron* **2006**, *62*, 6107–6112. [[CrossRef](#)]
235. Takahashi, H.; Matsumoto, K.; Ueda, M.; Miyake, Y.; Fukuyama, Y. Biomimetic syntheses of neurotrophic americanola and isoamericanola by horseradish peroxidase (HRP) catalyzed oxidative coupling. *Heterocycles* **2002**, *56*, 245–256. [[CrossRef](#)]
236. Bruschi, M.; Orlandi, M.; Rindone, B.; Rummakko, P.; Zoia, L. Asymmetric biomimetic oxidations of phenols using oxazolidines as chiral auxiliaries: The enantioselective synthesis of (+)- and (-)-dehydrodiconiferyl alcohol. *J. Phys. Org. Chem.* **2006**, *19*, 592–596. [[CrossRef](#)]
237. Singleton, V.L.; Cilliers, J.J.L. Characterization of the Products of Nonenzymic Autoxidative Phenolic Reactions in a Caffeic Acid Model System. *J. Agric. Food Chem.* **1991**, *39*, 1298–1303. [[CrossRef](#)]
238. Agata, I.; Hatano, T.; Nishibe, S.; Okuda, T. A tetrameric derivative of caffeic acid from *Rabdosia japonica*. *Phytochemistry* **1989**, *28*, 2447–2450. [[CrossRef](#)]
239. Bogucki, D.E.; Charlton, J.L. A non-enzymatic synthesis of (S)-(-)-rosmarinic acid and a study of a biomimetic route to (+)-rabdosin. *Can. J. Chem.* **1997**, *75*, 1783–1794. [[CrossRef](#)]
240. Belozero, O.A.; Deigin, V.I.; Khrushchev, A.Y.; Dubinnyi, M.A.; Kublitski, V.S. The total synthesis of sevanol, a novel lignan isolated from the thyme plant (*Thymus armeniacus*). *Tetrahedron* **2018**, *74*, 1449–1453. [[CrossRef](#)]
241. Datta, P.K.; Yau, C.; Hooper, T.S.; Yvon, B.L.; Charlton, J.L. Acid-catalyzed cyclization of 2,3-dibenzylidenesuccinates: Synthesis of lignans (±)-cagayanin and (±)-galbulin. *J. Org. Chem.* **2001**, *66*, 8606–8611. [[CrossRef](#)]
242. Ishikawa, R.; Yoshida, N.; Akao, Y.; Kawabe, Y.; Inai, M.; Asakawa, T.; Hamashima, Y.; Kan, T. Total syntheses of (+)-sesamin and (+)-sesaminol. *Chem. Lett.* **2014**, *43*, 1572–1574. [[CrossRef](#)]
243. Tanaka, M.; Mukaiyama, C.; Mitsunashi, H.; Maruno, M.; Wakamatsu, T. Synthesis of Optically Pure Gomisi Lignans: The Total Synthesis of (+)-Schizandrin, (+)-Gomisin A, and (+)-Isoschizandrin in Naturally Occurring Forms. *J. Org. Chem.* **1995**, *60*, 4339–4352. [[CrossRef](#)]
244. Tanaka, M.; Ohshima, T.; Mitsunashi, H.; Maruno, M.; Wakamatsu, T. Total syntheses of the lignans isolated from *Schisandra chinensis*. *Tetrahedron* **1995**, *51*, 11693–11702. [[CrossRef](#)]
245. Fischer, J.; Reynolds, A.J.; Sharp, L.A.; Sherburn, M.S. Radical carboxylation approach to lignans. Total synthesis of (-)-arctigenin, (-)-matairesinol, and related natural products. *Org. Lett.* **2004**, *6*, 1345–1348. [[CrossRef](#)]
246. Xia, Y.; Zhang, Y.; Wang, W.; Ding, Y.; He, R. Synthesis and bioactivity of erythro-nordihydroguaiaretic acid, threo(-)-saururenin and their analogues. *J. Serb. Chem. Soc.* **2010**, *75*, 1325–1335. [[CrossRef](#)]
247. Holmes, T.L.; Stevenson, R. Arylnaphthalene Lignans. Synthesis of Justicidin E, Taiwanin C, Dehydrodimethylconidendrin, and Dehydrodimethylretrodendrin. *J. Org. Chem.* **1971**, *36*, 3450–3453. [[CrossRef](#)]
248. Maclean, I.; Stevenson, R. Synthesis of (±)-otobain. *J. Chem. Soc. C Org.* **1966**, *0*, 1717–1719. [[CrossRef](#)]
249. Ting, C.P.; Tschanen, E.; Jang, E.; Maimone, T.J. Total synthesis of podophyllotoxin and select analog designs via C–H activation. *Tetrahedron* **2019**, *75*, 3299–3308. [[CrossRef](#)]
250. Gardner, K.D.; Reed, W.P.; Evan, A.P.; Zedalis, J.; Hylarides, M.D.; Leon, A.A. Endotoxin provocation of experimental renal cystic disease. *Kidney Int.* **1987**, *32*, 329–334. [[CrossRef](#)]
251. Jiang, Y.; Yu, B.; Fang, F.; Cao, H.; Ma, T.; Yang, H. Modulation of chloride channel functions by the plant lignan compounds kobusin and eudesmin. *Front. Plant Sci.* **2015**, *6*, 1–11. [[CrossRef](#)]
252. Osmakov, D.I.; Andreev, Y.A.; Kozlov, S.A. Acid-sensing ion channels and their modulators. *Biochemistry* **2014**, *79*, 1528–1545. [[CrossRef](#)] [[PubMed](#)]
253. Osmakov, D.I.; Khasanov, T.A.; Andreev, Y.A.; Lyukmanova, E.N.; Kozlov, S.A. Animal, Herb, and Microbial Toxins for Structural and Pharmacological Study of Acid-Sensing Ion Channels. *Front. Pharmacol.* **2020**, *11*, 991. [[CrossRef](#)] [[PubMed](#)]
254. Osmakov, D.I.; Koshelev, S.G.; Lyukmanova, E.N.; Shulepko, M.A.; Andreev, Y.A.; Illes, P.; Kozlov, S.A. Multiple Modulation of Acid-Sensing Ion Channel 1a by the Alkaloid Daurisoline. *Biomolecules* **2019**, *9*, 336. [[CrossRef](#)] [[PubMed](#)]

-
255. Osmakov, D.I.; Koshelev, S.G.; Palikov, V.A.; Palikova, Y.A.; Shaykhutdinova, E.R.; Dyachenko, I.A.; Andreev, Y.A.; Kozlov, S.A. Alkaloid Lindoldhamine Inhibits Acid-Sensing Ion Channel 1a and Reveals Anti-Inflammatory Properties. *Toxins* **2019**, *11*, 542. [[CrossRef](#)] [[PubMed](#)]
256. Osmakov, D.I.; Koshelev, S.G.; Andreev, Y.A.; Dubinnyi, M.A.; Kublitski, V.S.; Efremov, R.G.; Sobolevsky, A.I.; Kozlov, S.A. Proton-independent activation of acid-sensing ion channel 3 by an alkaloid, lindoldhamine, from *Laurus nobilis*. *Br. J. Pharmacol.* **2018**, *175*, 924–937. [[CrossRef](#)]